SYNTHESIS OF CNT-TITANIA-SILICA NANOCOMPOSITE THIN FILMS: THE EFFECT OF HEAT TREATMENT ON PHOTOCATALYTIC ACTIVITY

A THESIS SUBMITTED TO
THE GRADUATE SCHOOL OF NATURAL AND APPLIED SCIENCES
OF
MIDDLE EAST TECHNICAL UNIVERSITY

BY

TUĞÇE KIRBAŞ

IN PARTIAL FULFILLMENT OF THE REQUIREMENTS
FOR
THE DEGREE OF MASTER OF SCIENCE
IN
CHEMICAL ENGINEERING

SEPTEMBER 2014

Approval of the thesis:

SYNTHESIS OF CNT-TITANIA-SILICA NANOCOMPOSITE THIN FILMS: THE EFFECT OF HEAT TREATMENT ON PHOTOCATALYTIC ACTIVITY

submitted by **TUĞÇE KIRBAŞ** in partial fulfillment of the requirements for the degree of **Master of Science in Chemical Engineering Department, Middle East Technical University** by,

Prof. Dr. Canan Özgen _______________
Dean, Graduate School of **Natural and Applied Sciences**

Prof. Dr. Halil Kalıpçılar _______________
Head of Department, **Chemical Engineering**

Prof. Dr. Gürkan Karakaş _______________
Supervisor, **Chemical Engineering Dept., METU**

Examining Committee Members:

Prof. Dr. Timur Doğu _______________
Chemical Engineering Dept., METU

Prof. Dr. Gürkan Karakaş _______________
Chemical Engineering Dept., METU

Prof.Dr. Hayrettin Yücel _______________
Chemical Engineering Dept., METU

Assoc. Prof. Dr. Ayşen Yılmaz _______________
Chemistry Dept., METU

Assoc. Prof.Dr. Sena Yaşyerli _______________
Chemical Engineering Dept., Gazi Uni.

Date: **15.09.2014**

I hereby declare that all information in this document has been obtained and presented in accordance with academic rules and ethical conduct. I also declare that, as required by these rules and conduct, I have fully cited and referenced all material and results that are not original to this work.

Name, Last name : TUĞÇE KIRBAŞ

Signature :

ABSTRACT

SYNTHESIS OF CNT-TITANIA-SILICA NANOCOMPOSITE THIN FILMS: THE EFFECT OF HEAT TREATMENT ON PHOTOCATALYTIC ACTIVITY

Kırbaş, Tuğçe
M.S., Department of Chemical Engineering
Supervisor : Prof. Dr. Gürkan Karakaş

September 2014, 139 pages

In this study, CNT-TiO_2-SiO_2 nanocomposites were synthesized by sol-gel process and the thin films over glass substrates were fabricated by dip coating method. The effects of CNT addition, heat treatment temperature and atmospheres on the structure and photocatalytic properties were examined. The thin films were prepared with and without carbon nanotubes and the heat treatment was carried out at different temperatures in the range of 300-600^{o}C under air and nitrogen atmosphere. Characterization of the samples was performed by thermal analysis, XRD, SEM&EDS, elemental carbon analysis, XPS and UV-Vis spectroscopy. Thermal analysis indicated that the oxidation temperature of carbon nanotubes was reduced significantly by the presence of TiO_2-SiO_2 and considerable amount of carbon is oxidized under nitrogen atmosphere. XRD studies showed that the crystallinity is enhanced by heat treatment temperature. The SEM images revealed that CNTs were successfully incorporated in thin film structure. Elemental carbon analysis was performed to obtain the residual carbon amount after heat treatment. The results were consistent with thermal analysis and showed that quantity of carbon is decreasing with increasing temperature under both air and nitrogen atmospheres. UV-Vis Spectroscopy indicated the photoabsorption edge of thin films is at UV region which is in agreement with titania. XPS studies showed that the reduction of Ti^{4+} to Ti^{3+} sites during heat treatment under nitrogen flow and these oxygen vacancies over the surface are known as effective sites for photocatalysis. The photocatalytic activity tests were performed by monitoring the degradation of metyhylene blue under UV irradiation in the presence of the thin film. The CNT-added samples have higher photocatalytic activity than the TiO_2-SiO_2 sample. And also higher heat treatment temperatures favor the photocatalytic activity until the sintering. The most photocatalycally active sample is found as the CNT-TiO_2-SiO_2 thin film that was heat treated at 500^{o}C under air atmosphere.

Keywords: Titanium dioxide, silica, carbon nanotubes, photocatalysis, thin film

ÖZ

KNT-TİTANYA-SİLİKA NANOKOMPOZİT İNCE FİLMLERİN SENTEZİ: ISIL İŞLEMİN FOTOKATALİTİK AKTİVİTEYE ETKİSİ

Kırbaş, Tuğçe
Yüksek Lisans, Kimya Mühendisliği Bölümü
Tez Yöneticisi : Prof.Dr.Gürkan Karakaş

Eylül 2014, 139 sayfa

Bu çalışmada, KNT-TiO_2-SiO_2 nanokompoziti sol-jel prosesi ile üretilmiş ve daldırma metodu ile cam yüzeyinde ince film üretilmiştir. Karbon eklenmesi, ısıl işlem sıcaklığı ve ısıl işlem atmosferinin ince film yapısına ve fotokatalitik özelliklerine etkisi incelenmiştir. İnce filmler karbon nanotüp eklenerek ve eklenmeden hazırlanmış ve hava ve azot ortamlarında 300-600^oC aralığında farklı sıcaklıklarda ısıl işleme tabii tutulmuştur. Örneklerin karakterizasyonu, ısıl analiz, XRD, SEM&EDS, elemental karbon analizi, XPS ve UV-Görünür bölge spektroskopisi kullanılarak gerçekleştirilmiştir. Isıl analiz sonucunda, TiO_2-SiO_2 varlığının karbon nanotüplerin oksitlenme sıcaklığını anlamlı miktarda düşürdüğü ve azot altında ısıl işlem sonucu kayda değer miktarda karbonun oksitlendiği görülmüştür. Isıl işlem sıcaklığı arttıkça kristallenmenin arttığı XRD analizi kullanılarak gözlenmiştir. SEM görüntüleri karbon nanotüplerin başarılı bir şekilde film yapısına yerleştiğini göstermiştir. Elementel karbon analizi, ısıl işlemin ardından filmde kalan karbon miktarını bulmak için yapılmıştır. Sonuçlar ısıl analiz ile uyumlu olmakla beraber karbon nanotüp miktarının her iki atmosferde ısıl işlem sıcaklığı ile azaldığını göstermiştir. UV-Görünür bölge spektroskopisi örneklerin ışık absorpsiyon sınırının UV bölgesinde olduğunu ve titanyum dioksit ile uyumlu olduğunu göstermiştir. XPS çalışmaları, azot altında ısıl işlem süresince Ti^{4+}’nın Ti^{3+}’ya indirgendiğini ve ince film yüzeyinde, fotokatalitik aktivite için önemli olduğu bilinen oksijen boşlukları olduğunu göstermiştir. Fotokatalitik aktivite testleri, UV ışınlaması altında ince filmlerin metilen mavisini bozmasını gözlemleyerek gerçekleştirilmiştir. Karbon nanotüp eklenmiş örneğin eklenmemiş olandan daha aktif olduğu bulunmuştur. Ayrıca ısıl işlem sıcaklığının artmasının, sinterleşme olana dek, fotokatalitik aktiviteyi arttırdığı gözlenmiştir. Fotokatalitik olarak en aktif örneğin KNT-TiO_2-SiO_2 ile hazırlanan ve hava ortamında $500^{o}C$’de ısıl işleme tabi tutulan ince film olduğu bulunmuştur.

Anahtar kelimeler: Titanyum dioksit, silisyum dioksit, karbon nanotüp, fotokataliz, ince film

To my family

ACKNOWLEDGEMENTS

First I would like to express my deep gratitude to my supervisor Prof.Dr. Gürkan Karakaş for his academic guidance and valuable support throughout my studies. Also I want to thank him for encouragement and his motivating speeches when I am confused.

I should thank METU Central Laboratory for their help with characterization studies. I would like to thank my labmates Merve Çınar Akkuş for her friendship and patience, Cemre Avşar for her enjoyable conversations and nice hospitableness and Emre Yılmaz for his collaborative, motivating and friendly manner furthermore he answers my all questions forebearingly. I also thank to rest of my friends from METU Chemical Engineering Department, especially, Gence Taşdemir, Tülay Bursalı, Özgen Yalçın, Seval Gündüz and S.Gökçe Avcıoğlu for their valuble friendship. I am also thankful to my housemate, classmate and fellow traveller Burçin İkizer for her support, enjoyable moments and delicious foods.

I would like to express my deepest gratitude to my lovely friends Seval Cankurt, S.Deniz Coşkun and Fulya Özsan who always stand by me. Also I want to extend my thanks to my friends from the 7th Art Cinema and Photography Community for their help to change my perspective on life.

I am especially grateful to my fellow sufferer Yasemin Sönmez for her invaluable friendship, heartfelt understanding and helpful contributions while writing the thesis.

I owe a big thank to my parents Hayat and Aydemir Kırbaş for their endless love, encouragement, moral and material support during my studies. Also I would like to thank my sympathetic brother Çağrı Kırbaş for his great fellowship and sense of humor.

Finally, I want to express my heartfelt thanks to Onur who always stands by me with an eternal friendship, great support, encouragement and deep love.

TABLE OF CONTENTS

CHAPTERS

LIST OF TABLES

TABLES

LIST OF FIGURES

FIGURES

LIST OF ABBREVIATIONS

CNT	Carbon nanotube
DTA	Differential Thermal Analysis
EDS	Energy Dispersive X-Ray Spectroscopy
KOH	Potassium Hydroxide
METU	Middle East Technical University
SEM	Scanning Electron Microscopy
SiO_2	Silicon dioxide
TGA	Thermogravimetric Analysis
TiO_2	Titanium dioxide
TTIP	Titanium tetraisopropoxide
UV-Vis	Ultraviolet-Visible Spectroscopy
XRD	X-Ray Diffraction
XPS	X-Ray Photoelectron Spectroscopy

CHAPTER 1

INTRODUCTION

Photocatalysis is a useful method for the removal of the pollutants from air and water. Photocatalysis is a photochemical reaction which uses a photocatalyst. The main advantage of the photocatalysis is the capability of reduction and oxidation reactions at room temperature. TiO_2 is the most widely used photocatalyst because of its unique photocatalytic properties such as oxidative strength, photostability and redox selectivity [1].

TiO_2 is a metal oxide semiconductor that has a wide usage area varies from color industry to electronics, new generation materials and catalyst area. The nontoxicity, long stability and low cost make titania available for the present and future studies. The photocatalytic studies were accelerated with the work from Fujishima and Honda in 1972 [2].

The photocatalytic activity of titania depends on many factors such as crystallinity, crystalline phase, grain size and surface area. Titanium dioxide have three crystalline phases; anatase, rutile and brookite. The rutile is the most stable phase whereas anatase phase is metastable and brookite is rare phase. Although there are some contradictory results in literature, anatase is known more photocatalytically active than rutile phase which is formed by heat treatment by phase transition. The titania as prepared by sol-gel synthesis has an amorphous structure, which has no significant photocatalytic activity and it requires heat treatment process for crystallinity. Thus for high photocatalytic activity, the heat treatment must be carried out carefully to obtain desired phase composition by avoiding the phase transition.

The photocatalytic activity can be also enhanced by particle size, surface area, doping, noble metal loading or sensitizing. In this study, another metal oxide, silica was used as a support. SiO_2 is an amorphous material having very large surface area which can be synthesized by sol-gel method easily. SiO_2 may lead a shift the transition temperature of anatase to rutile toward higher temperature which provide the thermal stability to titania. Besides the crystallite size of titania is decreased due to the inhibition effect of silica on the growth of titania particles. The small particles contribute the higher surface area which enhances the photocatalytic activity [3]. In addition, the interface between TiO_2 and SiO_2 is known to enhance the photocatalytic activity of TiO_2. Significant number of work assigns Ti-O-Si sites as active sites for adsorption and photochemical reactions.

The synergetic effect of titania-carbon nanotube combination is a novel topic in photocatalysis due to their promising applications. Carbon nanotubes were added the mixed oxide matrix and the effect of CNTs on photocatalytic activity was investigated. The addition of carbon nanotubes improves surface area, dispersion of TiO_2 particles and density of active sites of titania. Also the rate of recombination of photogenerated electron-hole pair is decreased which results higher photocatalytic activity [4].

The application of photocatalysts as films has some advantages for the removal of pollutant in aqueous medium over the photocatalysts in powder form. The photocatalyst in powder form can decrease the degradation time compared to thin films because of larger catalyst to volume ratio but there are some problems in practice; difficulties in separation of the powder photocatalyst from the suspension, aggregation of photocatalyst particles at higher catalyst loading, impropriety for continuous flow systems. To overcome this problem, the photocatalyst should be applied as thin film which coated on support surfaces where the photocatalyst particles immobilized. The support must be transparent to the irradiation, have strong bond with photocatalyst and inert [5,6].

In this study, the CNT-TiO_2-SiO_2 nanocomposites were synthesized by sol-gel method and the thin films were fabricated over glass substrates by dip coating. Sol-gel technique allows the production of a variety of inorganic networks which can be formed from metal alkoxide solutions. Homogeneous composite mixtures can be prepared at ambient temperature by sol-gel [7]. The sol-gel process is compatible by spin, spray and dip coating methods which are more preferable over expensive vacuum deposition and sputtering techniques.

CHAPTER 2

LITERATURE REVIEW

2.1 Semiconductors

Semiconductor materials have electrical conductivity between conductors and insulators. The electrical conductivity of semiconductor materials depends on the movement of the electrons and holes within lattice.

The highest energy electrons fill the lower energy band, which is valance band while the upper energy band which is called conduction band is empty. The energy difference between valence band and conduction band is defined as band gap energy. The band gap energy of the materials is characteristic which is minimum required energy for the transition of an electron from the valence band to the conduction band. Electrons which can be excited by absorbing heat or light, leave holes at the valence band while jumping to the conduction band. The band gap energy determines the electrical conductivity of the materials. For conductors, electrons can move easily from one band to another due to the overlap of valance band and conduction band. On the other hand, insulators have a large band gap which prevents the formation of electron-hole pairs. Semiconductors have narrower band gap than the insulators so the electrons could be excited by absorbance of energetic photons UV-Vis radiation (Figure 2.1) [1,8]. The band gap energies of widely used semiconductors are tabulated in Table 2.1.

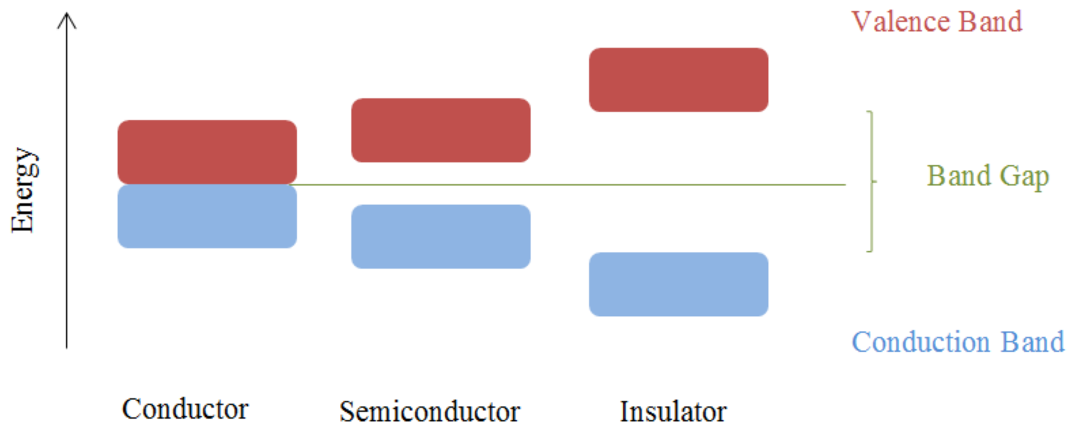

Figure 2.1 Band structures of conductors, semiconductors and insulators [3]

Table 2.1 Band gap energies of various semiconductors [3]

Semiconductor	Band Gap Energy (eV)
TiO_2 (anatase)	3.2
TiO_2 (rutile)	3.0
ZnO	3.2
ZnS	3.6
CdS	2.4
Fe_2O_3	2.3
WO_3	2.8

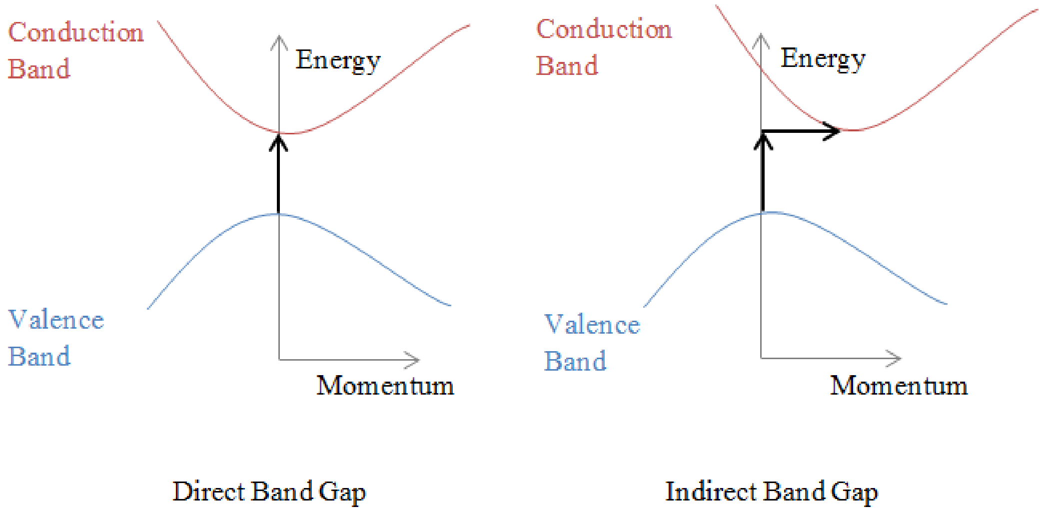

Figure 2.2 Direct and indirect band gap

The band gap is classified as direct band gap and indirect band gap. In a direct band gap semiconductor, the top of the valence band and the bottom of the conduction band are at the same momentum and so the electron and hole share the same momentum. The electrons at the valence band can be excited to the conduction band by absorbing a photon with an energy near the semiconductor band gap. Photons have almost zero momentum and cannot carry crystal momentum thus the maximum of valence band must be near the minimum of the conduction band for the excitation. In an indirect band gap semiconductor, the momentum of the conduction band and valence band is not equal to each other and so there is a difference between the electron and hole momentum. The maximum energy of the valence band occurs at a different value of the momentum to the minimum energy of the conduction band (Figure 2.2). In this case, photon energy is not sufficient for the excitation and so the electron must undergo a change in its momentum to generate an electron-hole pair. The momentum difference between valence and conduction bands supplements by the absorption or emission of a phonon which is a quantized mode of vibration in the crystal lattice. Therefore for an indirect band gap semiconductor, the excitation of the electrons from the valence band to the conduction band needs a couple of photon and phonon that provide the same momentum values for the energy bands.

The rate of formation of electron-hole pair is slower for an indirect band gap semiconductor than for a direct band gap semiconductor because it requires an additional energy for the excitation. The same procedure applies for the recombination of the electrons and holes so the recombination process is much more efficient for a direct band gap semiconductor whereas the process is mediated by a phonon for the indirect band gap. On the other hand, an indirect band gap semiconductor favors the photocatalytic activity due to the slow rate of the recombination of the electrons and holes.

As a semiconductor, titanium dioxide attracts great interest especially in photocatalysis due to its physical and chemical stability, low cost and nontoxicity. It is widely used in environmental processes as a photocatalyst for oxidation reactions of organic compound, in splitting water for hydrogen production, in photovoltaic cells and etc.

2.2 Titanium Dioxide (TiO_2)

Titanium dioxide is widely used as a photocatalyst in a variety of applications, including self-cleaning surfaces, air and water purification systems, sterilization and photoelectrochemical conversion. It has been the most widely studied material because of nontoxicity, low cost, chemical stability, long durability, transparency to visible light, superhydrophilicity and its strong oxidizing abilities for the decomposition of organic pollutants [9].

Titanium dioxide occurs in three crystalline phases as anatase, rutile and brookite. The crystal structures and some physical properties for these phases of titania are shown in Figure 2.3 and Table2.2, respectively. The unit cell type for anatase and rutile is tetragonal and for brookite is orthorhombic [10]. Both anatase and rutile phases are applied in photocatalytic reactions but the anatase is the more photocatalically active phase which is especially in the photodegradation of organic pollutants. Rutile is the most stable phase and anatase and brookite can transform to rutile when heated. Brookite is a rare phase that it is difficult to prepare the pure brookite without rutile or anatase even if at low calcination temperatures [10-12].

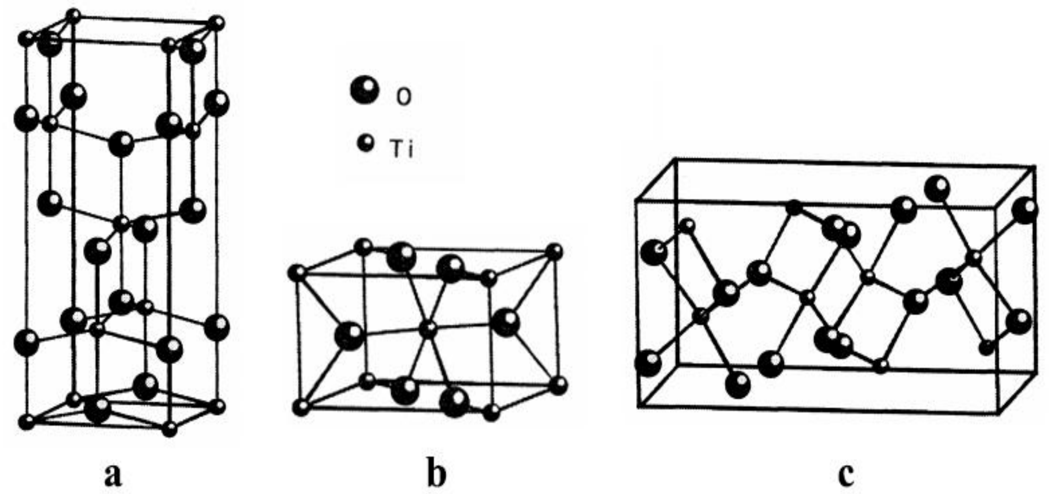

Figure 2.3 Crystal structures of titanium dioxide a) Anatase b) Rutile c) Brookite[10]

Table 2.2 Physical Properties of Anatase, Rutile and Brookite [10]

	Anatase	Rutile	Brookite
Crystal Structure	Tetragonal	tetragonal	orthorhombic
Lattice Constants	a=3.784	a=4.5936	a=9.184
	c=9.515	c=2.9587	b=5.447
			c=5.1445
Space Group	$I4_1$/amd	$P4_2$/mnm	Pbca
Molecule/cell	4	2	8
Volume/molecule(Å^3)	34.061	31.216	32.172
Density(g/cm^3)	3.79	4.13	3.99
Ti─O bond length(Å)	1.937(4)	1.949(4)	1.87-2.04
	1.965(2)	1.98(2)	
O─Ti─O bond angle	77.7°	81.2°	
	92.6°	90.0°	77.0°-105°

The band gap energies of bulk anatase and bulk rutile have been reported as 3.2 eV and 3.0 eV, respectively [10-15]. Both phases have significant photocatalytic activity but in most of the cases, the anatase has greater activity in spite of the higher band gap than rutile. It has been reported in many studies that anatase has an indirect band gap while rutile has a direct band gap [10,14]. Also anatase has wider optical absorption gap and smaller electron effective mass than rutile. It provides anatase with higher mobility for the charge carriers which means higher photocatalytic activity[13]. The rate of recombination of electron-hole can be reduced by the indirect band gap and so this leads to higher photocatalytic activity. There is a variety of reasons, such as crystal size, surface area, surface defects and porosity which affect the rate of recombination of the electrons and holes. The photocatalytic activity can change significantly due to the difference in these properties. Another reason for the higher photocatalytic activity of anatase can be the higher Fermi level of anatase than rutile by about 0.1eV. This provides anatase with a lower oxygen adsorption capacity and a higher level of hydroxyl groups on the surface which are very important for the photocatalytic activity.

2.3 Photocatalysis

Photocatalysis is widely applied method on self cleaning surfaces, antibacterial surfaces, decomposition of volatile organic compounds, water purification and water splitting. Among many materials for photocatalysis, titanium dioxide is close to being an ideal one for industrial use because of its availability and non-toxicicty. The lower cost, higher stability and the strength of the oxidizing are the main advantages of titanium dioxide over other semiconductor metal oxides [16].

According to the band model, an electron in an electron-filled valence band can be excited to a vacant conduction band by force of photoirradiation. The conduction band is separated by a forbidden band, a band gap from the valence band and an electron leaves a hole in the valence band while jumping over the band gap. The generated electrons and holes lead the reduction and oxidation reactions of the adsorbates on the surface of the photocatalyst [17].

The ability of adsorption of reactants which can be oxidized and reduced is important for a photocatalyst among with absorbing light efficiently. Also another important factor is the ability to transfer electrons between the bands of the semiconductor and the adsorbed compound which is controlled by the band gap energy position of the semiconductor and the redox potentials of the adsorbed particles. For the acceptor adsorbate, the redox potential should be below the conduction band of the semiconductor. For the donor adsorbate, the potential level should be above the valence band in order to give an electron to the hole in the valence band. The transfer of electrons from semiconductor to the acceptor adsorbate is called the reduction reaction and the transfer of electrons from the donor adsorbate to the semiconductor is called oxidation reaction. The mechanism of these reactions on the photocatalyst is showed in Figure 2.4.

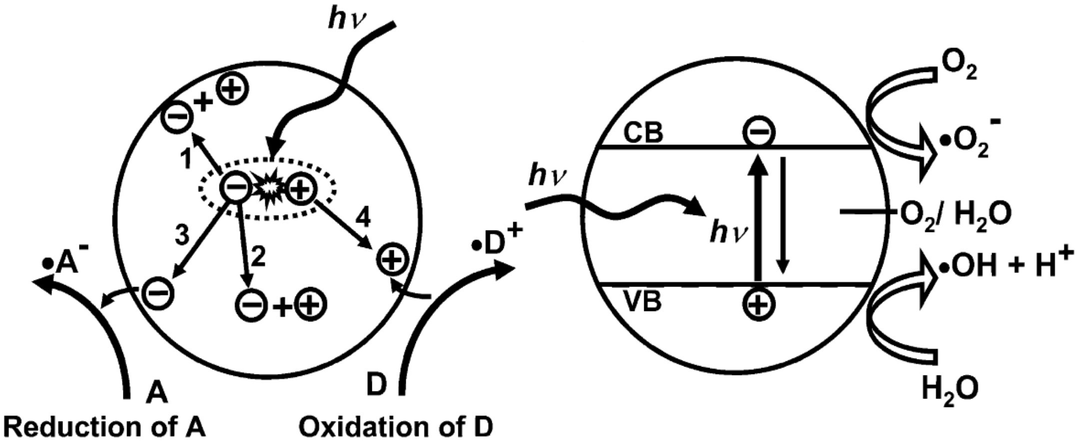

Figure 2.4 The mechanism of photocatalysis on a semiconductor particle [13]

In Figure 2.4, the main processes occurring on a semiconductor are represented. On the left particle, absorption of the photon, the formation of electron-hole pair and the migration of electron-hole are depicted. The recombination of electron-hole at the surface and bulk is showed with the arrows marked (1) and (2), respectively. The arrow marked (3) shows the reduction of acceptor and (4) shows the oxidation of donor. On the right particle, the electrons at the valence band are excited to the conduction band by absorption of a photon with energy of hυ. The excited electron is transferred to oxygen molecule to generate superoxide ion radical ($\bullet O_2^-$) and the electron is transferred from water molecule to the hole in the valence band in order to form hydroxyl radical (•OH) [13].

2.3.1 The steps of photocatalytic reactions of TiO_2

The photocatalysis mechanism of titanium dioxide is listed below step by step.

a) The first step of heterogeneous photocatalytic reactions is the formation of electron-hole pair when TiO_2 absorbs photons which have higher energy than the band gap of energy.

$$TiO_2 + \text{photon } (h\upsilon) \rightarrow TiO_2\ (h^+ + e^-)$$

b) The generated holes react with the electron from the donor adsorbate (RX_{ads}) e.g. surface hydroxyl groups;

$$h^+ + RX_{ads} \rightarrow RX^+_{ads}$$

$$h^+ + H_2O_{ads} \rightarrow \bullet OH_{ads} + H^+$$

$$h^+ + OH^-_{ads} \rightarrow \bullet OH_{ads}$$

c) The generated electrons is transferred to the adsorbed electron acceptor e.g. molecular oxygen;

$$O_{ads} + e^- \rightarrow O^-_{ads}$$

$$e^- + O_2 \rightarrow O_2^-$$

The second and third steps which are electron transfer reactions are the most important ones because the major oxidant radicals form in these steps.

d) The superoxide anion can continue to the reaction in aqueous phase and yield hydrogen peroxide which is highly oxidative compound.
Photoconversion of hydrogen peroxide also gives hydroxyl radical (•OH)

$$H^+ + O_2^- \rightarrow \bullet HO_2$$

$$H^+ + O_2^- + \bullet HO_2 \rightarrow H_2O_2 + O_2$$

$$H_2O_2 + h\upsilon \rightarrow 2\ \bullet OH_{ads}$$

For the oxidation of adsorbed organic contaminants, the hydroxyl radicals and superoxide anions are very active species. The organic compounds are oxidized by these radicals along with the reduction reactions and the chain reaction which initiated by the photoabsorption ends up.

The recombination of electron and hole may occur before the transfer to the surface of the particle due to some lattice defects, impurities and imperfections. Also the absence of electron scavengers (O_2 and H_2O) can cause the recombination of electron and hole instead of photocatalytic chain reactions. So the recombination of electron and hole decreases the activity of the photocatalyst. The photocatalytic efficiency (quantum efficiency) is defined by the ratio of the number of free radicals produced to the number photons used in the reaction [18]. Titanium dioxide has efficiency less than 10% because of large band gap and high recombination rate of charge carriers. Also photon energy of above 3.2 eV which denotes the wavelength 388nm is required to excite the titanium dioxide. For excitation, UV light can be used which has a high energy light with a wavelength range between 100-400 nm. However, the content of ultraviolet light in ambient light or solar radiation is less than 5% and brings an important limitation to the use of TiO_2 as photocatalyst [17].

In order to decompose the pollutants or contaminants over the surface photocatalically, the species (subject and precursor of the radicals) must be adsorbed on the surface of the photocatalyst. Thus the adsorption capacity which denotes high surface area and porosity should be considered for better activity. Otherwise the reduction and oxidation reaction cannot occur and excited electrons recombine with holes. On the other hand, the high surface area alone is not sufficient for higher photocatalytic activity. The crystallinity is also an important factor to affect the activity. Despite of the high surface area of some amorphous materials, these materials cannot show photocatalytic activity due to enormous charge recombination rate. In order to improve the crystallinity, heat treatment process is needed for photocatalysts. Heat treatment supplies an ordered crystal structure. Nevertheless, heat treatment at high temperatures can cause sintering in the photocatalyst and so less surface area. Besides for titanium dioxide, high heat treatment temperature and long heat treatment duration result a phase transition from anatase to rutile which can decrease the photocatalytic activity [19].

2.3.2 Improving the photocatalytic activity of TiO_2

The photocatalytic activity of titanium dioxide can be improved by modifying its electronic structure. There are several methods for the modification which includes doping the titanium dioxide with metals (W, V, Ce, Zr, Fe), oxides (ZnO, WO_3, SiO_2, CrO_3) and non-metals (C, N, S, P, F), sensitizing with dye and metal complexes and loading noble metals.

In doping method, dopants act as traps for the photogenerated electrons and holes and reduce the electron-hole recombination rate. Also the photoabsorption capacity of titanium dioxide can be increased by doping. Doping may lead to a decrease in the band gap energy of titanium dioxide and so a shift in adsorption edge to visible light.

Sensitization is a method that makes the titanium dioxide more sensitive to less energetic light with a sensitizing material which can be excited by less energetic photon than TiO_2. The sensitized titanium dioxide has a lower absorption edge than pure titanium dioxide due to the injection of electrons from an excited level of the sensitizing material into the conduction band of semiconductor.

Noble metal loading can enhance the photocatalytic activity of titanium dioxide due to their low Fermi levels. The excited electrons at the conduction band can be transferred to the loaded metal particle which decreases the electron-hole recombination rate.

2.3.2.1 The effect of SiO_2 on the photocatalytic activity of TiO_2

The photocatalytic activity of titania can be improved by the addition of silica which provides higher surface area with good adsorption capacity and thermal stability with higher crystallinity, also good transmission of UV light [20].

The addition of silica may reduce the particle size of titania and so increase the surface area by the formation of Si-O-Ti bonding which inhibits the growth of TiO_2 particles. Also small particle size decreases the electron-hole recombination probability and diffusion pathway which increase the accessibility of photons to the lattice [21]. The crystalline structure is another important factor for the photocatalytic activity. To obtain highly crystalline titania, it is required high heat treatment temperature. Anatase phase shows more photocatalytic activity than the others but anatase can easily transform into rutile at 500^oC due to its low thermal stability. Moreover the phase transition of anatase to rutile at high temperatures can cause a decrease in surface area which also decreases the photocatalytic activity of titania. The addition of silica is a solution to provide anatase with thermal stability which prevents the transformation of anatase to rutile even at high temperatures. Also it is reported that the presence of the silica increases the amount of the hydroxyl groups over the titania surface [20,22]. The improvements of silica on titania is affected from the ratio of SiO_2 to TiO_2 and the ideal ratio was reported about 0.5 by molar [23].

2.3.2.2 The effect of CNT on the photocatalytic activity of TiO_2

Carbon nanotubes have specific adsorption and electronic properties due to their peculiar morphology, the role of defects, the probability of opening or closing of the tubes. There is a synergetic interaction between CNT and metal oxides due to their intrinsic properties. The photocatalytic activity of carbon nanotube-titania composites has become an attractive topic in photocatalysis, because of their combination of electronic, adsorption mechanical and thermal properties [4]. Carbon nanotubes can provide high surface area, retardation of electron-hole recombination and new active sites for adsorption and reaction [24]. Beyond surface area, carbon nanotubes can be modified towards adsorbents of their surface groups. Carbon nanotubes formed alcohol, keto and acid moieties on their surfaces if they are treated by acids. To improve the adsorption of specific species, these groups can be tailored.

There are different mechanisms for the enhancement of the photocatalytic properties. First, CNT acts as a trap for photogenerated electrons. An electron is excited with a high energy photon and jumps to the conduction band. This electron is transferred into the CNTs and holes remain on the TiO_2 for redox reactions. Second, CNT acts as a sensitizer and transfer electrons to the TiO_2. The photogenerated electron is transferred to the conduction band and then formation of superoxide radicals by adsorbed molecular oxygen occurs. The positively charged nanotubes transfer an electron from the valence band of titania leaving a hole. Lastly, the hole can react with adsorbed water to generate hydroxyl radicals. The formation of carbon-oxygen titanium bond which extends the absorption edge to longer wavelengths may be another possibility for the enhancement of the photocatalytic activity by carbon nanotubes [25].

The CNT-TiO_2 nanocomposites might be obtained by simple mixing of titania and CNT, thermal oxidation of Ti metal, sol-gel from titanium alkoxides, hydrothermal synthesis, PVD, CVD and electrophoretic deposition. Among them, the most widely used method is sol-gel technique [24].

2.4 Synthesis of Thin Films

Thin films are applied to the surfaces of glasses, ceramic tiles, steel bars due to their mechanical strength. Thus the coated surfaces may exhibit advanced new properties such as self-cleaning, hydrophobicity, anti-reflectance etc. To fabricate thin films, sol-gel technique has several advantages which allow the use of wet coating techniques such as spray, spin and dip coating methods. Also sol-gel method can be applied for large surfaces to produce high quality glasses. Moreover it is one of the successful methods to synthesize the photocatalytic nanoparticles [26]. Sol-gel method allows the production of hybrid materials by using different substrates. The final product is homogeneous and at high purity. The reaction occurs at room temperature and the kinetic of reaction, the particle size and shape can be controlled easily. The wet process prevents the inhalation of hazardous dusts. On the other hand, the precursors may be expensive and health hazardous. Also loss of the chemicals used in sol-gel is high due to the long processing time.

2.4.1 Sol-Gel Process

Sol-gel synthesis is a process which defined as the formation of a colloidal suspension (sol) followed by hydrolysis and polimerisation of the precursor which are the usually inorganic metallic salts or metal alkoxides. The three main steps of sol-gel synthesis are hydrolysis, alcohol condensation and water condensation (Figure 2.5). There are a lot of factors that have an influence on the hydrolysis and condensation like pH, concentration of catalyst, water/alkoxide ratio and temperature [27].

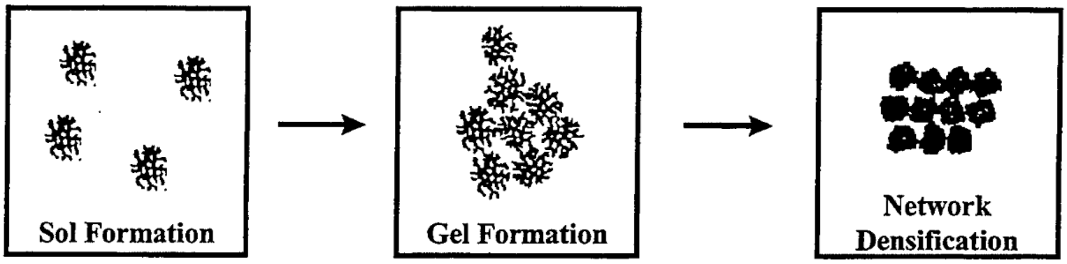

Figure 2.5 Process scheme of sol-gel synthesis [28]

In sol-gel synthesis of metal alkoxides, the ractions of hydrolysis and condensations take place rapidly. For titania, titanium isopropoxide and titanium butoxide are the most commonly used precursors in the sol-gel synthesis. The mechanism of the hydrolysis reaction between the precursor and water is decribed as following [1].

$Ti(OR)_n + xH_2O \rightarrow Ti(OH)_x(OR)_{n-x} + xROH$

The hydrolysis reaction continues up to the formation of $Ti(OH)_n$ and then polymerization reactions start which are condensation dehydration and dealcoholation, respectively.

$Ti(OR)_n + Ti(OR)_{n-1}(OH) \rightarrow Ti_2O(OR)_{2n-2} + ROH$

$2Ti(OR)_{n-1}(OH) \rightarrow Ti_2O(OR)_{2n-2} + H_2O$

The overall reaction is

$Ti(OR)_n + n/2\ H_2O \rightarrow TiO_{n/2} + nROH$

The particles come together into a compact form as a result of condensation reactions and the metal oxide crystals form. After the hydrolysis and condensation reactions, the next step is gelation which obtains the final product structure. Along with the formation of gel, the shrinkages and porous structure occur since the network loses water and alcohol.

The type of titania precursor and chemical matrix in the sol-gel system are the main parameters that affects the morphology of the synthesized TiO_2. Also aging time and conditions have an impact on the structure of the particles since the condensation reaction continues and so further links are formed during aging. In addition higher surface area and porous structure can be obtained by long aging time. Moreover drying time can affect the pore structure. Fast drying can break down the cross-links due to the high pressures in the pores during the evaporating of water, alcohol and other volatile compounds in the sol-gel matrix.

2.4.1 Dip coating

For sol-gel process, there are several method for the preparation of thin films which are dipping, spinning are spraying. Dip coating has some advantages over the others such as high transfer efficiency, good contact between sol and substrate, ability for multi-layer coating, no limit for the shape of substrate and simple equipment [28].

In dip coating process, the substrate is immersed into the coating solution carefully with a constant rate. The substrate is kept in the solution for a while and then withdrawn without any vibration with a constant rate which is really slow to deposit the thin layer on the substrate. The excess liquid drains from the surface and the thin film is formed by the evaporation of the solvent (Figure 2.6). The constant velocity for dipping and pulling up is important to obtain uniform thin film coating. Also the viscosity and surface tension of the coating solution, evaporation rate affect the formation of the film [29].

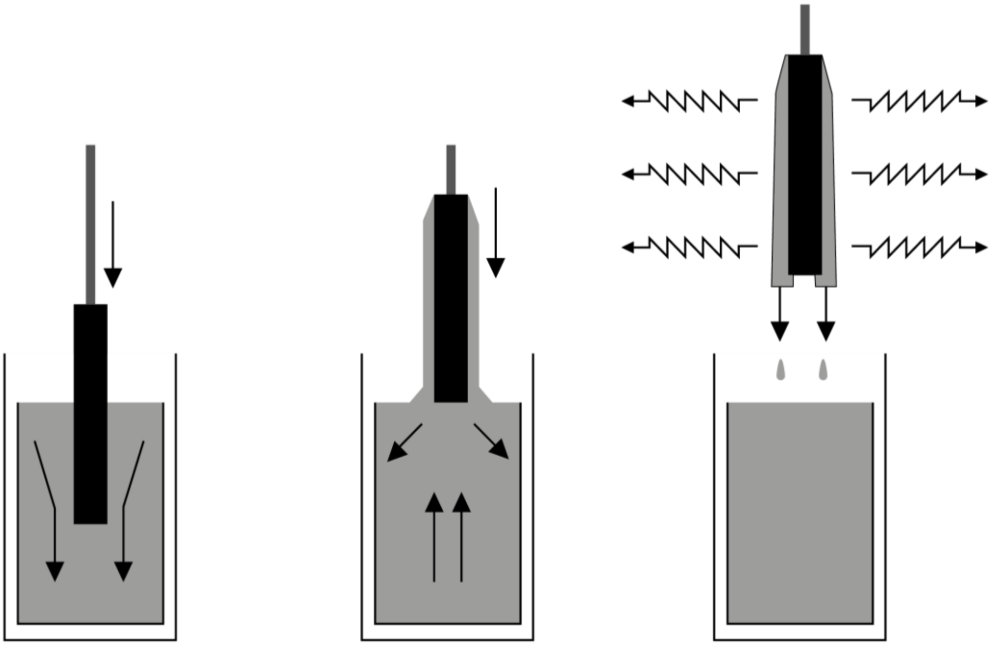

Figure 2.6 Dip coating process [29]

2.4.3 Thermal Treatment

The thermal treatment of the synthesized thin films is required for the phase transition from amorphous to the crystalline phase after drying. Generally, calcination is applied as a thermal treatment which made under an oxidizing atmosphere. Calcination process lead the burning out of the organic compounds and forming ordered crystal structure by diffusing of the inorganic species.

The photocatalytic activity of titania is significantly affected by the structural properties such as crystallinity, crystalline phase, particle size, surface area, pore size and distribution [9]. Calcination time and temperature have a strong effect on these properties. Short calcination duration and/or low calcination temperature cause low crystallinity while the long calcination time and/or high calcination temperature result in formation of rutile and sintering which decrease the surface area and so photocatalytic activity of titania. Also the phase transition of anatase to rutile is influenced by oxygen defects that created by the heat treatment temperature and atmosphere, redox reactions and dopants [30].

CHAPTER 3

EXPERIMENTAL

In this study, TiO_2-SiO_2 and CNT-TiO_2-SiO_2 thin films over glass substrates were synthesized with a colloidal solution by dip coating. The fabricated thin films were heat treated at different temperatures under air and nitrogen atmosphere. The coating solutions and carbon nanotubes were analyzed by TGA and DTA. The characterization of the thin films was carried out by thermal analyses, XRD, SEM, EDS, elemental carbon analysis, XPS and UV-Vis spectroscopy. The photocatalytic activity of the thin films was examined by the methylene blue degradation test.

3.1 Preparation of Thin Films Samples

3.1.1 Materials

The glass substrate and the chemicals used for the pretreatment of substrates and the synthesis of coating solution are listed as:

- Microscope slides by ISOLAB
- Titanium (IV) isopropoxide [TTIP, $C_{12}H_{28}O_4Ti$, 97%] by Aldrich (CAS number: 546-68-9)
- Acetic acid [Glacial acetic acid, CH_3CO_2H, 99.8-100.5%] by Sigma-Aldrich (CAS Number: 64-19-7)
- LUDOX SM-30 colloidal silica [SiO_2, 30 wt. % suspension in H_2O] by Aldrich (CAS Number: 7631-86-9)

- Carbon nanotube [NANOCYL^{TM} NC7000 series, thin multi-wall carbon nanotubes] by Nanocyl
- 2-Propanol [Isopropanol, C_3H_8O, >99.5%] by Sigma-Aldrich (CAS Number: 67-63-0)
- Ethanol [Ethyl alcohol, C_2H_6O, >99.8%] by Sigma-Aldrich (CAS Number: 64-17-5)

3.1.2 Pretreatment of Glass Substrates Materials

Microscope slides with a dimension 26 mm x 76 mm x 1 mm were used as soda-lime glass substrates. The substrates were washed with distilled water and then immersed into 1.0 N KOH solution for 48 hours in order to improve the wetting properties. After etching process with KOH, the substrates were rinsed with distilled water till pH 7 and subsequently ultrasonicated in ethanol for 1 hour. Then the substrates were rinsed with distilled water again and finally dried at 100^{o}C for 1 hour.

3.1.3. Synthesis of Sol-Gel Solution

The sol-gel method was applied to prepare the coating solution. The titania nanoparticles can be synthesized as follows [32]: 30 ml Ti (IV) of isopropoxide were added into 60 ml of glacial acetic acid by drop wise while continuous stirring. After 10 minute stirring, 30 ml of deionized water was added very slowly in the mixture. The reaction of this process is:

$$Ti(OCH(CH_3)_2)_4 + 2H_2O \rightarrow TiO_2+4(CH_3)_2CHOH$$

During the addition of water, white precipitates form which disappears by stirring overnight. The final clear solution was stored at room temperature for hydrolysis.

In order to prepare the titania-silica mixed oxide nanoparticles, LUDOX was used as silica precursor. The molar TiO_2/SiO_2 ratio was selected as 0.5 and the amount of water in silica suspension for this ratio was calculated. Then the recipe of sol-gel was revised as 21.7 ml of deionized water and 8.3 ml of LUDOX instead of 30 ml of deionized water. After this point, the mixture is called TiO_2-SiO_2 and the thin films that synthesized from this mixture are called TiO_2-SiO_2 thin films. The TiO_2-SiO_2 mixture was mixed with carbon nanotubes and then called CNT-TiO_2-SiO_2 also the thin films that synthesized from this mixture are called CNT-TiO_2-SiO_2 thin films. In order to prepare the coating solution for CNT-TiO_2-SiO_2 thin films, 50 ml of TiO_2-SiO_2 clear solution were taken and the carbon nanotubes were added into this solution with a ratio as 5% by weight. The mixture after CNT addition was ultrasonicated for 5 min at a period with 2 s pulse and 2 s standby in order to prevent the aggregations of carbon nanotubes. Also the mixture without carbon nanotubes was ultrasonicated in the same way to obtain same properties for the mixture. The sonication process was performed by SONICS 500W Vibracell with 35% amplitude. Both of two mixtures, TiO_2-SiO_2 and CNT-TiO_2-SiO_2 were kept in a plastic beaker for gelation.

3.1.4 Preparation of Thin Film Samples

The TiO_2-SiO_2 and CNT-TiO_2-SiO_2 thin films were obtained from the prepared sol-gel solution over the pretreated glass substrates by using dip coating technique. The glass substrates were immersed into the solution with a speed of 20 mm/s and withdrawn with a speed of 2 mm/s. After the drying at 100^{o}C for 15 min, the coated samples were heat treated in preheated tubular furnace (Protherm 1000W, PTF 12/50/250) under air or nitrogen atmosphere. The heat treatment was carried out at 300^{o}C, 400^{o}C, 500^{o}C and 600^{o}C under each atmosphere for 20 min.

The thin films are entitled according to composition, heat treatment atmosphere and temperature as shown in Table 3.3. The label of “T” points to the thin films which were synthesized by the TiO_2-SiO_2 mixture, and the label of “C” points to the thin films which were synthesized by the CNT-TiO_2-SiO_2 mixture. The label “A” shows the heat treatment atmosphere as air, and “N” shows as nitrogen. The numbers in the labels indicate the heat treatment temperature. In addition the thin films used in analyses as prepared (without heat treatment) labelled with “nonHT”.

Table 3.3 The codes of samples

Composition of Sol-Gel	Heat Treatment Atmosphere	Heat Treatment Temperature (^oC)	Sample Code
TiO_2-SiO_2	AIR	300	T-A300
TiO_2-SiO_2	AIR	400	T-A400
TiO_2-SiO_2	AIR	500	T-A500
TiO_2-SiO_2	AIR	600	T-A600
TiO_2-SiO_2	N_2	300	T-N300
TiO_2-SiO_2	N_2	400	T-N400
TiO_2-SiO_2	N_2	500	T-N500
TiO_2-SiO_2	N_2	600	T-N600
TiO_2-SiO_2	-	-	T-nonHT
CNT-TiO_2-SiO_2	AIR	300	C-A300
CNT-TiO_2-SiO_2	AIR	400	C-A400
CNT-TiO_2-SiO_2	AIR	500	C-A500
CNT-TiO_2-SiO_2	AIR	600	C-A600
CNT-TiO_2-SiO_2	N_2	300	C-N300
CNT-TiO_2-SiO_2	N_2	400	C-N400
CNT-TiO_2-SiO_2	N_2	500	C-N500
CNT-TiO_2-SiO_2	N_2	600	C-N600
CNT-TiO_2-SiO_2	-	-	C-nonHT

3.2 Characterization

The prepared thin films were characterized by different techniques to analyze the crystalline structure, surface morphology and surface composition of the thin films.

Also the effects of carbon nanotubes addition, heat treatment temperature and atmosphere on these properties were examined.

3.2.1 Thermal Analysis

Thermogravimetric analysis (TGA) and differential thermal analysis (DTA) were performed with a heating rate as 10^oC/min by Shimadzu DTG-60H Differential Thermal Gravimetric Analyser in METU Chemical Engineering Department. The coating solutions and bare carbon nanotubes were dried at 100^oC and then analyzed between room temperature and 900^oC under air and N_2 flow to investigate the interaction between carbon nanotubes and titania-silica nanoparticles due to heat treatment.

3.2.2 X-Ray Diffraction (XRD)

The crystalline phase of the thin films was examined by X-Ray diffraction analysis (Rigaku Ultima IV diffractometer) in METU Central Laboratory. The XRD analysis of the thin films were performed between 10^o and 90^o 2θ with a grazing angle of 0.5^o by using Cu source which has a wavelength as 0.15405 nm. The standard peaks of compounds were found by using Rigaku PDXL XRD Analysis Software.

3.2.3 Scanning Electron Microscopy (SEM) & Energy Dispersive X-Ray Spectroscopy (EDS)

The surface images of the thin films were obtained with magnitude as 100000x and 200000x and high voltage (30kV) by Quanta 400 F Field Emission Scanning Electron Microscope in METU Central Laboratory. The samples were coated with Au-Pd mixture by spraying to achieve sufficient conductivity and so prevent the electron charging on the surface due to electron beam.

The composition of the thin film surfaces was examined by JEOL JXA-8230 Electron Probe Microanalyzer among with SEM analysis in METU Central Laboratory. The measuring range of the EDS instrument is from B(5) to U(92).

3.2.4 Elemental Carbon Analysis

The amount of residual carbon in the film after heat treatment was analyzed by LECO CHNS-932 Elemental Analyzer in METU Central Laboratory. The synthesized thin films after heat treatment were scraped off from the glass surface carefully by a spatula in order to make the films into powder. The elemental carbon analyses for the samples were repeated two times and the quantity of carbons in films was calculated as the average of two results.

3.2.5 X-Ray Photoelectron Spectroscopy (XPS)

X-ray photoelectron spectroscopy analysis was used to investigate the surface composition of the thin film. The survey scans of the samples and high resolution XPS spectra of Ti 2p, O 1s, C 1s and Si 2p were obtained by Physical Electronics PHI VersaProbe II Scanning XPS Microprobe in METU Central Laboratory. The spectrum of the elements was deconvoluted by using XPSPEAK 4.1 software.

3.2.6 UV-Visible Spectroscopy

The UV-Visible spectra of the thin films were obtained in the wavelengths between 280-800 nm by Shimadzu 2550 UV- Vis spectrophotometer in METU Chemical Engineering Department. The uncoated but pretreated glass substrate was used a reference sample to eliminate the absorptivity of the substrate. In addition the direct and indirect band gap energies of the samples were calculated by using the absorbance data against the incident wavelength.

3.3 Photocatalytic Activity Test

The photocatalytic activity test was based on the methylene blue degradation capacity of the thin films under UV irradiation. The TiO_2-SiO_2 and CNT-TiO_2-SiO_2 thin films were examined in order to reveal the effect of CNT addition, heat treatment atmosphere and temperature on photocatalytic activity. The photocatalytic degradation tests were performed at room temperature in a sterilizer cabinet with a mercury lamp (PHILIPS TUV 15W 1SL-254 nm) as UVC light source. Shimadzu 2550 UV- Vis spectrophotometer is used for the observation of the decrease in methylene blue absorbance by irradiation time. In order to determine the relation between absorbance and concentration of methylene blue, the calibration curve was prepared by using the absorbance data of the methylene blue solutions at different concentration (2,4,6,8 and 10ppm). For photocatalytic activity test, the each thin film were immersed into 10ml of 2ppm methylene blue solution and then irradiated at a distance of 6 cm from the lamp. The methylene blue samples were taken from the irradiated solutions in the presence of thin films every half an hour and their UV-Vis spectra were obtained between 200-800nm. In addition, 10ml of 2ppm methylene blue solution without any thin film sample was irradiated in same way to determine the photodegradation of the dye solution.

CHAPTER 4

RESULTS AND DISCUSSION

In this study, the effect of carbon nanotubes on the photocatalytic activity of TiO_2-SiO_2 nanocomposite thin films have been investigated. The titania solution was prepared by the sol-gel method and the TiO_2-SiO_2 and 5% carbon nanotube containing CNT-TiO_2-SiO_2 thin film samples were fabricated by dip coating. The effect of heat treatment temperature and atmopshere on the crystal structure, textural properties and photocatalytic activity were examined. The heat treatment was applied at 300^{o}C, 400^{o}C, 500^{o}C and 600^{o}C under air and N_2 atmosphere.

4.1 Characterization

The dried coating solutions and bare carbon nanotubes were analyzed by thermal analysis. The thin film samples were characterized XRD, SEM, elemental carbon analysis (CHNSO), XPS and UV-Vis spectroscopy. The effect of heat treatment and CNT addition on the structure was examined by thermal analysis, XRD and elemental carbon analysis. SEM and XPS techniques were applied in order to obtain information about the surface morphology and structure. The optoelectronic properties of the thin films were examined by UV-Vis spectroscopy.

4.1.1 Thermal Analysis of the Coating Solutions and Carbon Nanotubes

The response of the sol-gel synthesized samples and bare carbon nanotubes to heat treatment under air and N_2 atmosphere was examined by thermogravimetric analysis (TGA) and differential thermal analysis (DTA). The thin film coating solutions (TiO_2-SiO_2 and CNT-TiO_2-SiO_2) which prepared by sol-gel method were dried at 100^oC and made into powder for analysis. These powder samples and also bare carbon nanotubes were heated at a ramp of 10^oC/min to 900^oC with 75ml/min air or nitrogen flow rate. The sampling time of thermal analysis is 1s and the weight of samples for air and nitrogen flows is showed in Table 4.4.

Table 4.4 Sample weights for thermal analysis

Powder Sample	**Weight (mg)**	
	AIR	N_2
CNT	1.637	3.141
TiO_2-SiO_2	19.118	16.207
CNT-TiO_2-SiO_2	10.948	10.149

As a first step, the thermal behavior of bare carbon nanotubes was studied. The thermal analysis of CNT under air flow, there is only one peak at 632^oC due to oxidation reaction of carbon as shown in Figure 4.1. The TGA curve shows 86.5% weight lost which indicates the formation of ash and presence of some impurities. Under N_2 flow, no significant weight loss for CNT was observed in TGA curve as shown in Figure 4.2. These results indicate that MWCNT sample is volatiles free but contains some noncombustible impurities.

For the TiO_2-SiO_2 powder sample, the first weight loss under air flow was observed within temperature interval of 50-150^oC in TGA curve, which was attributed to the removal of adsorbed water and the release of acetic acid and other volatiles such as reaction products of condensation reaction of TTIP with water (Figure 4.3). The second weight loss occurred within temperature interval of 240-400^{o}C and total weight loss is about 40%. The DTA peak was observed onset with second weight loss indicates exothermic reaction around 360^{o}C due to the oxidation or decomposition of organic residuals. The exothermic peak at 450^{o}C might be attributed to crystallization of amorphous titania where no significant weight loss was observed. The third DTA peak is around 820^{o}C which can be attributed to the phase transition from anatase to rutile while there is no weight loss. These results are in good agreement with literature [32, 33]. In Figure 4.4, similar thermal behavior but less weight loss were observed in TGA of sample heated in N_2 flow. Heat treatment under N_2 resulted with similar weight loss except any distinctive exothermic oxidation reaction around 360^{o}C. Heat treatment under inert N_2 atmosphere may cause coke deposition due to the pyrolysis and decomposition of organic residuals.

The CNT-TiO_2-SiO_2 powder sample containing carbon nanotubes as 5% by weight was analyzed and the influence of presence of CNT in sol-gel under air atmosphere was shown in Figure 4.5. The weight loss between 50-250^{o}C in TGA curve is attributed to removal of adsorbed water and other residual compounds. In DTA curve, the peaks were observed at 363^{o}C and 487^{o}C which were attributed to decomposition of remaining sol-gel components and oxidation reaction of CNT, respectively. About 5% weight loss at 487^{o}C is consistent with added amount of CNT into sol-gel. It is clearly stated that the oxidation temperature of CNT decreased from 632^{o}C to 487^{o}C dramatically in the presence of TiO_2 and SiO_2. It is clear that the decomposition of carbon nanotubes was catalyzed by the presence of titania and silica. Similar results were also reported in literature and explained by the use of lattice oxygen of anatase to formation C-O bond for TiO_2-coated carbon nanotubes [34, 35]. On the other hand, the crystallization peak around 800^{o}C was not resolved well. The thermal behavior of CNT-TiO_2-SiO_2 powder under N_2 flow is presented in Figure 4.6. As it is seen from figure, the peak of oxidation of volatile organics was not observed in absence of molecular oxygen. Broad exothermic peak was observed in the temperature range of 380-500^{o}C which is ascribed with the CNT oxidation.

Interestingly the same total weight loss was observed with the sample heated under air flow. The broad exothermic peak might be attributed to CNT oxidation in the absence of molecular oxygen can be explained by the oxidation of CNTs by surface oxygen or -OH species.

$$Ti^{4+}\text{-}O_2 + C \rightarrow CO_x + Ti^{3+}$$

$$Ti^{4+}\text{-}OH + C \rightarrow CO_x + Ti^{3+} + H_2O$$

In order to clarify and ensure the suggested mechanism for CNT oxidation under inert atmosphere, new sets of experiments were planned. The CNT-TiO_2-SiO_2 samples were heat treated at different temperature and analyzed by X-ray photoelectron spectroscopy and elemental carbon analysis for this purpose.

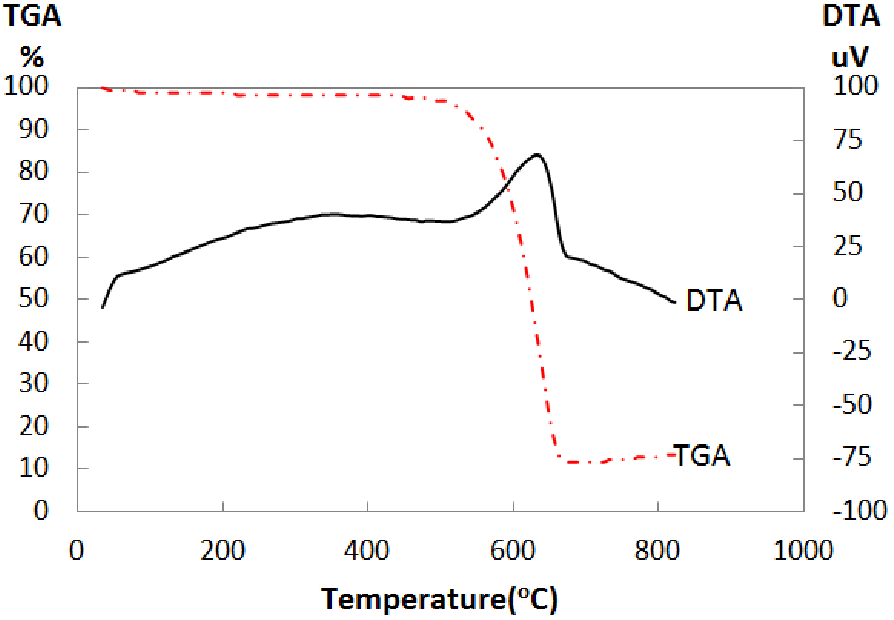

Figure 4.1 Thermal analysis of CNT sample under air flow

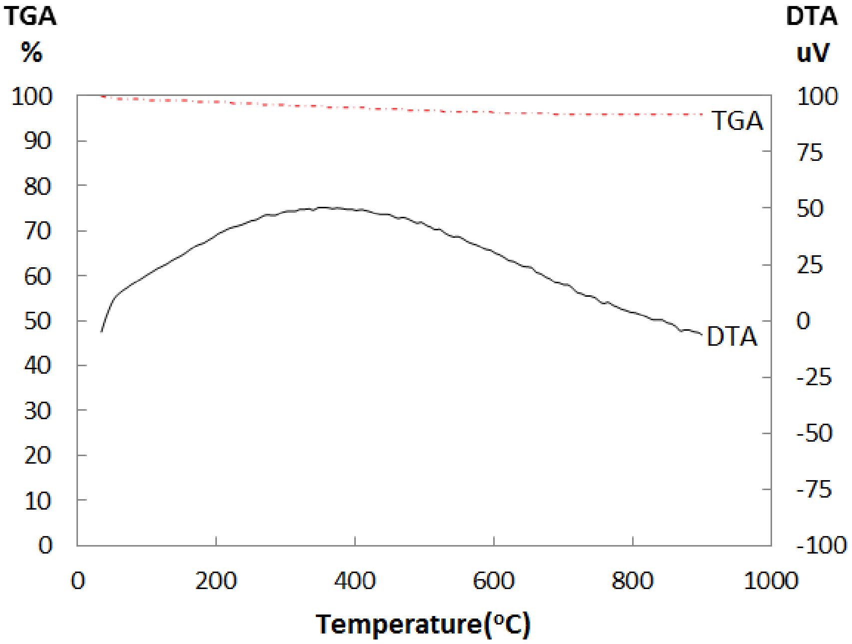

Figure 4.2 Thermal analysis of CNT sample under N_2 flow

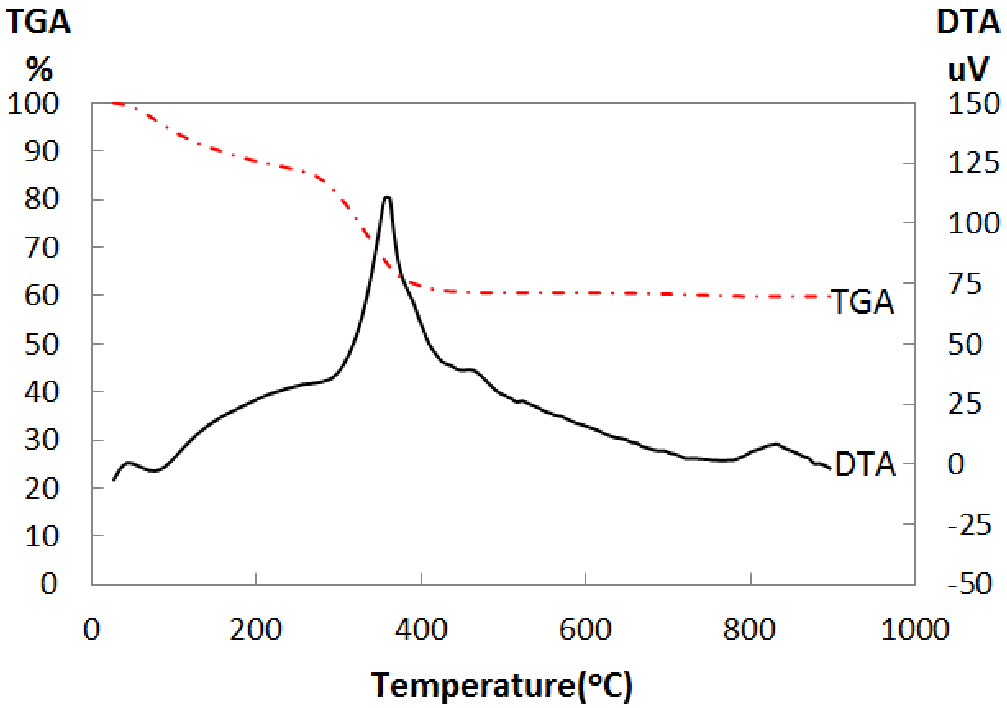

Figure 4.3 Thermal analysis of TiO_2-SiO_2 powder sample under air flow

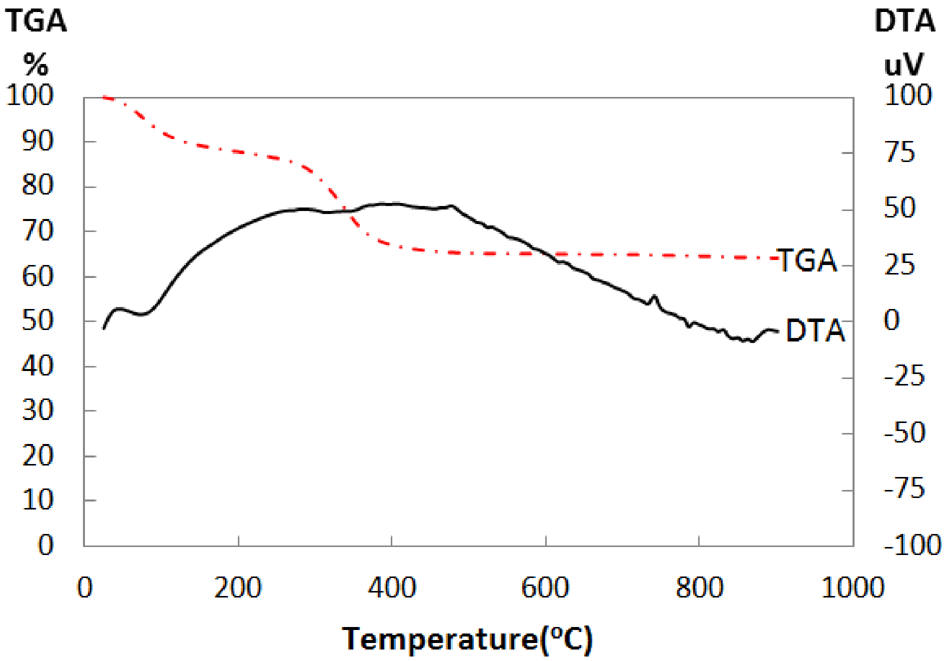

Figure 4.47 Thermal analysis of TiO_2-SiO_2 powder sample under N_2 flow

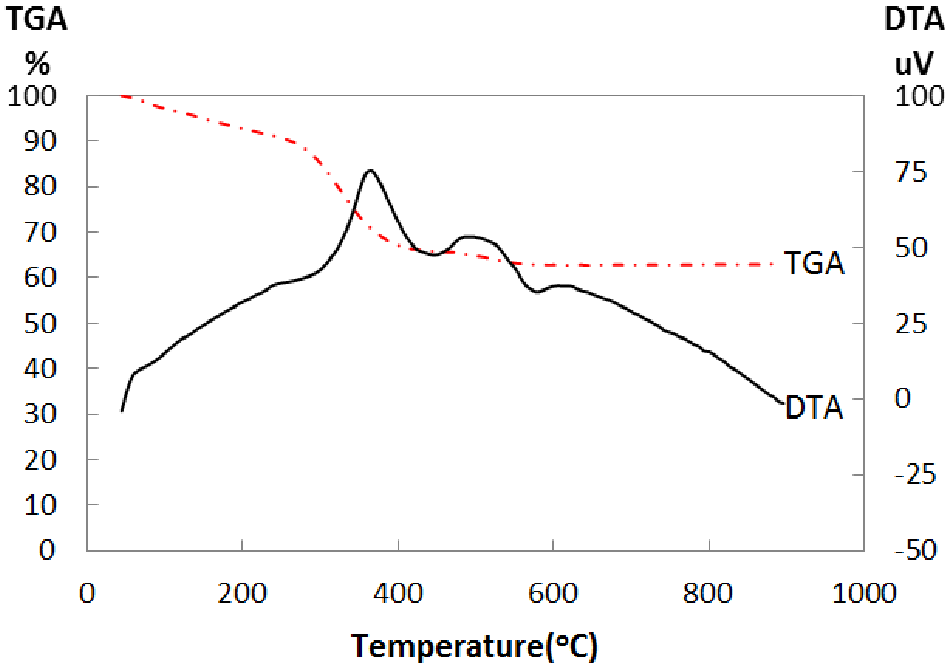

Figure 4.5 Thermal analysis of CNT-TiO_2-SiO_2 powder sample under air flow

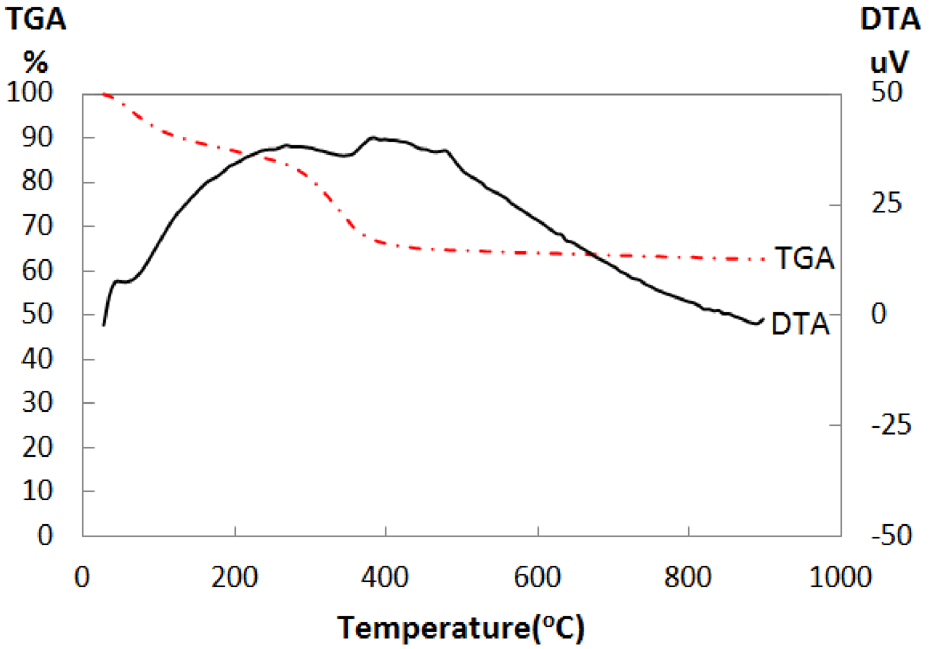

Figure 4.6 Thermal analysis of CNT-TiO_2-SiO_2 powder sample under N_2 flow

4.1.2 X-Ray Diffraction Analysis

X-ray diffraction analysis of the thin film samples was performed to investigate the crystalline phase, crystallite size and the effect of CNT on crystal structure of TiO_2. The CNT-TiO_2-SiO_2 and TiO_2-SiO_2 thin film samples were examined after heat treatment at a temperature range from 300^{o}C to 600^{o}C under air and N_2 atmosphere. The XRD patterns of the all samples indicated that the crystallization of titania is enhanced by the heat treatment and only anatase phase was observed on the samples which has a higher photocatalytic activity than other forms, rutile and brookite for most of the photocatalytic reactions. The CNT peak which is at 2θ 26.5^{o} could not be resolved due to the amorphous nature of carbon nanotubes and low mass fraction (5wt %) compared with detection limits. On the other hand, the amorphous silica showed a smooth broad overtone within the range of 2θ 15-40^{o} values. After this point, the thin film samples will be remarked as shown in Table 3.3.

The XRD patterns of TiO_2-SiO_2 thin film samples that heat treated in air flow are given in Figure 4.7. T-A300 and T-A400 samples showed only a broad peak which indicates the presence of amorphous structure. As calcination temperature increases, a sharp main peak at 2θ 25.4^{o} is observed which is attributed to the anatase phase (ICDD PDF Card No: 01-070-6826). The XRD patterns of T-A500 and T-A600 samples exhibited diffraction peaks at 2θ 25.4^{o}, 38.1^{o}, 48.2^{o}, 54.3^{o}, 55.3^{o}, 63.1^{o}, 75.6^{o}, 83.2^{o} which are consistent with anatase (1 0 1), (0 0 4), (2 0 0), (1 0 5), (2 1 1), (2 0 4), (2 1 5), (2 2 4) planes, respectively. A phase transition from anatase to rutile above 500^{o}C heat temperature has been reported in literature extensively [3, 12, 30]. However, the rutile formation was not observed during heat treatment despite the calcination temperature is increased to 600^{o}C which can be explained by short heat treatment duration. 20-minute-treatment may be too short for anatase-rutile phase transition. The presence of silica for all samples was evidenced by overtones in the background at 2θ 15^{o}-30^{o} range. In Figure 4.8, the XRD patterns of the TiO_2-SiO_2 thin film samples treated under N_2 atmosphere are given. In comparison with Figure 4.7, TiO_2-SiO_2 thin film samples treated under N_2 flow exhibit similar XRD patterns with the thin film samples that heat treated under air flow. Hence the presence of oxygen in heat treatment atmosphere does not affect the crystallinity significantly. The spectra of T-N300 and T-N400 samples indicate the presence of amorphous TiO_2 and the broad diffraction overtones at 2θ 15-30^o range can be explained by the presence of amorphous silica in the thin film. The XRD patterns of T-N500 and T-N600 samples matched with anatase phase only thus there is no rutile formation.

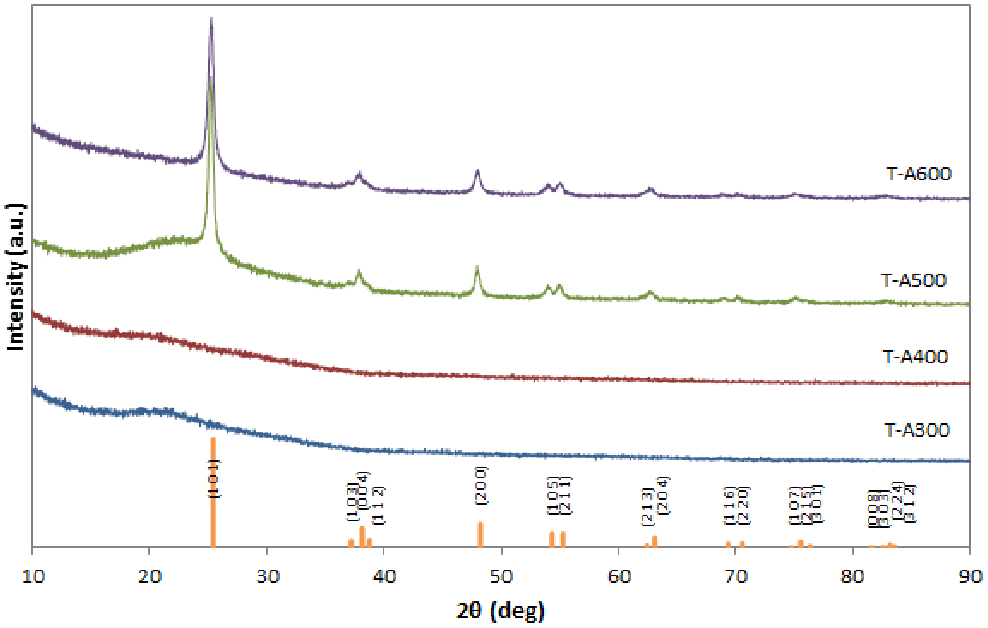

Figure 4.7 XRD patterns of TiO_2-SiO_2 thin films that heat treated under air atmosphere

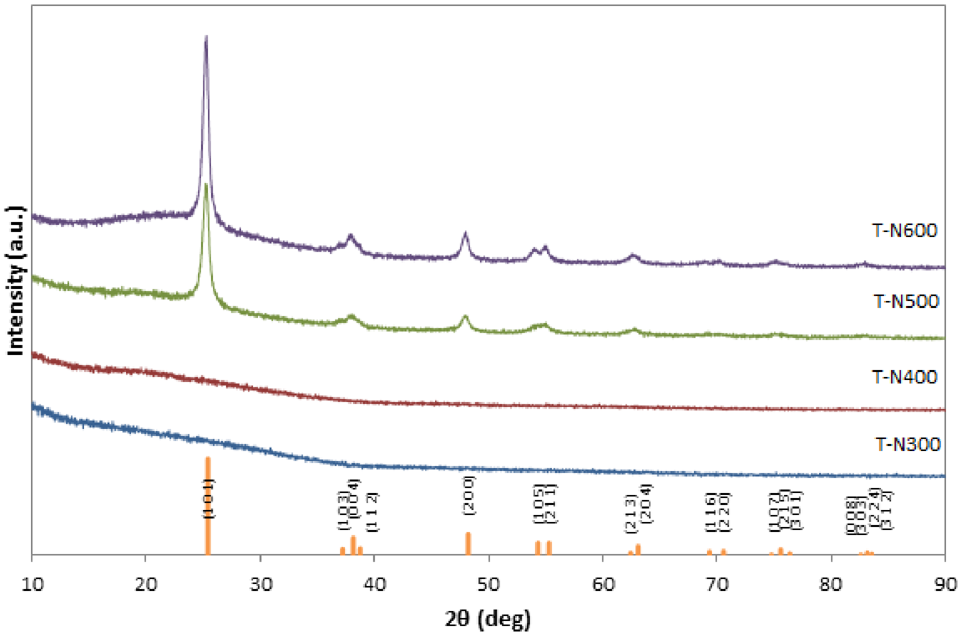

Figure 4.8 XRD patterns of TiO_2-SiO_2 thin films that heat treated under N_2 atmosphere

The effect of CNT on the crystallinity was also examined by XRD analysis. The XRD pattern of C-nonHT sample has no peak so the film can be associated with amorphous structure. As illustrated in Figure 4.9, the CNT-TiO_2-SiO_2 samples that heat treated under air flow show increasing crystallinity with temperature. In the spectra of C-A300 and C-A400 samples, small peak observed at 2θ 25.4^o is assigned as (101) plane of anatase peak. Thus, in the presence of carbon nanotubes, the anatase formation began at 300^{o}C for under air atmosphere while the crystallization temperature of TiO_2-SiO_2 thin film samples was above 400^{o}C. Thus the presence of CNT facilitates the crystallization formation reaction. This can be explained by reduction of activation energy for crystallization or formation of hot spots during heat treatment due to oxidation of CNTs. This possibility could be cleared out by examining the XRD analysis of the CNT-TiO_2-SiO_2 thin film samples that heat treated under N_2 atmosphere (Figure 4.10). The crystallinity of the samples that are heat treated at 300 and 400^{o}C under nitrogen flow are very low. Therefore, the anatase formation at 400^{o}C is facilitated by CNT oxidation in the presence of air under the experimental conditions applied.

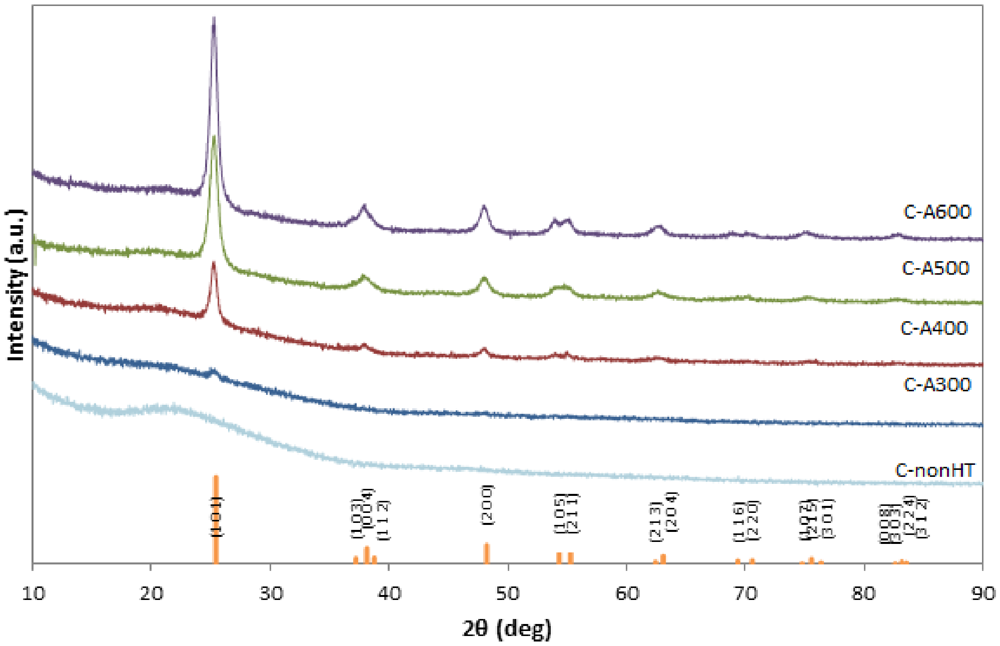

Figure 4.9 XRD patterns of CNT-TiO_2-SiO_2 thin films that heat treated under air atmosphere

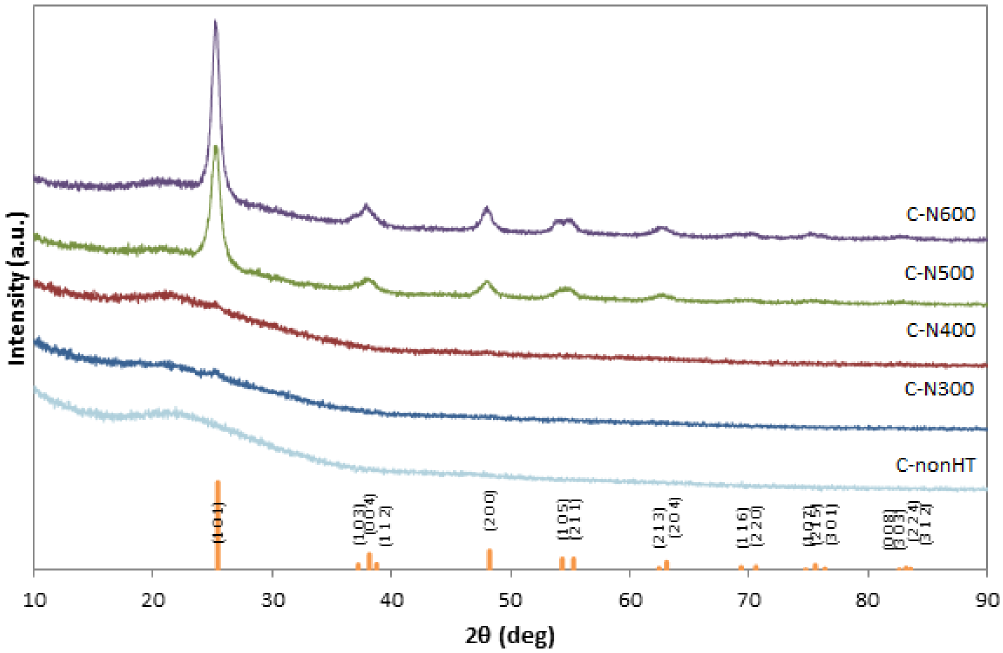

Figure 4.10 XRD patterns of CNT-TiO_2-SiO_2 thin films that heat treated under N_2 atmosphere

The average crystallite size of samples were determined by Scherrer equation considering anatase peak at 2θ 25.4^{o} corresponding to (1 0 1) plane.

$$D = \frac{0.9\lambda}{B_{\frac{1}{2}} \cos\theta}$$

Where D is the crystallite size, λ is the wavelength of the incident X-ray beam (0.154 nm for Cu Kα source), $B_{1/2}$ is the full-width at half maximum in radian and θ is the diffraction angle. The calculated crystallite sizes of the analyzed samples are tabulated in Table 4.5. It can be concluded that, the crystal growth is suppressed by the presence of carbon nanotubes both in the presence of air and nitrogen.

Table 4.5 Crystallite size of TiO_2-SiO_2 and CNT-TiO_2-SiO_2 samples that were heat treated at different temperature under air and N_2 atmosphere

Sample	Crystallite Size(nm)		Sample	Crystallite Size(nm)	
	AIR	**N_2**		**AIR**	**N_2**
T-300	-	-	**C-300**	11.7	-
T-400	-	-	**C-400**	12.5	-
T-500	17.4	12.1	**C-500**	9.7	8.3
T-600	14.9	14.0	**C-600**	10.7	10.0

4.1.3 Scanning Electron Microscopy Analysis & Energy Dispersive X-Ray Spectroscopy

The CNT-TiO_2-SiO_2 thin film samples were analyzed by SEM to investigate the efects of calcination temperature and atmosphere on morphology. The SEM images revealed that the CNTs were successfully incorporated into TiO_2-SiO_2 matrix and thin films have smooth and homogeneous surface. Some cracks were observed due to densification of thin films during heat treatment and sintering. The average diameter of bare multiwalled carbon naotubes was given as 9.5 nm (see App.A) and when carbon nanotubes are incorporated with TiO_2-SiO_2 matrix, the diameter increses significantly (~20 nm) which indicates the compatibility of sol-gel colloidal mixture and carbon nanotubes. As seen in Figure 4.11, the diameter of carbon nanotube in CNT-TiO_2-SiO_2 thin film after heat treatment in air flow at 450^{o}C was measured as 22 nm. The SEM analysis through cracks indicate the presence of carbon nanotubes coated with a layer of TiO_2-SiO_2. The bright and high contrast spots indicate the high electron density on the tips of carbon nanotubes as a result of conductance and local charging. Therefore, carbon nanotubes and TiO_2-SiO_2 layer are subject to different chemical environments. TiO_2-SiO_2 particles that surround CNT may contribute to the physical and chemical properties including catalytic activity.

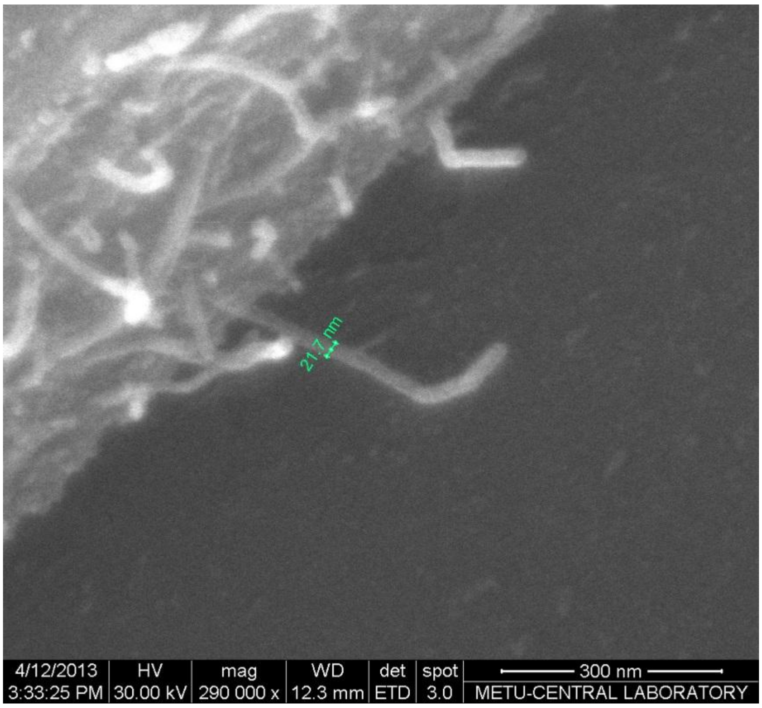

Figure 4.11 The measured diameter of CNT in thin film after heat treatment at 450°C under air atmosphere

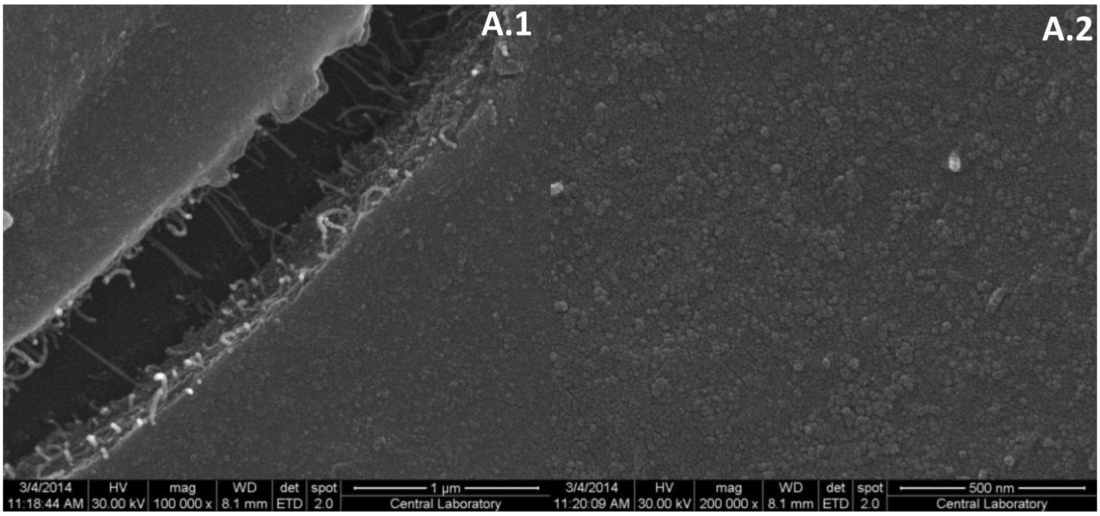

Figure 4.12 SEM Images of CNT-TiO_2-SiO_2 thin film (non-heat treated) A.1) surface crack A.2) surface

The SEM images of the synthesized CNT-TiO_2-SiO_2 thin film without heat treatment are shown in Figure 4.12. The effect of heat treatment under air and nitrogen atmosphere is shown in Figure 4.13 to Figure 4.16. It is obviously seen from the images that, there is no significant change between the images of non-heat treated and heat treated samples at 300°C in air and N_2 atmospheres (Figure 4.13). Carbon nanotubes are homogeneously dispersed and incorporated with a TiO_2-SiO_2 structure.

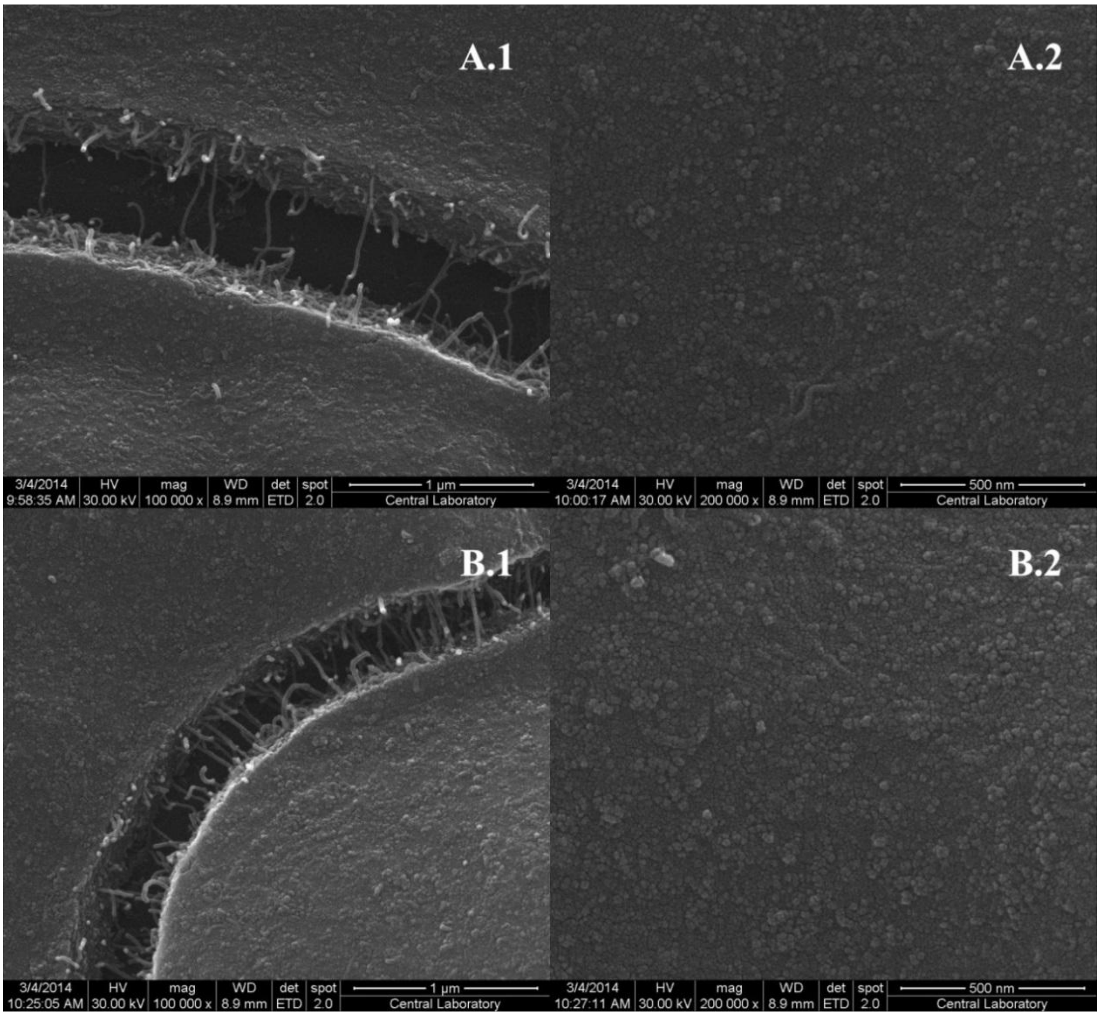

Figure 4.13 SEM Images of CNT-TiO_2-SiO_2 thin film 1) surface crack 2) surface after heat treatment at 300°C under A) air B) N_2 atmosphere

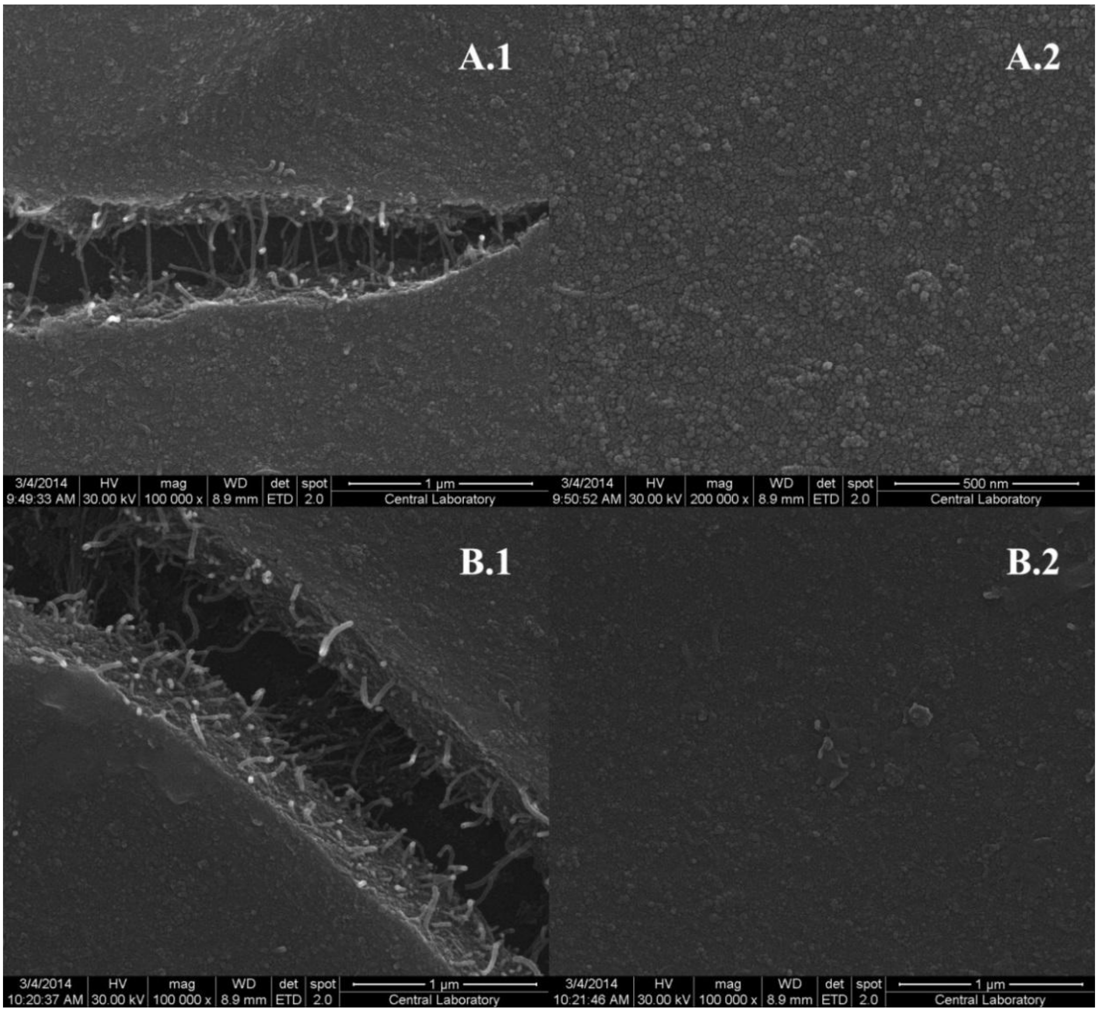

Figure 4.14 SEM Images of CNT-TiO_2-SiO_2 thin film 1) surface crack 2) surface after heat treatment at 400°C under A) air B) N_2 atmosphere

The representative SEM images of C-A400 and C-N400 samples are shown in Figure 4.14. The presence of CNTs was still observed intensively in the cracks of the films. The textural properties of C-A400 and C-N400 are similar to C-A300, C-N300 and C-nonHT samples. By increasing heat treatment temperature, the quantity of carbon nanotubes in the film decreased which can be attributed by oxidation reaction. In Figure 4.15, it can be seen that the amount of CNT in the film that heat treated under air flow and N_2 flow at 500°C is considerably less than the sample heat treated at 400°C. The interesting thing is the decrease in the quantity of CNTs after heat treatment in N_2 atmosphere. These results are in good agreement with the TGA analysis. In the absence of oxygen, carbon nanotubes oxidized by surface oxygen and hydroxyl species.

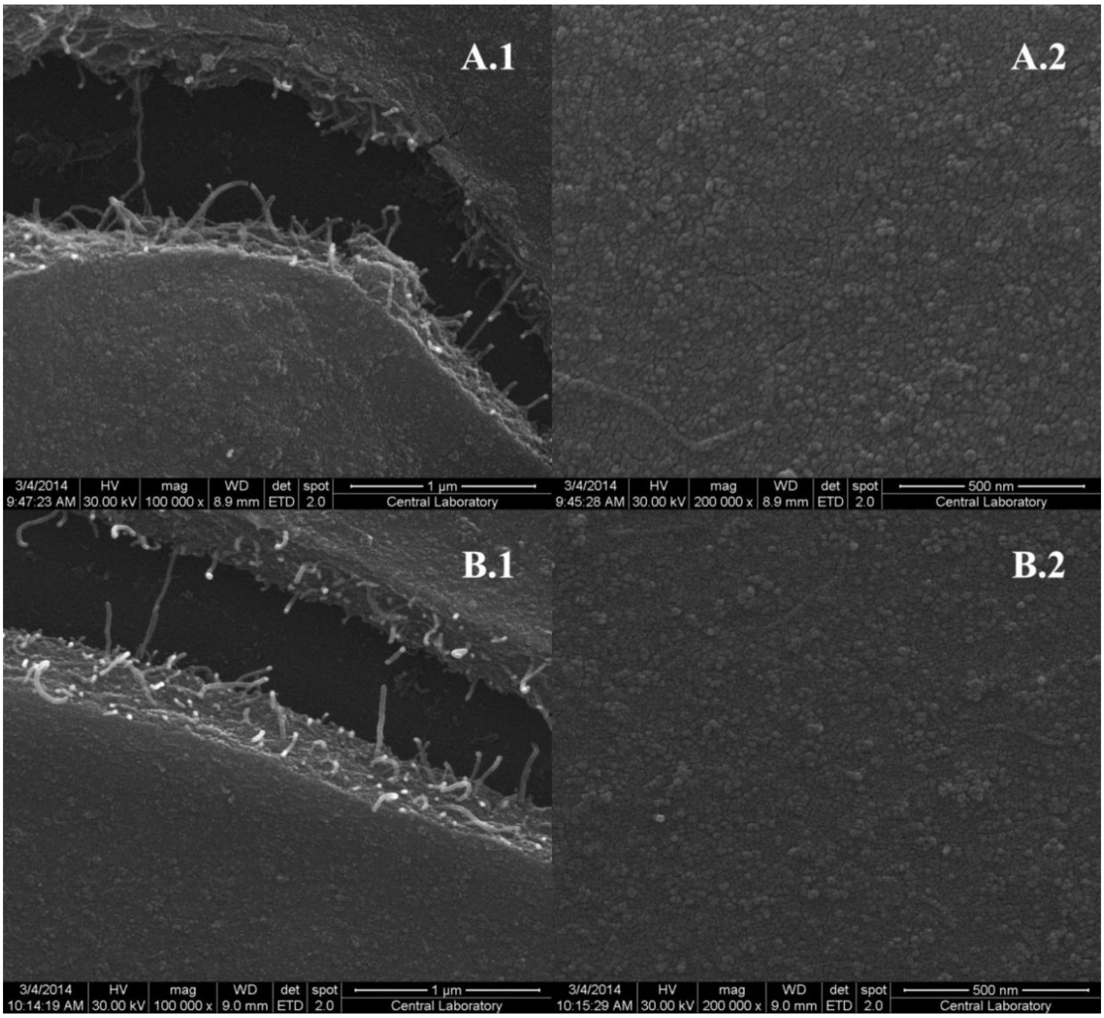

Figure 4.15 SEM Images of CNT-TiO_2-SiO_2 thin film 1) surface crack 2) surface after heat treatment at 500°C under A) air B) N_2 atmosphere

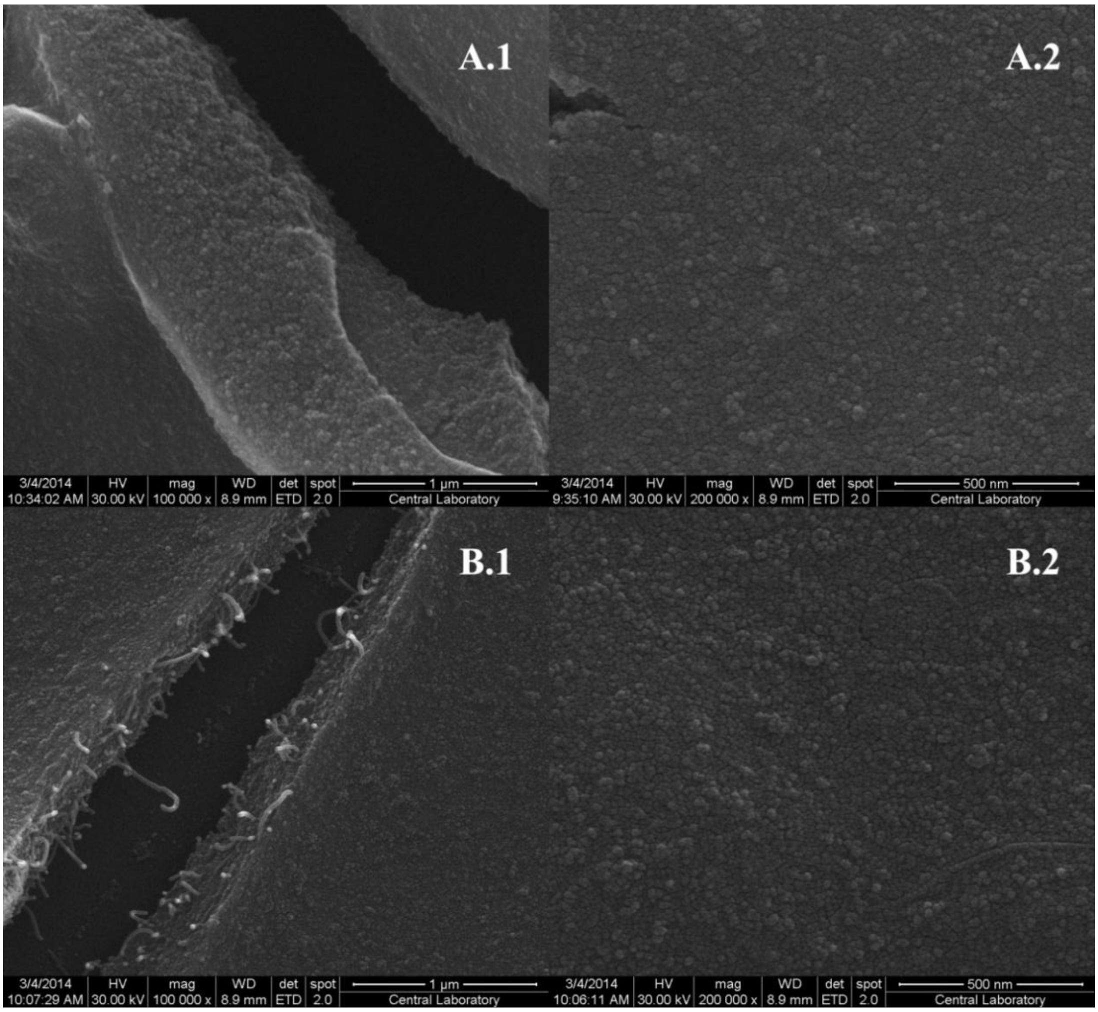

Figure 4.16 SEM Images of CNT-TiO_2-SiO_2 thin film 1) surface crack 2) surface after heat treatment at 600^oC under A) air B) N_2 atmosphere

In Figure 4.16, the SEM images of CNT-TiO_2-SiO_2 thin film samples that heat treated at 600^oC under air and N_2 atmosphere are shown. As it is seen from the images, the sample treated under air flow has no evidence about the carbon nanotubes which indicates complete oxidation. On the other hand, the sample heat treated under N_2 flow still has some residual carbon nanotubes as expected.

The EDS analysis of the thin film samples are presented in Table 4.6. The decrease in carbon quantity was observed in all samples paralel with increasing temperature.

Altough the EDS analysis covers a significant depth, no carbon was observed on the samples treated at 600^{o}C under both air and nitrogen atmosphere. The determination of carbon is difficult for EDS analysis because of poor detection limit and sensitivity. The detection limit of EDS instrument starts from atomic number 5(B) with a sensitivity of 0.1 weight%. The carbon content of C-N600 sample may be most likely under the sensitivity due to oxidation of carbon nanotubes. In addition the carbon composition of the thin films samples was obtained much higher than the added amount of carbon nanotubes due to the intrumental error. This result also indicates that the EDS analysis is incapable for the determination of carbon which may be attributed to detection limit. In order to clarify the effect of the heat treatment temperature and atmosphere on the carbon composition of the thin film samples, the elemental carbon analysis was applied to the thin films.

Table 4.6 EDS Analysis for carbon content of CNT-TiO_2-SiO_2 thin films that heat treated at different temperatures under air and N_2 atmosphere

	C wt %	
Sample	**AIR**	**N2**
C-nonHT	19.39	19.39
C-300	17.58	18.16
C-400	16.02	19.64
C-500	6.43	13.6
C-600	-	-

4.1.4 Elemental Carbon Analysis

The residual carbon quantity in the CNT-TiO_2-SiO_2 thin film samples were also determined by CHNSO elemental analysis. For this purpose, the CNT-TiO_2-SiO_2 thin films were heat treated at different temperatures under air and N_2 atmosphere and then the samples that were scraped off form the glass surface were analyzed. The powdered samples were analyzed with two measurements and the error was calculated according to the average value. The instrumental error is about 0.7% for carbon analysis.

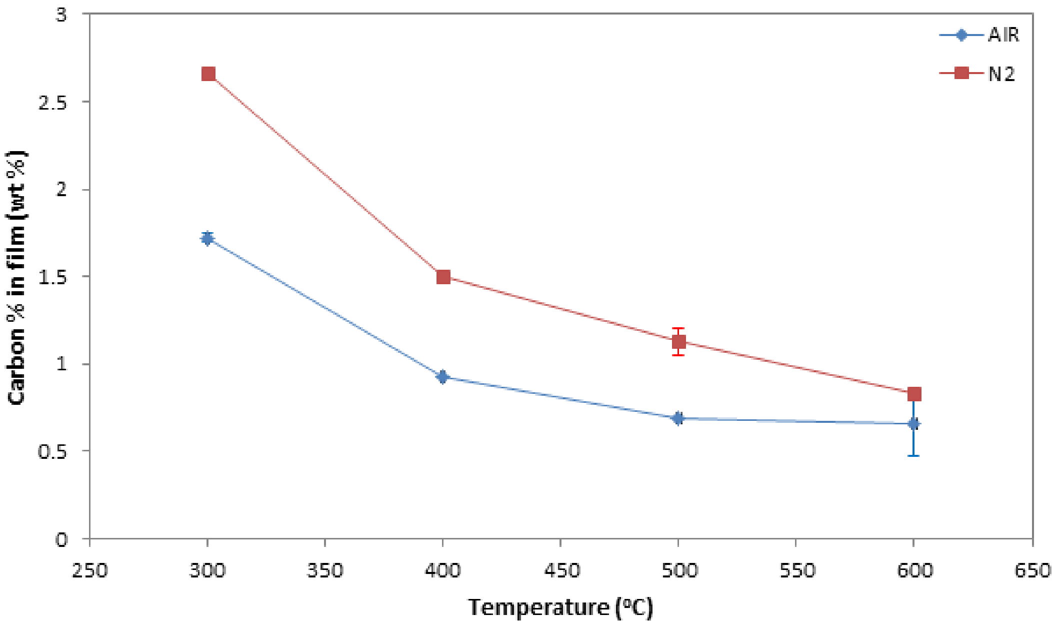

Figure 4.17 Elemental carbon analysis of CNT-TiO_2-SiO_2 thin films after heat treatment

As it seen in Figure 4.17, the amount of carbon was decreasing with increasing heat temperature under both of heat treatment atmospheres. The carbon analysis of the thin film samples treated under air and N_2 atmosphere exhibit similar results. The carbon nanotubes are oxidized by molecular oxygen in the presence of air and surface oxygen and hydroxyl species under nitrogen atmosphere. In order to ensure these results, XPS analysis were also performed.

4.1.5. X-Ray Photoelectron Spectroscopy

The effect of the heat treatment temperature and the atmosphere on the surface composition of the samples was analyzed by X-ray photoelectron spectroscopy (XPS). For this purpose, CNT-TiO_2-SiO_2 samples heat treated between 300-600°C under air and nitrogen flow were characterized by XPS. The survey scan and high resolution spectra of Ti 2p, O 1s, C 1s and Si 2p were investigated. All spectra were corrected with respect to the literature value of binding energy of C 1s 284.4 eV corresponding to C-C bond of MWCNT [36]. The high resolution spectrum of Ti 2p is composed of two main peaks of Ti $2p_{3/2}$ and Ti $2p_{1/2}$ at 458.6 and 464.3 eV respectively with a Ti $2p_{3/2}$ - Ti $2p_{1/2}$ splitting of 5.72eV and FWHM values of 0.98eV and 1.97eV [37]. Ti 2p high resolution spectrum of CNT-TiO_2-SiO_2 sample treated at 300°C under air confirmed the presence of Ti $2p_{3/2}$ and Ti $2p_{1/2}$ peaks and the spectrum deconvoluted by using XPS PEAK4.1 software (Figure 4.18). Two peaks were perfectly fitted corresponding to Ti $2p_{3/2}$ at 458.2 eV and Ti $2p_{1/2}$ at 464.3 eV between χ^2 values of between 1.94 and 3.07. These results are in good agreement with literature [37]. FWHM values of Ti $2p_{3/2}$ and Ti $2p_{1/2}$ peaks were determined as 1.44eV and 2.25eV which indicates a significant peak broadening. The peak broadening might be explained by differential charging as a result of complex structure of CNT-TiO_2-SiO_2 samples comprising of discrete conducting (MWCNTs), semiconducting (TiO_2) and insulator (SiO_2) domains. The presence of insulating domains over conducting and semiconducting structures and resulting dielectric discontinuity across the interface cause a significant peak broadening.

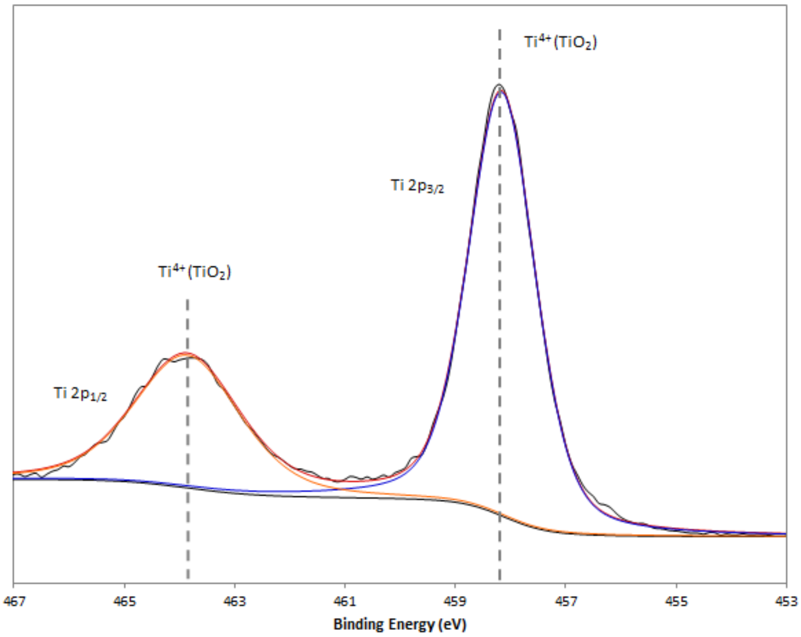

Figure 4.18 Ti 2p XPS spectrum for the C-A300

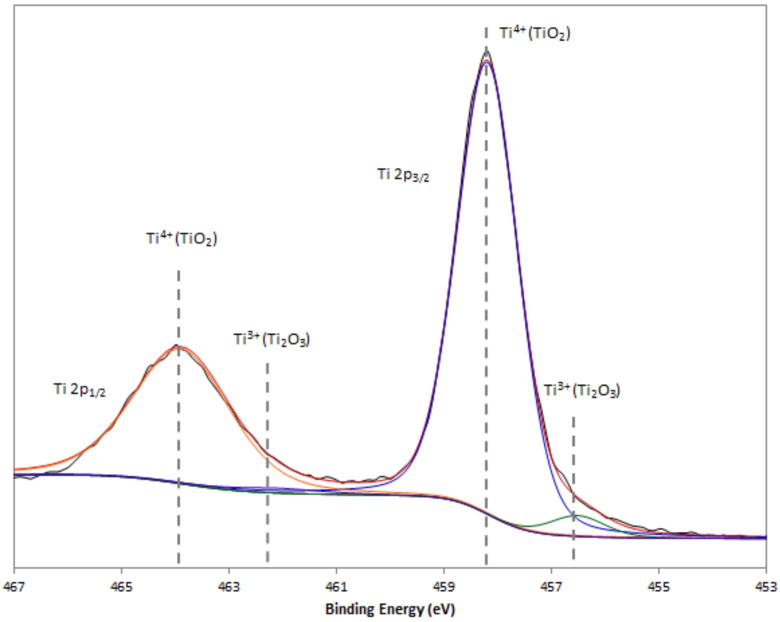

Figure 4.19 Ti 2p XPS spectrum for the C-N300

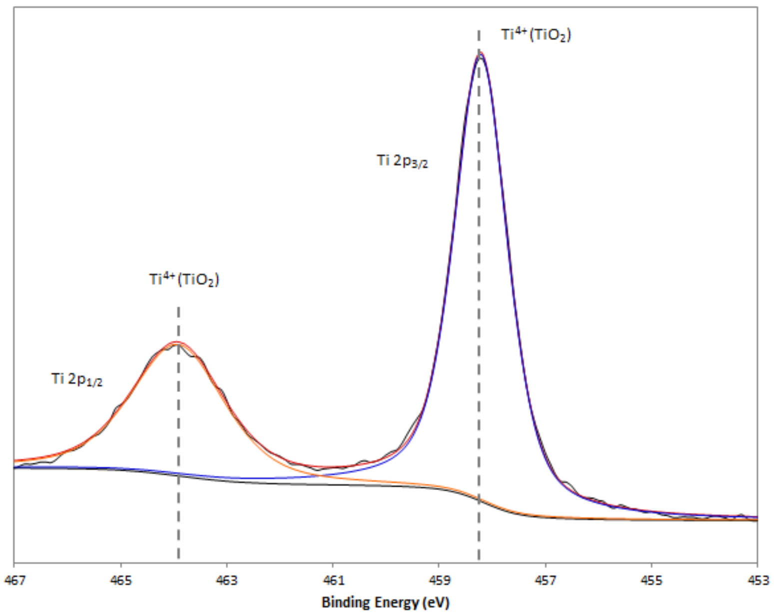

Figure 4.20 Ti 2p XPS spectrum for the C-A600

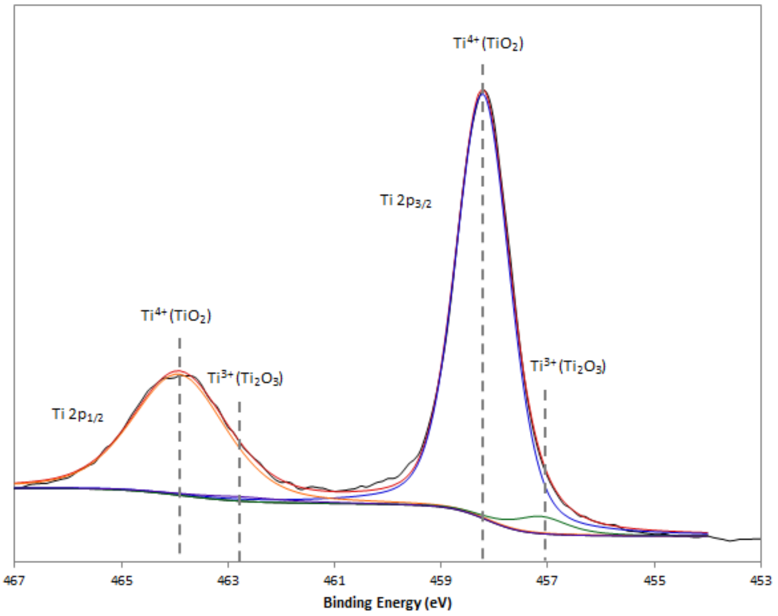

Figure 4.21 Ti 2p XPS spectrum for the C-N600

Ti 2p spectrum of CNT-TiO_2-SiO_2 sample heat treated under nitrogen atmosphere is shown in Figure 4.19. The spectrum was analyzed by using the same Ti $2p_{3/2}$ and Ti $2p_{1/2}$ binding energies, (458.2 eV and 464.3eV), Ti $2p_{3/2}$ - Ti $2p_{1/2}$ splitting values (5.72eV) and FWHM values. The peak asymmetry and the presence of tail at the lower binding energy indicate the presence of other Ti species over the surface. As shown in Figure 4.19, the fitted spectrum exhibits two new peaks at 456.6 eV and 462.2 eV which can be assigned into Ti^{3+} species. The peaks positions and Ti $2p_{3/2}$ - Ti $2p_{1/2}$ splitting values (5.6 eV) for Ti^{3+} are in good agreement with literature [37]. The formation of oxygen vacancies at 300°C under nitrogen atmosphere can be explained by oxidation of carbon nanotubes at elevated temperatures.

$$2TiO_2 + C \rightarrow Ti_2O_3 + CO$$

The formation of Ti^{3+} sites were also observed in the spectra of Ti 2p obtained for the samples heat treated under nitrogen atmosphere at 400°, 500° and 600°C as shown in Figure 4.20 and Figure 4.21. The Ti^{3+} sites have important impact on the photocatalytic activity. Therefore, Ti 2p spectra of the samples treated at 300°C, 400°C, 500°C and 600°C under nitrogen flow were analyzed by XPS PEAK4.1 and peak areas are presented in Table 4.7. As it is seen from the table, the area or the number of Ti atoms over the surface increases significantly with heat treatment temperature which can be explained by the removal of carbon and volatile residuals from the sol-gel synthesis. On the other hand, the ratio of Ti^{3+}/T^{4+} remains almost constant. Therefore, it can be inferred that Ti^{4+} and Ti^{3+} coexist on the surfaces of CNT-TiO_2-SiO_2 samples heat treated under nitrogen atmosphere.

The presence of Ti^{3+} defects and oxygen vacancies has a special importance on the photocatalytic activity [38]. Numerous surface reactions are affected by Ti^{3+} defects since it is a good reactive agent for many adsorbates. In literature, it is mentioned that reduced titania (TiO_{2-x}) which contains Ti^{3+} defects shows photocatalytic activity in visible light region [39]. In this study, the visible light absorption was not observed in the UV-Vis spectra of the CNT-TiO_2-SiO_2 thin films which are in

Section 4.1.6. On the other hand Ti^{3+} sites can provide the reactive compounds for the reduction of an electron-hole pair recombination rate which increases the photocatalytic activity. In the presence of O_2, Ti^{3+} defects can react with oxygen easily that results the formation of radicals such as $\bullet O_2^-$, •OH. In addition, the carbon pyrolysis can cause the reduction of the Ti^{4+} (TiO_2) in the surface to Ti^{3+} and formation of OH groups in the presence of water [40]. This also explains the presence of Ti^{3+} defects on the CNT-TiO_2-SiO_2 samples that heat treated under N_2 atmosphere.

Table 4.7 Deconvolution results of Ti 2p spectra: Ti 2p peak area versus heat treatment temperature under nitrogen atmosphere.

Temperature (°C)	Ti^{4+} (TiO_2)		Ti^{3+} (Ti_2O_3)		**Ti^{3+}/T^{4+}**
	Ti $2p_{3/2}$	**Ti $2p_{1/2}$**	**Ti $2p_{3/2}$**	**Ti $2p_{1/2}$**	
300	14729	7364	632	316	0.043
400	17560	8780	725	362	0.041
500	18077	9038	914	457	0.051
600	19307	9653	936	468	0.048

Heat treatment in the presence of carbon and nitrogen may cause the formation of carbides (TiC) and nitrides (TiN). The binding energy of Ti^{4+} $2p_{3/2}$ in TiC is 454.9 eV which is not observed in any of the spectra [41]. Survey scans do not indicate any nitrogen species which would be detected by N 1s core level located at 397.1 eV (Ti-N) and 399.5eV (N-O) (see App.B) [42].

Si 2p high resolution spectra of the samples were analyzed and presented in from Figure 4.22 to Figure 4.25. The CNT-TiO_2-SiO_2 samples heat treated under air and nitrogen atmosphere exhibit similar binding energies between 102.4–103.2 eV, which corresponds to Si^{4+} that is in good agreement with literature for SiO_2 [43]. Similar to Ti 2p case, significant peak widening was also observed in Si 2p spectra.

In literature FWHM for SiO_2 is given as 1.41 eV, however, the Si 2p spectra were analyzed by XPS PEAK4.1 and optimum peak fit were obtained by FWHM values of 2.1 eV which can be explained by differential charging over SiO_2 domains. Si 2p peak areas are shown in Table 4.8. XPS technique is not sensitive to silicon. As it is seen from table, the concentration of SiO_2 is not homogeneous over the surface. SiO_2 colloidal solution (LUDOX) might not be homogeneously mixed by TiO_2 during the sol-gel synthesis. Also the cracks over the thin film caused by thermal shrinkage during heat treatment may cause exposure of glass substrate by electron beam and SiO_2 from glass substrate interfere with SiO_2 in thin film during the analysis. The cracks over the thin film samples can be seen in SEM images in Section 4.1.3. Yet, the low atomic sensitivity factor of Si 2p is also possibility. Atomic sensitivity factor for Si 2p is 0.27 which is almost 7 times lower than Ti 2p (1.8) and XPS is not a strong technique for Si 2p quantification.

Table 4.8 Deconvolution results of Si 2p spectra: Si 2p peak area versus heat treatment temperature under air and nitrogen atmosphere

Temperature (^{o}C)	AIR		N_2	
	Si 2p Peak Position	**Peak Area**	**Si 2p Peak Position**	**Peak Area**
300	103	4641	102.4	1583
400	102.9	2623	103.2	3189
500	103.1	5479	102.4	2447
600	102.7	5682	102.9	2668

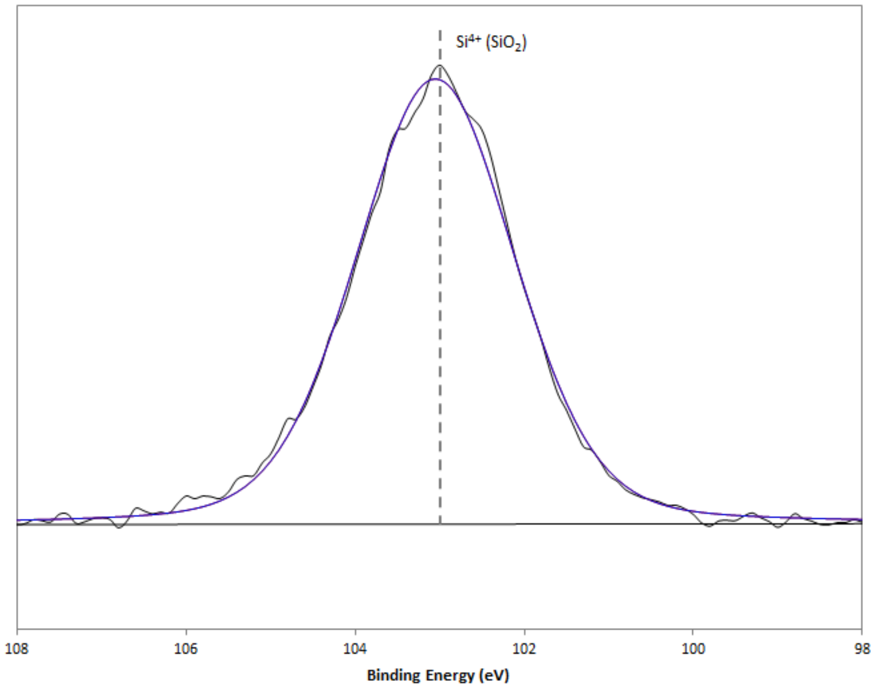

Figure 4.22 Si 2p XPS spectrum for the C-A300

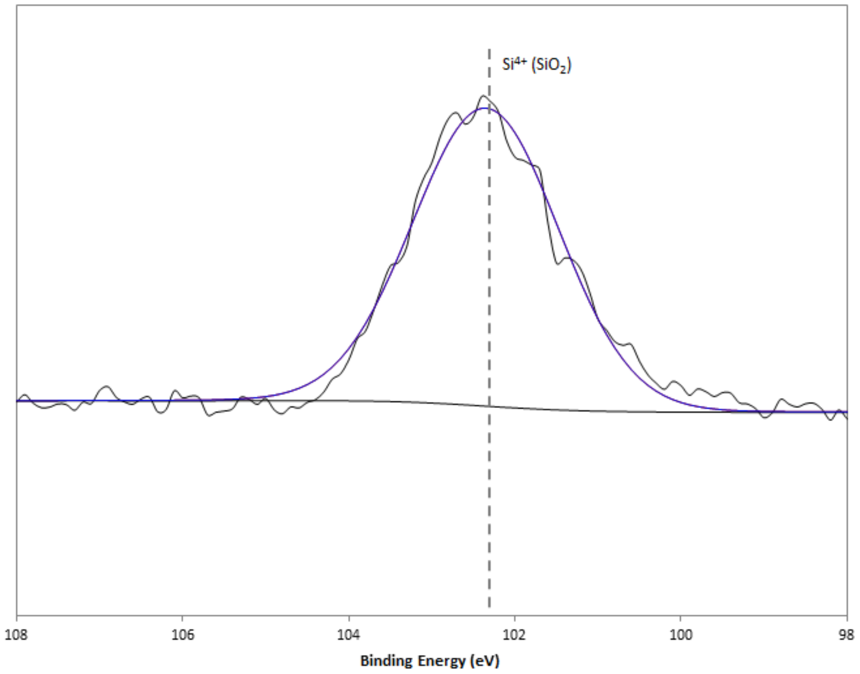

Figure 4.23 Si 2p XPS spectrum for the C-N300

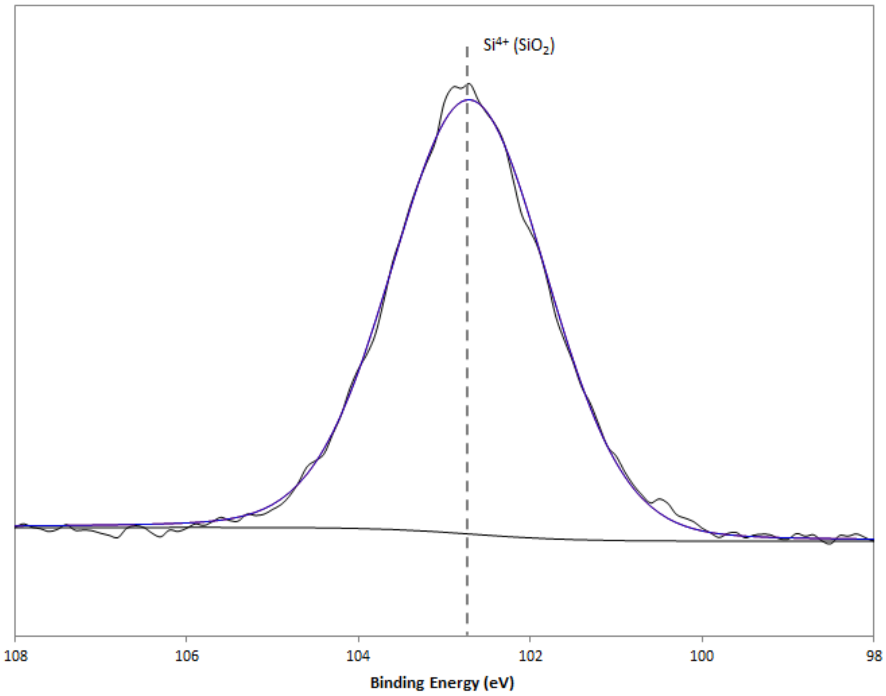

Figure 4.24 Si 2p XPS spectrum for the C-A600

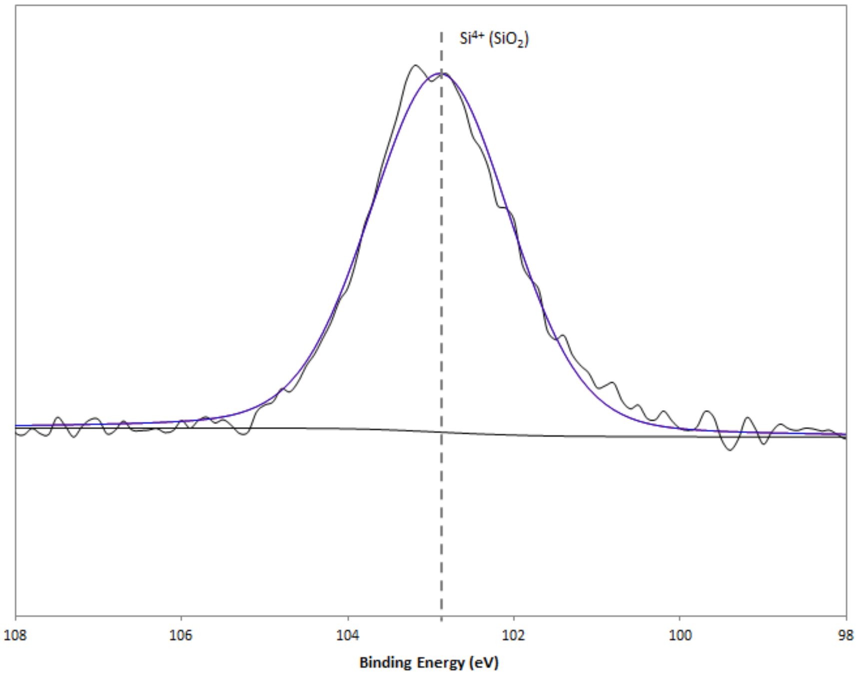

Figure 4.25 Si 2p XPS spectrum for the C-N600

The high resolution O 1s spectrum of the samples heat treated under air and nitrogen atmosphere were also analyzed. O 1s spectra of the samples exhibit very complex multiplet splitting as shown in from Figure 4.26 to Figure 4.29. O1s core level of the samples deconvoluted by assigning the major bands at 529.7eV and 532.05 eV for the oxygen in Ti-O-Ti and Si-O-Si respectively with FWHM of 1.44eV (Figure 4.26). In literature, the band at 531.1 eV can be attributed as oxygen in Ti-Si interface (Ti-O-Si), Ti_2O_3 and surface hydroxyl species (Ti-OH). On the other hand Ti-O-Si is not resolved in Ti 2p and Si 2p core level deconvolution. Therefore the possibility of the formation of Ti-O-Si could be eliminated and the band at 531.1eV can be assigned to Ti-OH and Ti_2O_3. Deconvolution analysis of O 1s core level by XPSPEAK4.1 revealed the presence of two more bands at 533.0 eV and 534.4 eV. These peaks are assigned into oxygen in O-C=O (533.0eV) and C-O (534.5eV) [36]. Therefore, O1s core level analysis of CNT-TiO_2-SiO_2 sample treated at 300^oC under air flow rate showed the presence of TiO_2, SiO_2, Ti_2O_3 and oxygenated carbon species over the surface (Figure 4.26). When the same sample is heat treated under nitrogen atmosphere, oxygenated carbon species could not be detected indicating the lack of free oxygen (Figure 4.27). Therefore, the carbon oxidation under air and nitrogen atmosphere results with different oxidation mechanisms as expected. Under air flow, oxygen rich MWCNT surface is oxidized while lattice oxygen is used under nitrogen atmosphere. When the heat treatment temperature increased, similar O1s spectra were obtained. However, the intensity of the peaks for oxygenated carbon species decreased significantly (Figure 4.28 and Figure 4.29). The quantitative analysis based on the peak area of Ti 2p and O 1s revealed the surface stoichiometry of TiO_x ($1.85<x<2.2$) by using the atomic sensitivity factors for Ti 2p and O 1s as 1.8 and 0.66 respectively (Table 4.9).

Table 4.9 Ti 2p and O 1s quantitative analysis for TiO_x

Temperature (°C)	AIR			N_2		
	Ti 2p	**O 1s**	**x**	**Ti 2p**	**O 1s**	**x**
300	10857.2	24115.2	2.22112	12273.9	23269.7	1.89587
400	12710.6	23497	1.84862	14633.3	29436.4	2.0116
500	13332.2	25197	1.88993	15063.9	32086.4	2.13002
600	12855	23772.7	1.8493	16088.9	32030.3	1.99083

The presence of surface hydroxyl group (–OH) on the surface has an importance role for the photocatalysis. After the photon adsorption, the electron and hole move to the surface where the reduction and oxidation reactions occur with the adsorbed species. The formed h^+ is trapped by –OH or surface H_2O to generate the hydroxyl radical (•OH) and e^- reacts with free oxygen to generate superoxide radical anion (O_2^-). The hydroxyl radical is highly active and can oxidize the organic compounds that adsorbed on the surface. Thus the photocatalytic activity can be enhanced by the hydroxyl groups that act as precursors for the hydroxyl radical (•OH) [44].

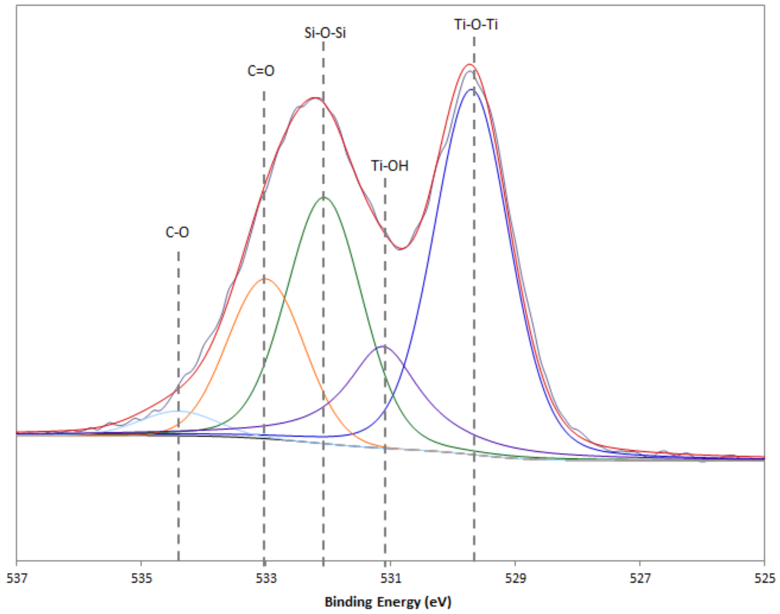

Figure 4.26 O 1s XPS spectrum for the C-A300

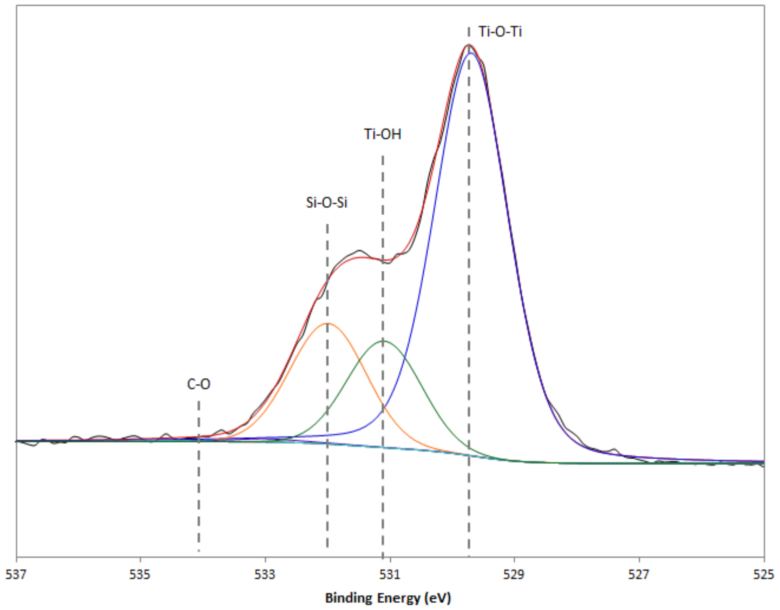

Figure 4.27 O 1s XPS spectrum for the C-N300

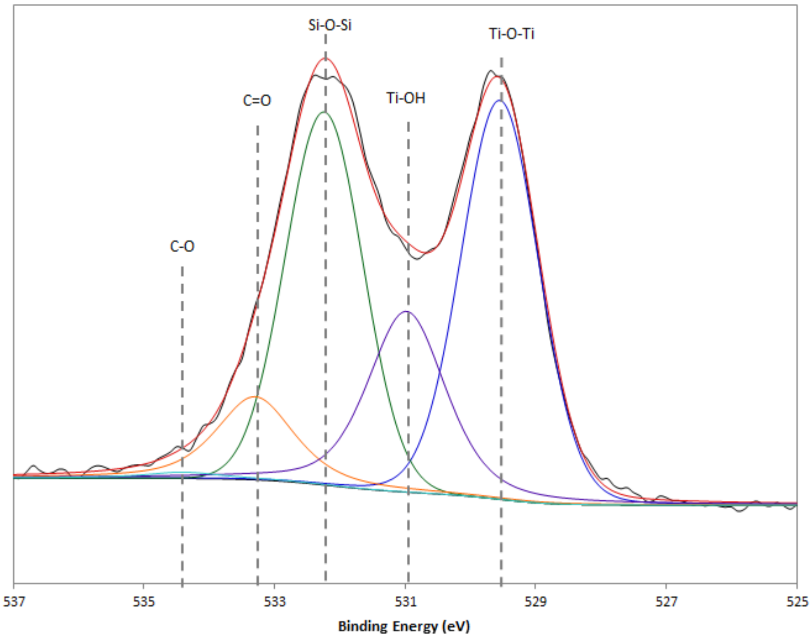

Figure 4.28 O 1s XPS spectrum for the C-A600

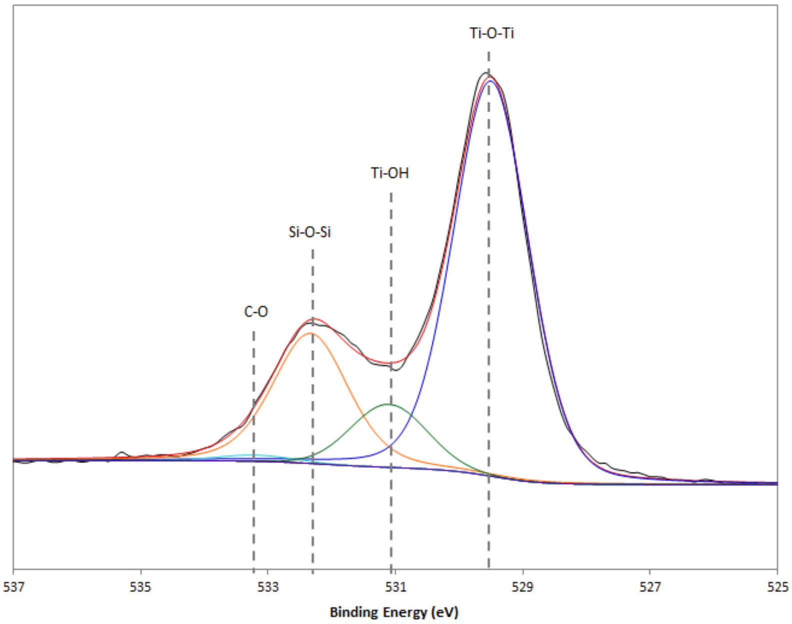

Figure 4.29 O 1s XPS spectrum for the C-N600

Similar to O 1s core level, high resolution XPS spectra of the samples exhibited complex multiplet splitting (between Figure 4.30 and Figure 4.33). Deconvolution of the C 1s spectra revealed the presence of pristine MWCNT structure (C-C) at 284.4eV which is good agreement with literature [36]. The samples treated at 300^{o}C under air and nitrogen flow exhibited similar C1s spectra and two more carbon species over the surface at 286.9ev and 288.6eV which can be assigned to C-O and O-C=O species (Figure 4.30 and Figure 4.31). C1s core level XPS analysis is very difficult because of adventitious carbon contamination, low atomic sensitivity (0.25) and discrepancies in the literature regarding peak positions and FWHM values of different species. Therefore, quantitative analysis at this point will be ambiguous and over interpretation and discussed only qualitatively. As it is seen from Figure 4.32 and Figure 4.33, heat treatment at 600^{o}C under air flow cause a significant asymmetry on the band. Careful deconvolution of C 1s revealed a new peak at 285.5eV which indicates the formation of carbon fragments which are not in tubular structure. The same trend was observed on the C1s spectrum of the samples heat treated at 400^{o}C and 500^{o}C under air flow (see App.B). These results indicate that MWCNT structure oxidized by molecular oxygen during heat treatment above 300^{o}C which is in good agreement with TGA results. On the other hand, carbon structure oxidized by lattice oxygen in the presence of inert nitrogen atmosphere. The amount of residual carbon can be approximated by peak areas of graphitic structure and carbon fragments at 284.2eV and 285.5eV respectively. As it is seen from Table 4.10, amount of carbon over surface significantly reduced by heat treatment above 500^{o}C. The effect of molecular oxygen is more significant than lattice oxygen on carbon oxidation.

Table 4.10 Total peak area of MWCNT C-C and carbon fragments at the binding energy of 284.2eV

Temperature (^{o}C)	Peak Area	
	AIR	**N_2**
300	4057	4464
400	4161	3969
500	2554	3195
600	2197	3120

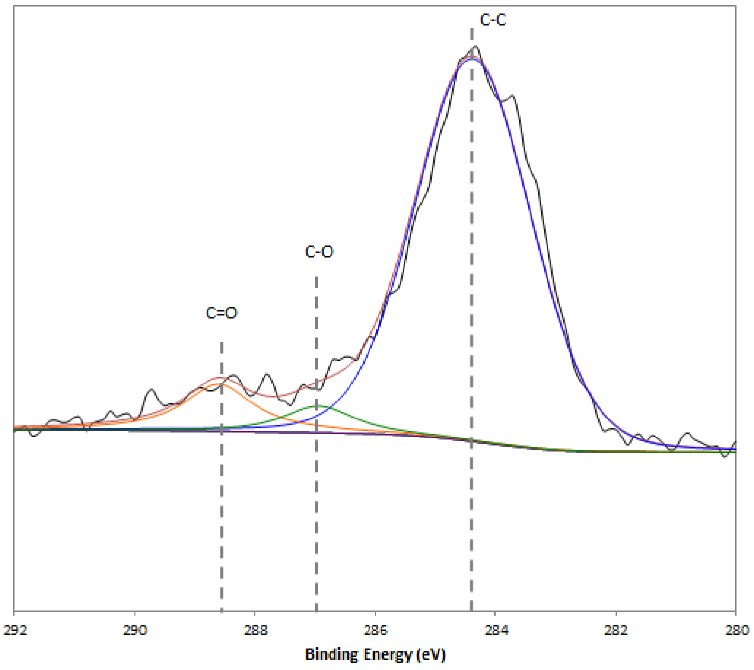

Figure 4.30 C 1s XPS spectrum of C-A300

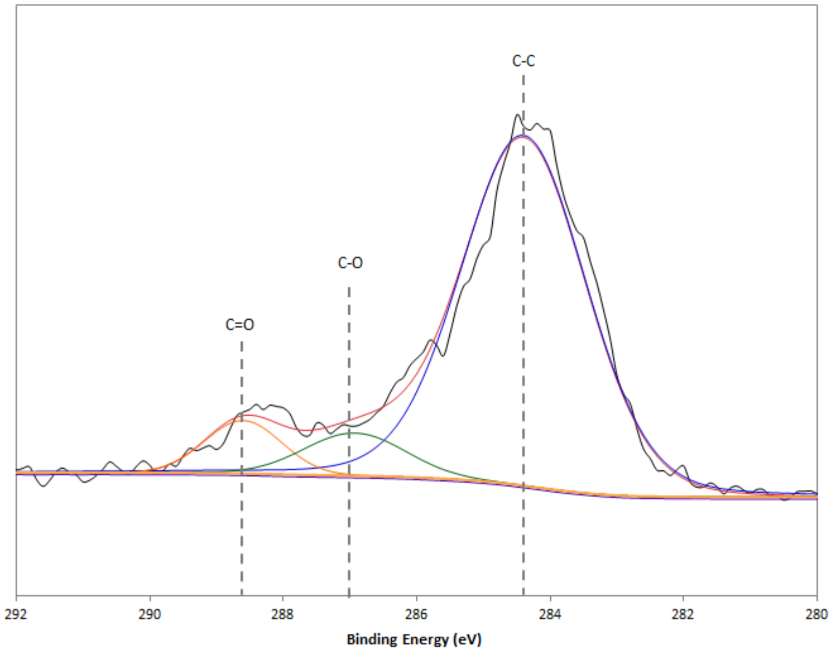

Figure 4.31 C 1s XPS spectrum of C-N300

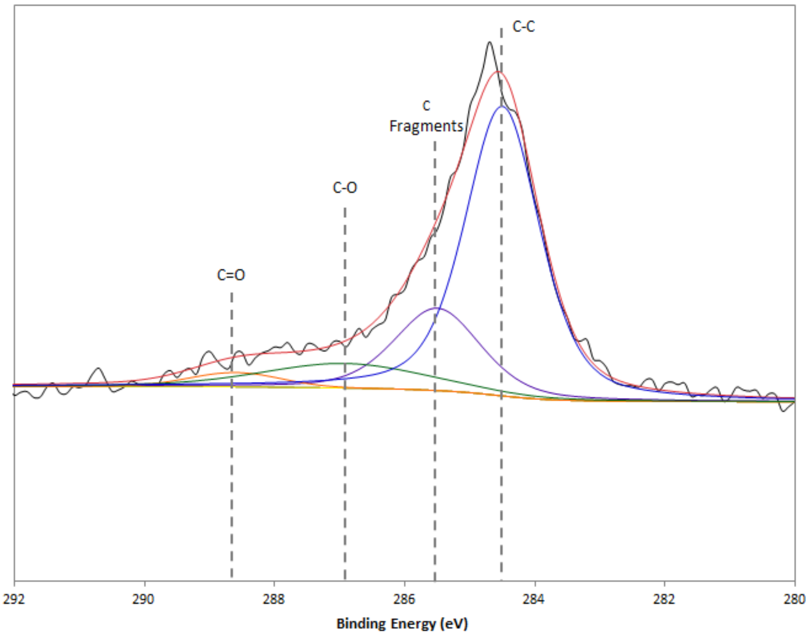

Figure 4.32 C 1s XPS spectrum of C-A600

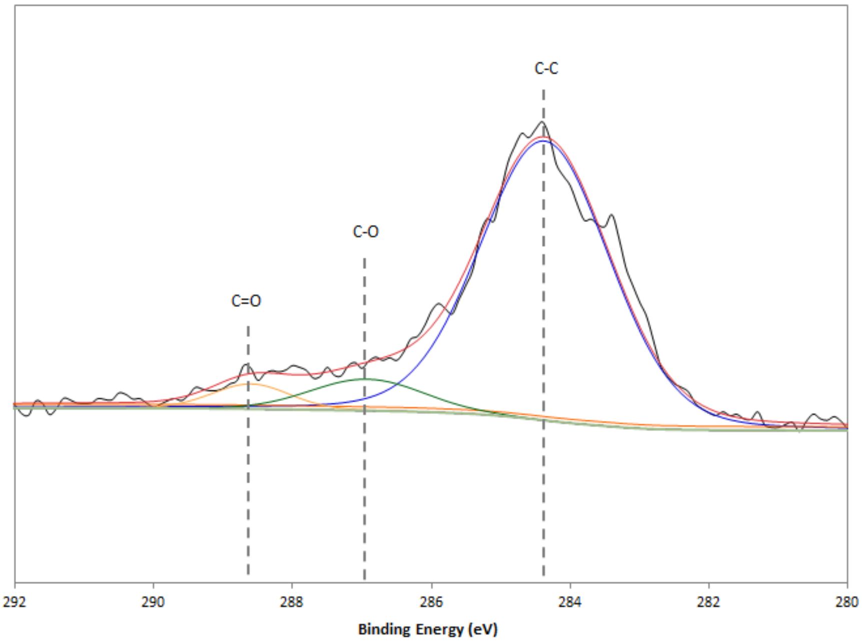

Figure 4.33 C 1s XPS spectrum of C-N600

4.1.5 UV-Visible Spectrophotometry and Band Gap Calculation

The effect of the addition of carbon nanotubes, heat treatment temperature and atmosphere on band gap energy of the thin films was investigated by using the UV-Vis spectra of the thin films.

The TiO_2-SiO_2 and CNT- TiO_2-SiO_2 thin films were examined after heat treatment at different temperatures under air and N_2 atmosphere. The UV-Vis spectrum of the thin film that coated over glass was obtained between 200-800nm by using bare glass as a blank sample for UV-Vis spectrophotometer. The UV-Vis spectra of the films are shown in from Figure 4.34 toFigure 4.37. The absorption curves of the thin films are similar and it is seen that the absorption edge of the thin films appeared in UV-A region at about 365nm which is consistent with TiO_2 anatase phase. The heat treatment temperature and atmosphere have no significant impact on the absorption of the thin films. In addition, the absorption edge of CNT-added thin films is also similar to TiO_2-SiO_2 thin films and the addition of carbon nanotubes has no significant effect on absorption edge. The difference in the intensity of absorbance for the samples may explained by the thickness of the films. The thicker film absorbs the light more than the thin ones. This difference also shows that the films cannot be prepared exactly the same although the same procedure is followed.

The band gap energy of the thin film samples were calculated by evaluating the UV-Vis absorption data. For semiconductors, the general expression which is $(\alpha.h\upsilon)^m$ versus hυ relates the absorption coefficient to the band gap energy where á is the absorption coefficient, hυ is the light energy depends on wavelength where h is the Planck constant and υ is the ratio of speed of light to wavelength of the incident light, *m* is an integer or semi-integer. The intercept of the expression, which is a straight line gives the direct band gap energy when m is 2, the indirect band gap energy when m is ½. Figure 4.38 shows the plot $(\alpha.h\upsilon)^2$ vs hυ which is used to determine the direct band gap energy of TiO_2-SiO_2 thin films that heat treated at 300°C under air and N_2 atmosphere. The direct band gap energies are obtained for T-A300 and T-N300 samples as 3.76 eV and 3.67 eV, respectively. In Figure 4.39, the plot $(\alpha.h\upsilon)^{1/2}$ vs hυ gives the indirect band gap energies for the same samples as 3.42 eV and 3.25, respectively. The results for the band gap determination of the TiO_2-SiO_2 and CNT-TiO_2-SiO_2 thin films are showed in Table 4.11.

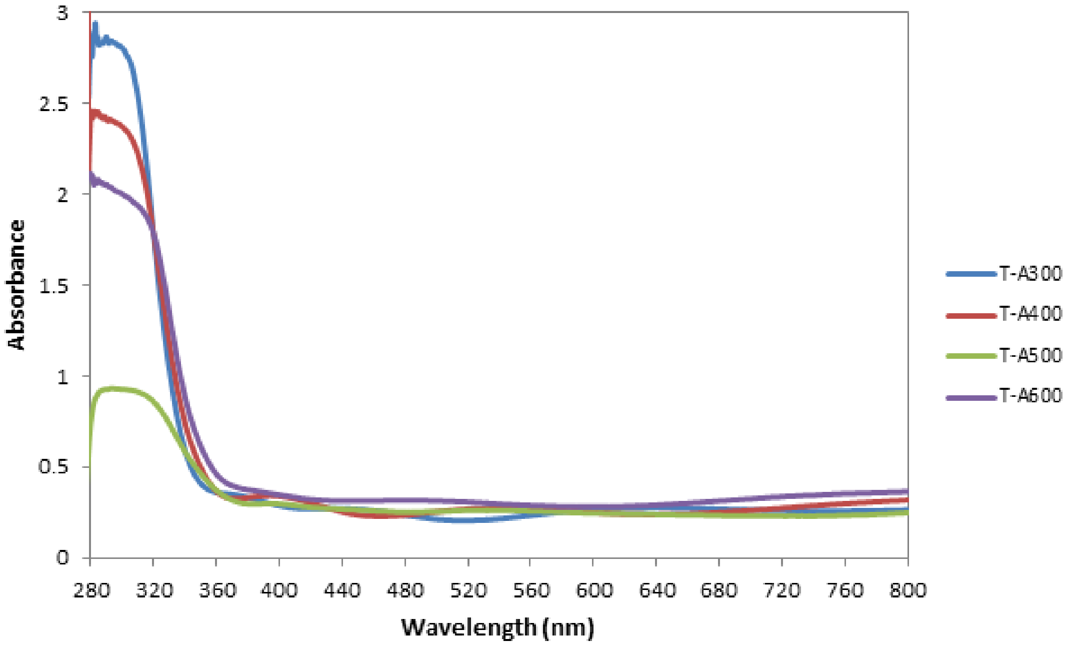

Figure 4.34 UV-Vis Spectra of TiO_2-SiO_2 thin films that heat treated under air atmosphere

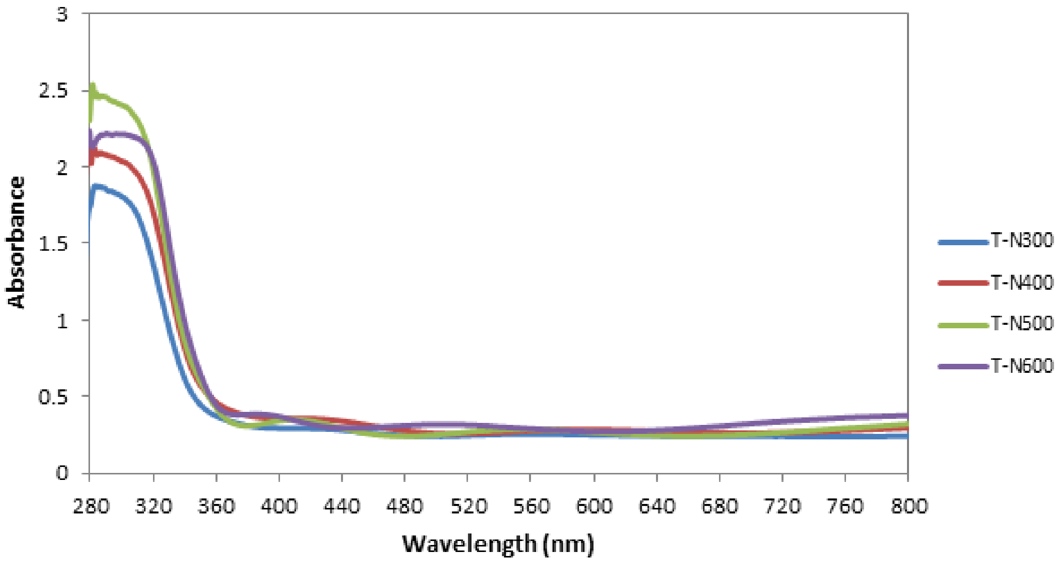

Figure 4.35 UV-Vis Spectra of TiO_2-SiO_2 thin films that heat treated under N_2 atmosphere

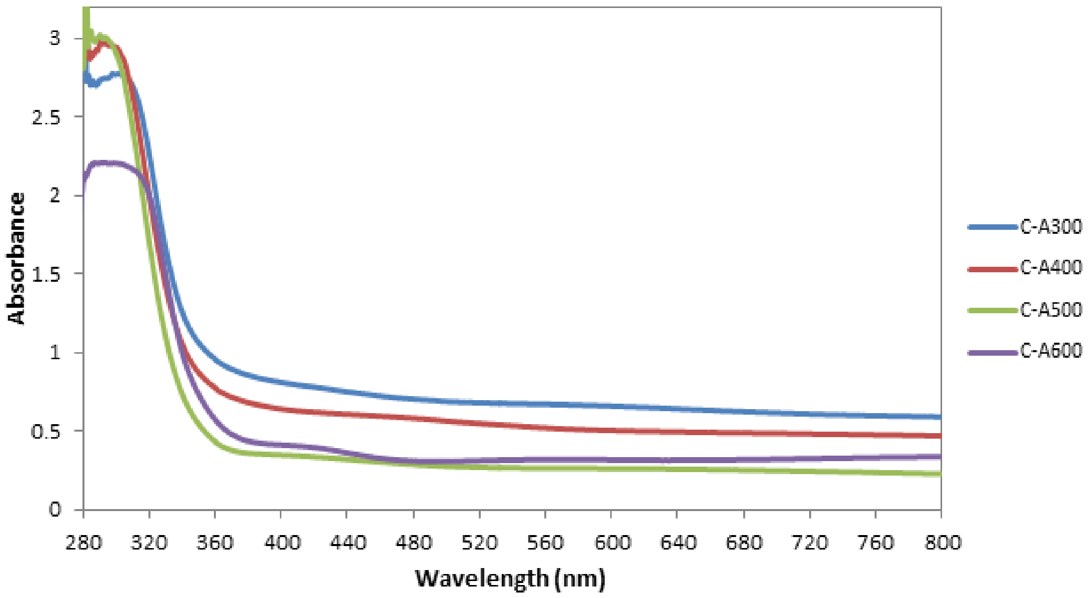

Figure 4.36 UV-Vis Spectra of CNT-TiO_2-SiO_2 thin films that heat treated under air atmosphere

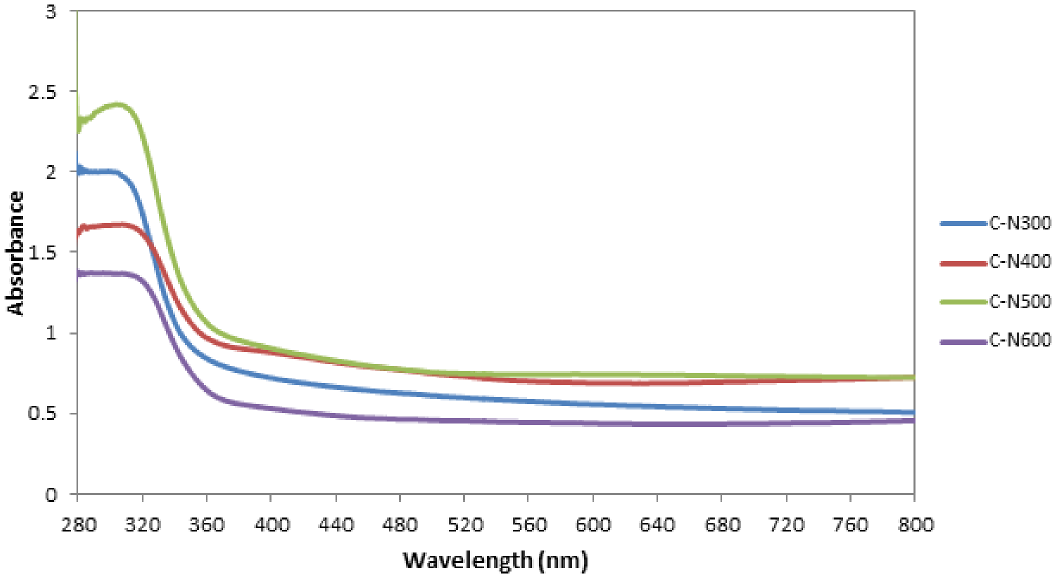

Figure 4.37 UV-Vis Spectra of TiO_2-SiO_2 thin films that heat treated under N_2 atmosphere

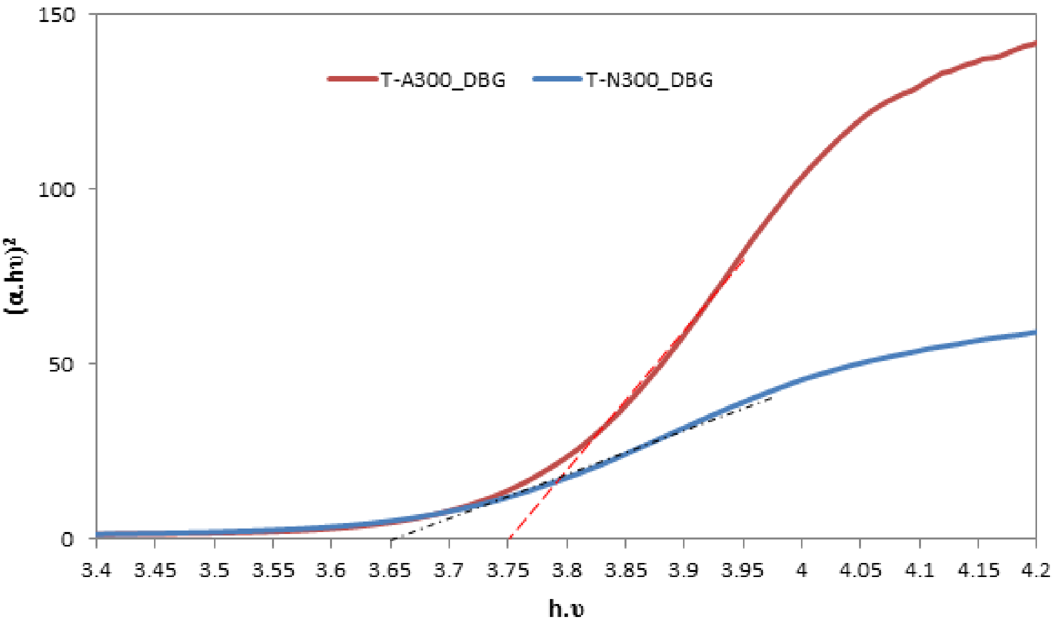

Figure 4.38 Direct band gap determination of T-300 sample

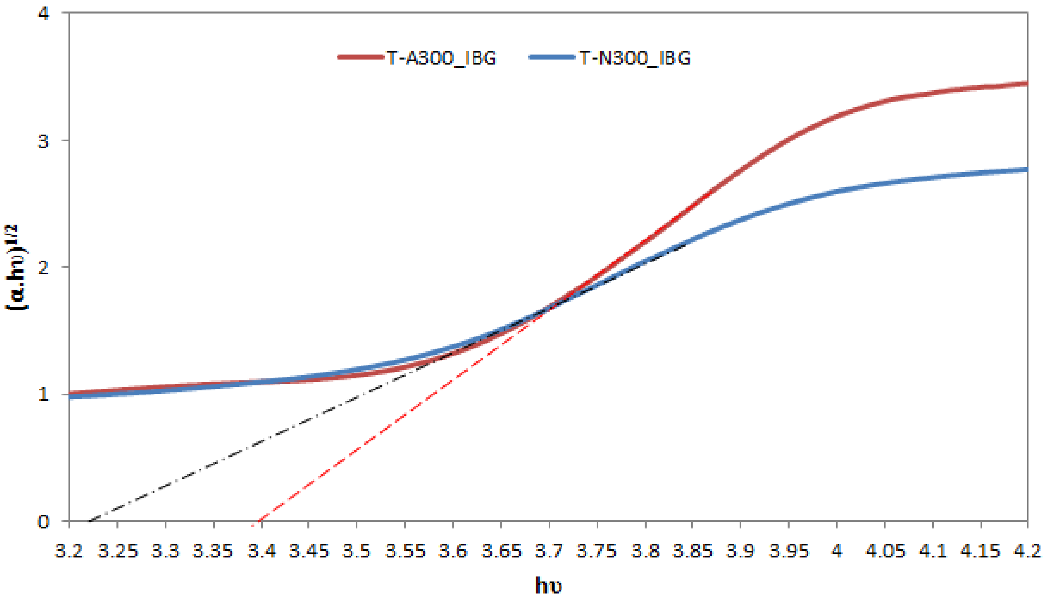

Figure 4.39 Indirect band gap determination of T-300 sample

Table 4.11 Direct and indirect band gap energies of TiO_2-SiO_2 and CNT-TiO_2-SiO_2 thin films that heat treated under air and N_2 atmosphere

Sample	Direct Band Gap(eV)		Indirect Band Gap(eV)	
	AIR	**N_2**	**AIR**	**N_2**
T-300	3.8	3.7	3.4	3.3
C-300	3.7	3.6	3.1	3.0
T-400	3.7	3.6	3.3	3.2
C-400	3.7	3.4	3.2	2.5
T-500	3.5	3.7	2.9	3.2
C-500	3.8	3.6	3.3	2.8
T-600	3.6	3.6	3.2	3.2
C-600	3.6	3.5	3.2	2.8

The direct band gap energies of TiO_2-SiO_2 that heat treated under air changes between 3.8-3.5eV while the indirect band gap of these samples changes between 3.4-2.9eV (see App.C). It is seen that heat treatment at different temperature under N_2 atmosphere didn’t affect the band gap energy significantly. The direct band gap energies of the TiO_2-SiO_2 samples heat treated under N_2 atmosphere are between 3.8-3.6 eV while the indirect band gap of these samples decreases from 3.3eV to 3.2eV by increasing heat treatment temperature. The carbon nanotubes addition results the similar direct band gap energies with the bare samples except T-A500. On the other hand the change in indirect band gap energies of CNT-TiO_2-SiO_2 thin films that heat treated under air or N_2 atmosphere are larger than the samples without carbon nanotubes except T-A500. The indirect band gap energies of CNT-TiO_2-SiO_2 that heat treated under N_2 atmosphere varies between 3.0-2.5eV which is significantly lower than the TiO_2-SiO_2 thin films. The minimum band gap energy indicates the higher photocatalytic activity hence it is expected in photocatalytic activity test that CNT-TiO_2-SiO_2 samples that heat treated under N_2 atmosphere show more activity. Also T-A500 sample is photocatalytically more active according to the indirect band gap energy.

4.2 Photocatalytic Activity Test

The photocatalytic activity of thin films was determined by methylene blue degradation test under UV light irradiation. In order to investigate the effect of CNT addition, heat treatment atmosphere and temperature on photocatalytic activity, the TiO_2-SiO_2 and CNT-TiO_2-SiO_2 thin films that heat treated at different temperature under air and N_2 atmosphere were analyzed. The thin films after heat treatment were immersed in 10 ml 2 ppm methylene blue solution and then irradiated for 180 minutes at a distance of 6cm perpendicular to the UV-C lamp irradiating at 254nm. The concentration change of methylene blue was followed by sampling the reaction mixture at 30-minute intervals and analysis of unreacted methylene blue by determining absorption at 664.5nm by UV-Vis Spectrophotometer. Generally the photocatalytic activity was obtained by examining the degradation of methylene blue over thin film surface after the adsorption in dark. The UV light irradiation after adsorption equilibrium is not convenient for the films of this study. The difference in surface areas of the films due to heat treatment caused the different amount of methylene blue deposition on the films and so the photocatalytic decomposition of adsorbed methylene blue cannot be measured on an equal basis. Also the CNT-TiO_2-SiO_2 thin films are blackish that makes the detection of methylene blue on film difficult for UV-Vis Spectrophotometer.

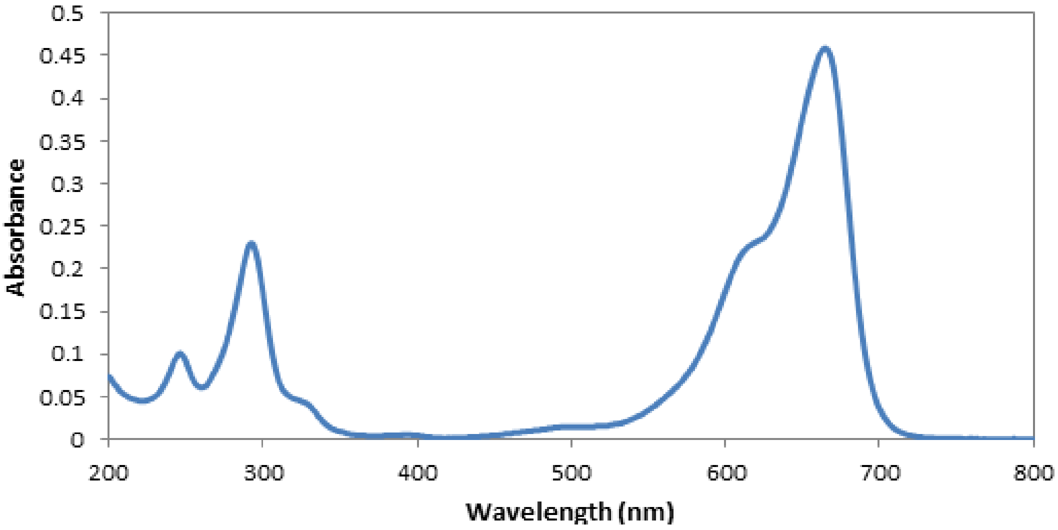

Figure 4.40 UV-Vis Spectrum of 2 ppm Methylene Blue

The ultraviolet-visible spectrum of the prepared 2ppm methylene blue is shown in Figure 4.40. The strong maximum peak of methylene blue is at 664.5nm and the degradation was observed for all samples by the decrease of absorbance at this wavelength during the reaction.

The heat treatment process enhances the photocatalytic activity due to improvement of the morphological and textural properties such as crystallinity and surface area. XRD analyses reveal the crystallinity of thin films. In order to show the effect of heat treatment on the surface area, the heat treated thin films immersed into 10ml 2ppm methylene blue solution and then kept in dark for 24h. The concentration of methylene blue solution was measured by the UV-Vis Spectrophotometer after the adsorption in dark. The methylene blue adsorption by CNT-TiO_2-SiO_2 thin films that heat treated under N_2 atmosphere was shown in Figure 4.41. The decrease absorbance at 664.5nm indicates the increase in surface area so the thin films. As mentioned before, the photocatalytic activity test based on the adsorbed dye on film surface is not convenient because of different surface areas of thin films due to heat treatment temperature. In this study, the adsorption equilibrium in dark was not considered before the photocatalytic activity test and also the photocatalytic activity was measured by the decrease in concentration of methylene blue solution in the beaker not on the film.

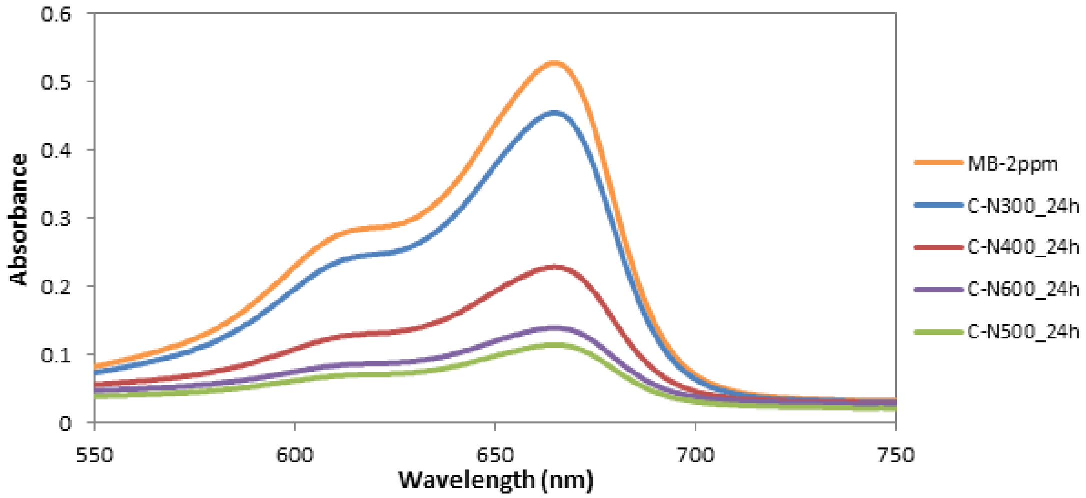

Figure 4.41 UV-Vis Spectra of methylene blue solution after the adsorption of $CNT-TiO_2-SiO_2$ thin films that heat treated under N_2 atmosphere in dark for 24h

In order to obtain the decrease in concentration of methylene blue solution, the relationship between concentration and absorbance was determined by the calibration curve and the degradation was measured by comparing of the absorbance and calibration equation. The degradation of 2ppm methylene blue solution during 180-minute-irradition is shown in between Figure 4.42 and Figure 4.48. Methylene blue is a sensitive dye to UV and even visible light. As shown in Figure 4.42, the concentration of methylene blue solution was decreased by irradiation time without any photocatalyst due to absorption. It is a common problem for photocatalytic activity tests that based on the decomposition of dyes. On the other hand, easiness of the measurement of dye concentration is a big advantage of this method. So both photo-degradation and photocatalytic degradation must be considered together while the decrease in concentration of methylene blue solution is evaluated.

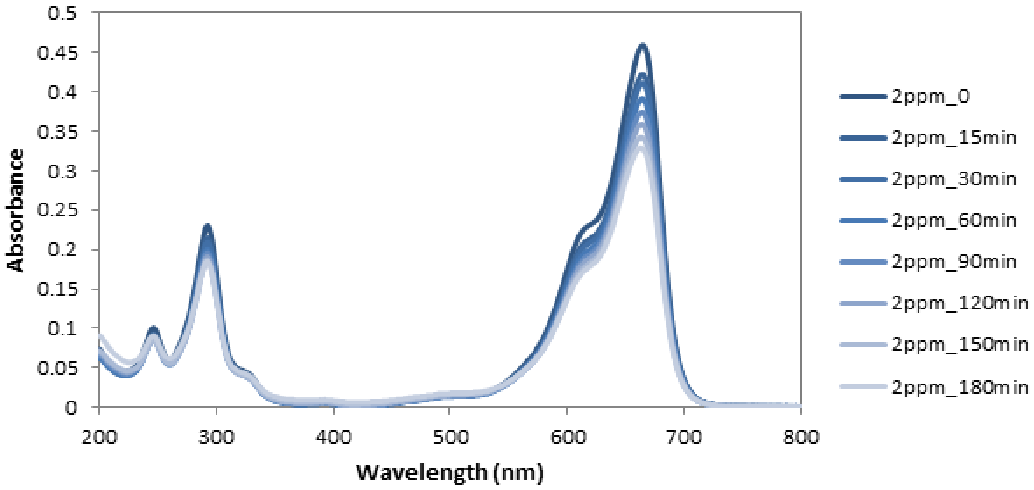

Figure 4.42 Photo-Degradation of methylene blue solution under UV-C irradiation without photocatalyst

The TiO_2-SiO_2 and CNT-TiO_2-SiO_2 samples that non heat treated and heat treated at 600°C under air and N_2 atmosphere are selected to show the change in UV-Vis spectrum of the reaction mixture with respect to time. The time course of reaction and the change in UV-Vis spectrum with respect to time for other samples are presented in Appendix D. All prepared thin film samples demonstrated significant photocatalytic activity on the degradation of methylene blue solution except C-nonHT.

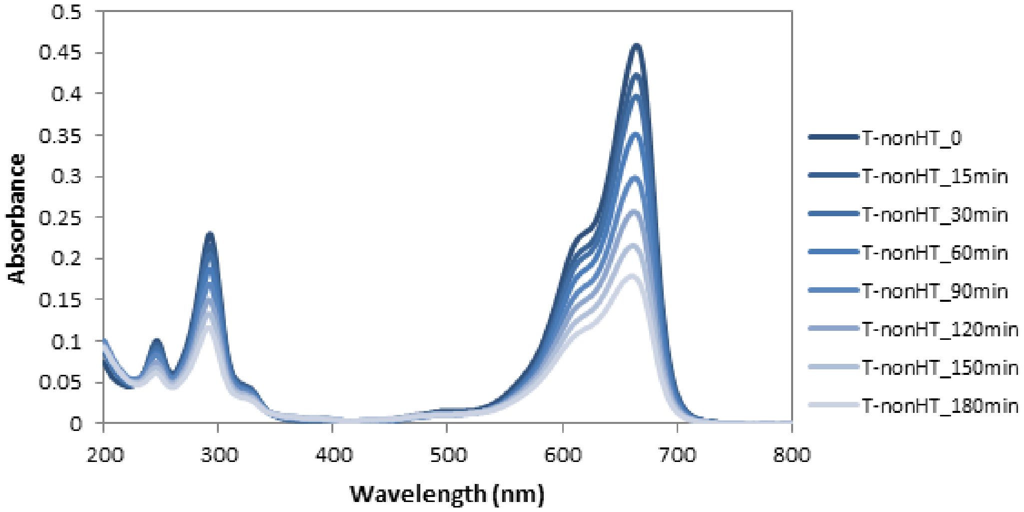

Figure 4.43 Photocatalytic degradation of methylene blue solution by T-non HT under UV-C irradiation

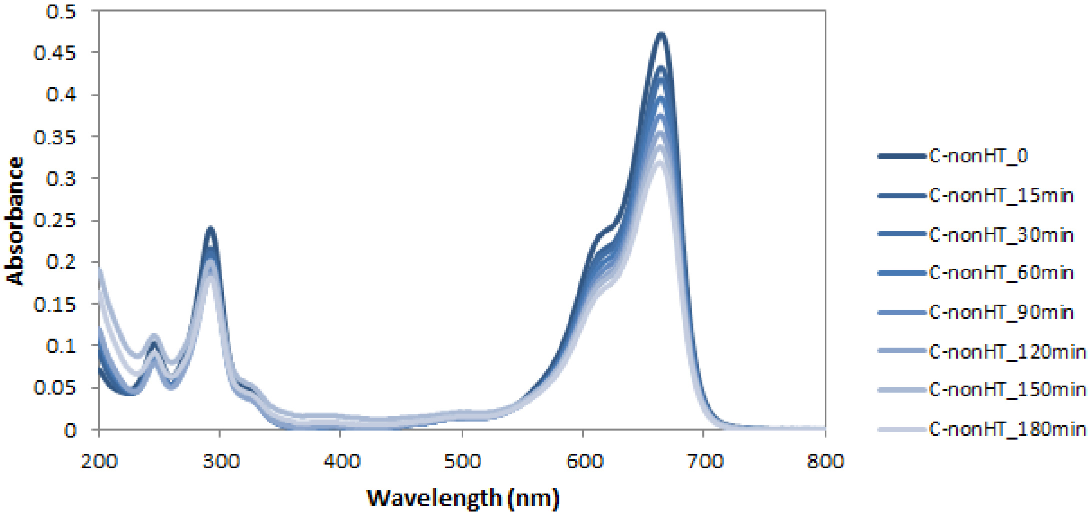

Figure 4.44 Photocatalytic degradation of methylene blue solution by C-nonHT under UV-C irradiation

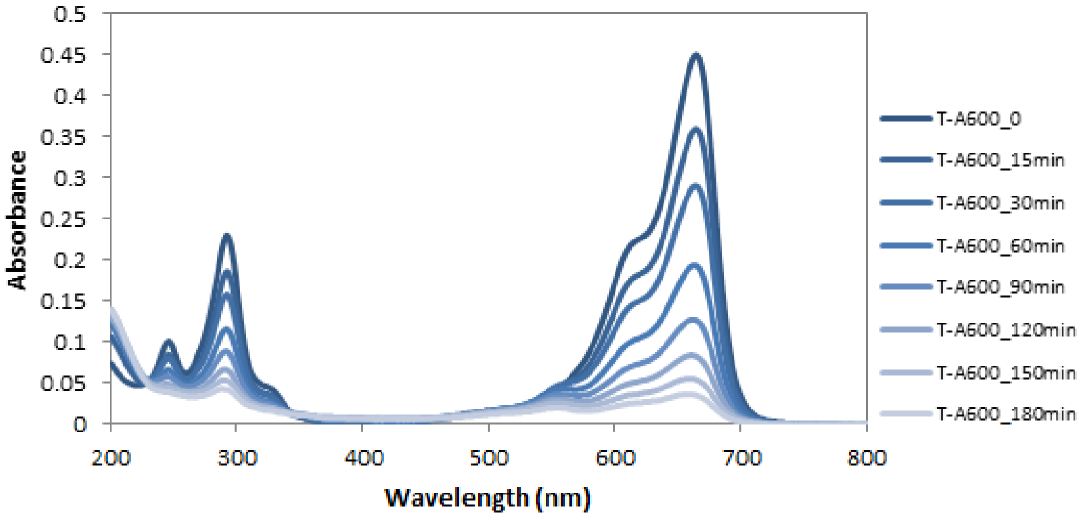

Figure 4.45 Photocatalytic degradation of methylene blue solution by T-A600 under UV-C irradiation

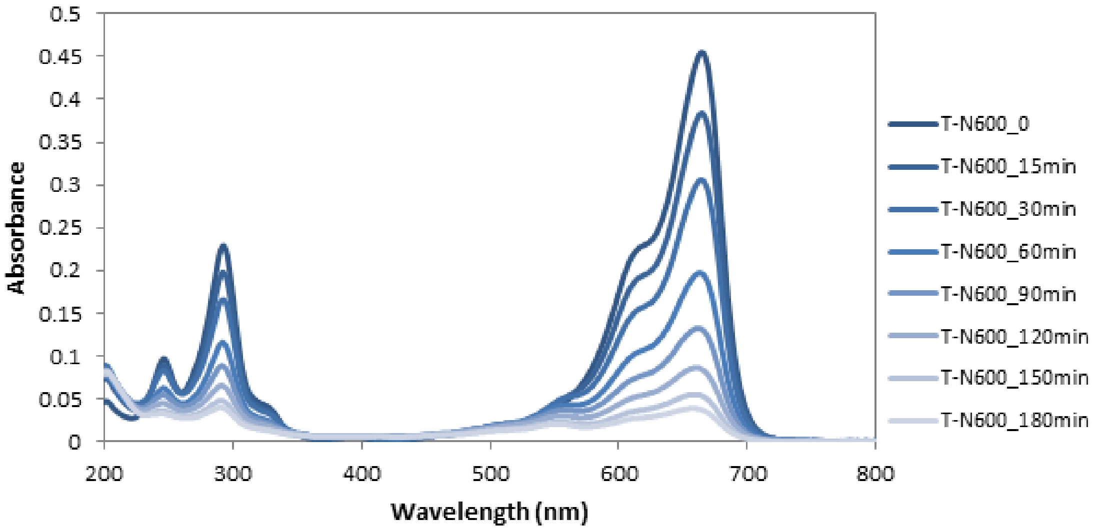

Figure 4.46 Photocatalytic degradation of methylene blue solution by T-N600 under UV-C irradiation

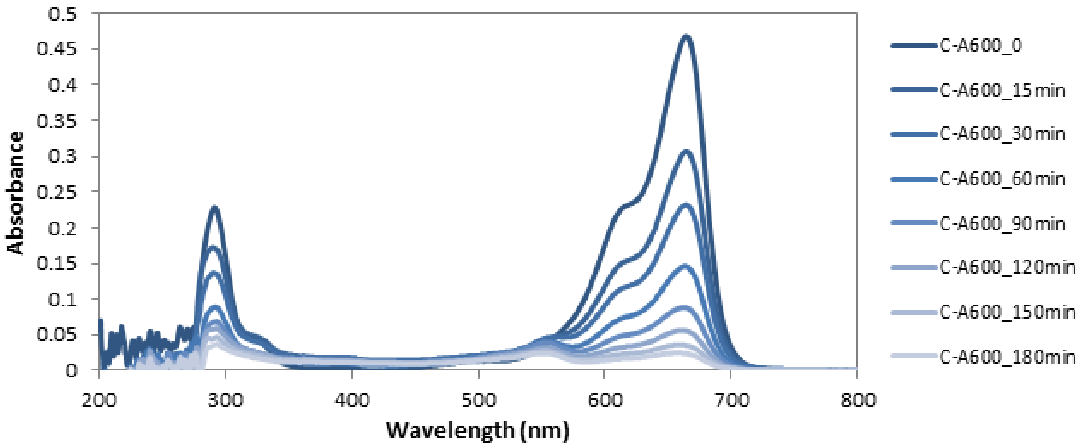

Figure 4.47 Photocatalytic degradation of methylene blue solution by C-A600 under UV-C irradiation

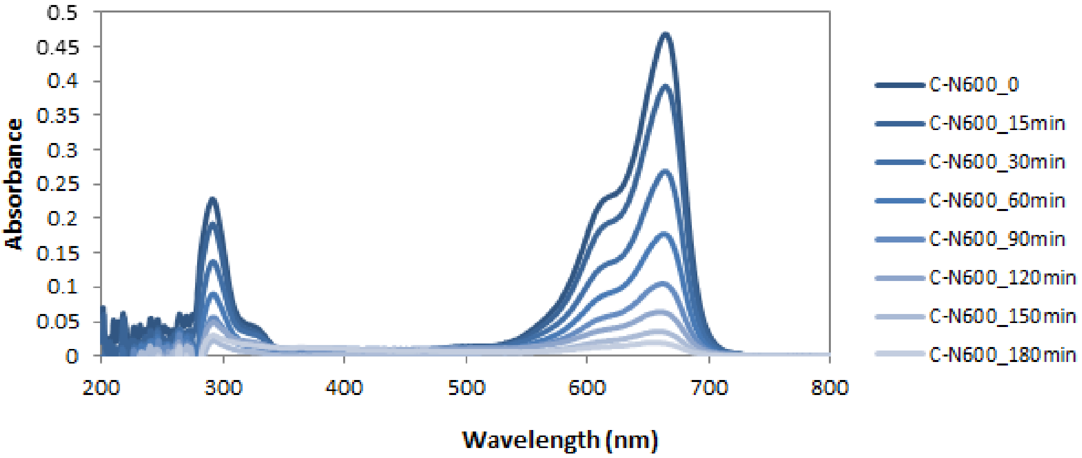

Figure 4.48 Photocatalytic degradation of methylene blue solution by C-N600 under UV-C irradiation

The photocatalytic activities of thin film samples as a function of irradiation time are shown in from Figure 4.49 to Figure 4.52. For a good understanding, the self-degradation of 2ppm methylene blue was also given in figures. The decrease in methylene blue absorbance at 664.5nm was converted to change in concentration by calibration equation and then the degradation percent was calculated by the ratio of difference of concentration at that time and at start to first concentration. The non-heat treated thin films have lower photocatalytic activity therefore it can be clearly stated that the heat treatment process enhances the photocatalytic activity of both TiO_2-SiO_2 and CNT-TiO_2-SiO_2 thin films. The photocatalytic activities of TiO_2-SiO_2 samples that non-heat treated and heat treated under air atmosphere are shown in Figure 4.49. At the end of 180 minutes of irradiation, 28% of the methylene blue photodegraded without any photocatalyst. On the other hand, 62%, 80%, 87% 85% and 92% degradation was observed over TiO_2-SiO_2 thin films, heat treated at 300^oC, 400^oC, 500^oC and 600^oC under air flow respectively. In Figure 4.50, the methylene blue conversion over bare TiO_2-SiO_2 thin film samples heat treated under nitrogen flow is shown. Similar to samples treated under air flow, 74%, 83%, 88% and 92% conversion were achieved at 300^oC, 400^oC, 500^oC and 600^oC respectively. The heat treatment under N_2 atmosphere can suppress the crystalline formation that caused lower photocatalytic activity.

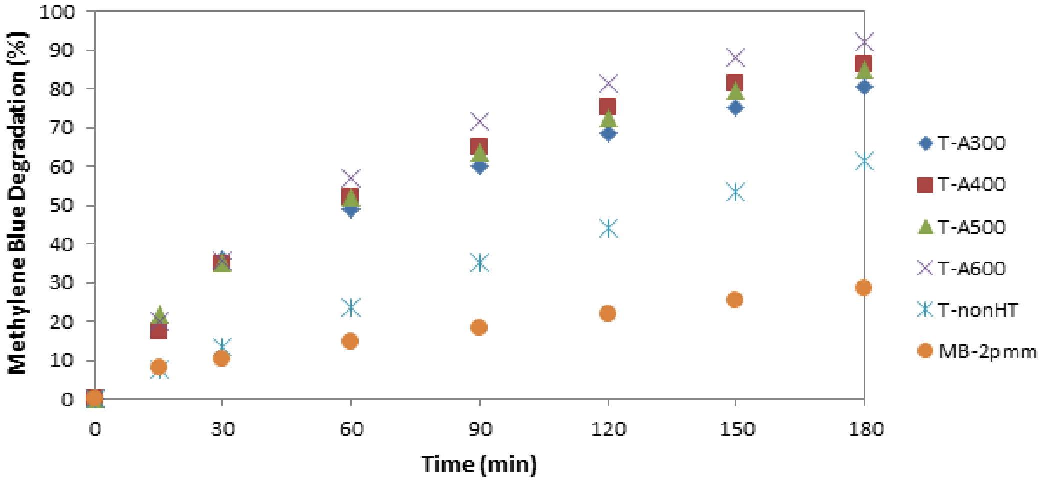

Figure 4.49 Photocatalytic activity of TiO_2-SiO_2 thin films that heat treated under air atmosphere

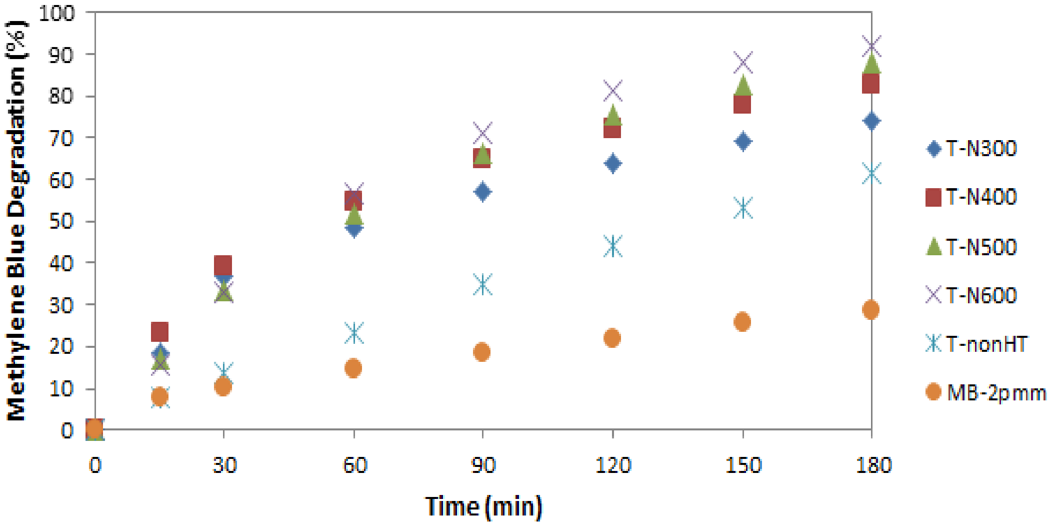

Figure 4.50 Photocatalytic activity of TiO_2-SiO_2 thin films that heat treated under N_2 atmosphere

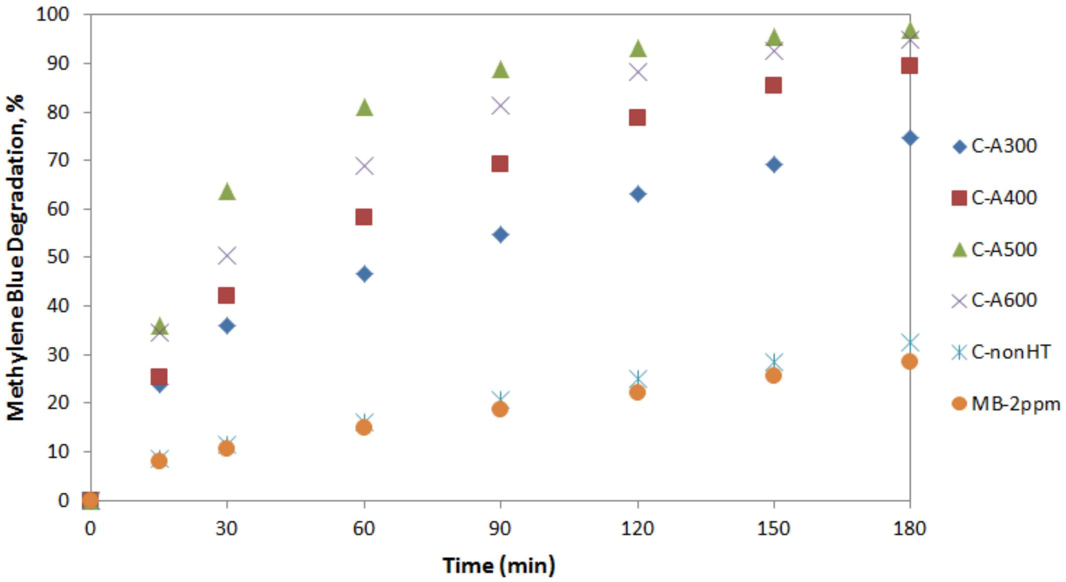

Figure 4.51 Photocatalytic activity of CNT-TiO_2-SiO_2 thin films that heat treated under air atmosphere

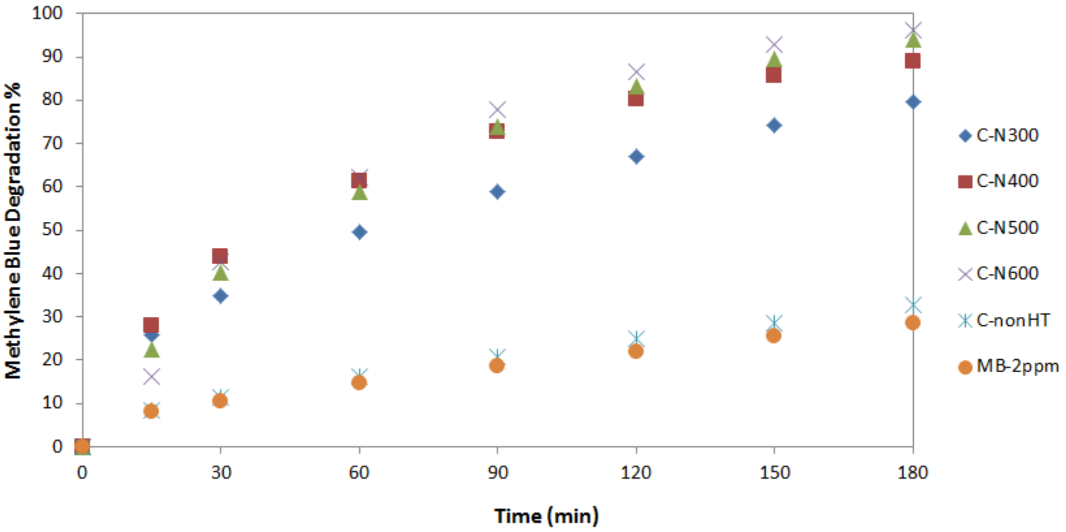

Figure 4.52 Photocatalytic activity of CNT-TiO_2-SiO_2 thin films that heat treated under N_2 atmosphere

The decomposition of methylene blue over CNT-TiO_2-SiO_2 thin film samples heat treated under air and nitrogen atmosphere are given in Figure 4.51 and Figure 4.52. The C-A500 sample has a higher initial photocatalytic activity; 80% degradation of methylene blue was achieved in 60 minutes. As shown in Figure 4.52, the samples that heat treated under N_2 atmosphere shows also similar activities. The non-heat treated sample showed almost no activity on the degradation of methylene blue but the photocatalytic activity increased by the heat treatment temperature. The sample heat treated at 600^oC under air atmosphere has lower activity than 500^oC which can be attributed to sintering of the film at high temperatures that caused the lower surface area. The maximum photocatalytic activity of TiO_2-SiO_2 thin films were achieved over T-A600 and T-N600 samples as 92% while the C-A500 and C-N600 samples have a photocatalytic activity as 96%. Besides the photocatalytic activity of T-A500 sample (85%) is dramatically lower than C-A500 (96%). It can be stated that the presence of carbon nanotubes in TiO_2-SiO_2 thin films make a contribution to photocatalytic activity depending on the heat treatment temperature and atmosphere.

The kinetics of photocatalytic degradation reaction was examined to clarify the effect of carbon nanotubes, heat treatment temperature and atmosphere on photocatalytic activity. The photocatalytic degradation reaction which obeys the first-order kinetics is expressed as;

$$-\ln \frac{C_{methylene\ blue}}{{C_{methylene\ blue}}^{0}} = k.t$$

$C_{\text{methylene blue}}$ and ${C_{\text{methylene blue}}}^{0}$ are the concentration of methylene blue at that time and initial concentration which is 2ppm, t is the irradiation time and k denotes the overall degradation rate constant of reaction. The plot of $-\ln(C_{\text{methylene blue}}/{C_{\text{methylene blue}}}^{0})$ versus time is a straight line which reveals the degradation reaction kinetics as first order. The rate constants for each reaction were obtained from the slopes of the lines and tabulated in Table 4.12. The rate constant of C-A500 sample is $0.0211 min^{-1}$ which is the maximum value as expected. The non-heat treated CNT-TiO_2-SiO_2

sample has the lowest rate constant as 0.0023min^{-1} which is nearly same with the rate constant of the self-degradation reaction. As discussed above, the addition of carbon nanotubes decreases the surface area of the thin film which results the low photocatalytic activity. On the other hand, it is obviously seen that the rate constant of CNT-TiO_2-SiO_2 thin films are higher than the TiO_2-SiO_2 thin films. Hence the photocatalytic activity of TiO_2-SiO_2 thin films can be enhanced significantly in the presence of carbon nanotubes.

Table 4.12 Rate constants of methylene blue degradation reaction

Heat Treatment Temperature (^oC)	Rate constant, k(min^{-1})			
	TiO_2-SiO_2		CNT-TiO_2-SiO_2	
	AIR	**N_2**	**AIR**	**N_2**
MB(2ppm)	0.002	0.002	0.002	0.002
nonHT	0.0051	0.0053	0.0023	0.0023
300	0.0095	0.0082	0.0082	0.093
400	0.0114	0.0105	0.0128	0.0132
500	0.0108	0.0119	0.0211	0.0153
600	0.0142	0.014	0.0174	0.0175

CHAPTER 5

CONCLUSIONS

The effect of CNT addition on the structure and photocatalytic activity of titania was examined. The coating solution is prepared by sol-gel technique and the thin films were coated on glass substrates by dip coating. The thin films were heat treated at different temperature under air and N_2 flow in order to investigate the effect of heat treatment temperature and atmosphere. The thin films were characterized by thermal analysis, X-ray diffraction, scanning electron microscopy and energy dispersive X-ray spectroscopy, elemental carbon analysis, X-ray photoelectron spectroscopy and UV-Visible spectroscopy. Photocatalytic activities of the thin films were tested by the methylene blue degradation test.

The effect of heat treatment on CNT-TiO_2-SiO_2 nanocomposites was examined by thermogravimetric analysis and differential thermal analysis. The bare carbon nanotubes which used in preparing the nanocomposite were analyzed under air and N_2 flow. The oxidation temperature of carbon nanotubes was found as 632^oC under air flow whereas no reaction was observed under nitrogen flow as expected. The colloidal solution which contains TiO_2-SiO_2 was dried and the powder was analyzed in same way. In air flow, the evaporation of adsorbed water and other volatiles (50-150^oC), oxidation or decomposition of organic residuals (~360^oC) and the crystallization (~450^oC) were observed while the total weight loss is about 40%. In N_2 flow, similar thermal behavior was exhibited for TiO_2-SiO_2 powder sample whereas the less mass loss was observed due to the absence of oxidizing atmosphere. The TGA analysis of CNT-TiO_2-SiO_2 powder sample under air flow exhibited the oxidation of CNT was at 487^oC which indicated dramatic decrease according to the bare CNT sample. The titania-silica catalyzed the oxidation reaction of CNTs. In N_2 flow, the oxidation of volatile organics cannot be observed but the total mass loss is the same with the sample heat treated under air flow. It may be caused by the oxidation of the carbon nanotubes by surface oxygen or –OH species which reduces the Ti^{4+} (TiO_2) to Ti^{3+}.

X-ray diffraction analysis indicated that the CNT addition enhanced the crystallinity at lower temperature under air flow while the TiO_2-SiO_2 thin film sample has a crystallization temperature above 500°C. It can be stated the oxidation of CNT may reduce the activation energy of crystallization during the heat treatment process. The different heat treatment atmospheres resulted in similar X-ray patterns. The phase of crystalline samples were consistent with only anatase and the phase transition of anatase to rutile did not observed even after the heat treatment at 600°C. It can be explained by the short heat treatment duration and the presence of silica. Silica may have a contribution to the thermal stability of the titania. From the crystallite size calculation, it was found that the addition of carbon nanotubes has an inhibition effect on the growth of the particles in both heat treatment atmospheres.

The scanning electron microscopy images showed that there is a good corporation with carbon nanotubes and TiO_2-SiO_2 particles. The surface of thin films was homogeneous and smooth but has some cracks on it. The carbon nanotubes were seen in these cracks but not over the surface. The diameter of the carbon nanotubes was increased from 9.5 nm to over 20 nm by the decoration of TiO_2-SiO_2 matrix. The images of the thin films that heat treated at different temperatures was similar merely the sample treated at 600°C. All carbon nanotubes were decomposed under air flow whereas they were still seen in N_2 flow. EDS analysis showed a decrease in the amount of carbon but the quantitative results were misleading due to the low sensitivity of EDS analysis to carbon element.

Elementel carbon analysis is in good agreement with the results of thermal analysis. The quantity of carbon in the film was decreased by increasing heat treatment temperature for both heat treatment atmospheres. Besides the decrease for the N_2 flow is near to the air flow results. In the oxidation of carbon nanotubes, the molecular oxygen in the presence of air was used while the surface oxygen and hydroxyl groups were used under nitrogen flow. To ensure, the thin films were analyzed by the X-ray photoelectron spectroscopy.

XPS analyses were applied to the CNT- TiO_2-SiO_2 samples. In the analysis of Ti, it was seen one more peak pair for the samples which were heat treated under nitrogen atmosphere. The peak was attributed to the presence of the Ti^{3+} species on the thin film surface which showed the formation of oxygen vacancies. Ti^{3+} species has a photocatalytically active role providing the oxidative radicals. The spectrum of O 1s showed the complex splitting which can be attributed the presence of Ti-O-Ti, Si-O-Si, O-C=O, C-O for the samples heat treated under air. The samples which treated under nitrogen atmosphere did not have the oxygenated carbon species due to the lack of free oxygen. Thus it can be clearly stated that the carbon oxidation during heat treatment follows different mechanisms under air an N_2 flow. The results revealed that the carbon nanotubes were oxidized by the free oxygen molecule under air flow whereas the lattice oxygen was used under nitrogen flow. The C 1s analysis proved the decrease of the amount of carbon by increasing temperature and the oxidative strength of the molecular oxygen in the presence of air is more for the carbon oxidation than the lattice oxygen.

UV-Vis spectroscopy indicated the light absorption edges of the thin films in UV region. The calculated band gap data showed that the neither heat treatment temperature nor heat treatment atmosphere have a significant effect on the band gap.

Photocatalytic activity tests revealed the heat treatment process enhances the photocatalytic activity of both TiO_2-SiO_2 and CNT-TiO_2-SiO_2 thin films due to improvement of the morphological and textural properties such as crystallinity and surface area. The lower activity of the sample heat treated at 600^oC under air atmosphere than 500^oC can be attributed to sintering of the film and so decrease in surface area. The methylene blue degradation reaction was indicated that the carbon nanotube added samples have higher photocatalytic activity than bare TiO_2-SiO_2 samples.

CHAPTER 6

RECOMMENDATIONS

The investigation of the surface area of the thin films is recommended to analyze the effect of the addition carbon nanotubes and silica, heat treatment temperature and atmosphere on the surface area and pore size.

The SEM and EDS analyses should be repeated on the different points of the film surface to increase the accuracy of the results.

The heat treatment temperature can be increased for the heat treatment under nitrogen atmosphere in order to improve the crystallinity by preventing the sintering. Also the formation of Ti^{3+} can be enhanced which leads the absorption edge of the samples to visible light.

The photocatalytic activity can be examined by antimicrobial activity test in order to gain insight about the antimicrobial properties of the thin films.

Different substrate surfaces can be chosen according to the application type of the future studies.

New wet coating techniques can be applied such as electrophoretic deposition (EPD) to obtain different surface properties.

REFERENCES

[1] Su, C., Hong, B.Y., Tseng C.M., *Sol–gel preparation and photocatalysis of titanium dioxide*, Catalysis Today, vol. 96, no. 3, pp. 119–126, 2004.

[2] Fujishima, A., Honda, K., *Electrochemical photolysis of water at a semiconductor electrode*, Nature, vol. 238, pp. 37-38, 1972.

[3] Tobaldi, D.M., Tucci, A., Škapin, A.S., Esposito, L., *Effects of* SiO_2 *addition on* TiO_2 *crystal structure and photocatalytic activity*, J. Eur. Ceram. Soc, vol. 30, no. 12, pp. 2481–2490, 2010.

[4] Oh, W., Chen, M., *Synthesis and characterization of CNT/*TiO_2 *composites thermally derived from MWCNT and Titanium(IV) n-Butoxide*, Bull. Korean Chem. Soc., vol. 29, no. 1, pp. 159–164, 2008.

[5] Hanel, A., Moren, P., Zaleska, A., Hupka, J., *Photocatalytic Activity of* TiO_2 *Immobilized on Glass Beads*, Physicochemical Problems of Mineral Processing, vol. 45, pp. 49-56, 2010.

[6] Sampaio, M.J., Silva, C.G., Marques, R.R.N., Silva, A.M.T., Faria, J.L., *Carbon nanotube-*TiO_2 *thin films for Photocatalytic Applications*, Catalysis Today, vol. 161, pp. 91-96, 2011.

[7] Young, S. K., *Overview of Sol-Gel Science and Technology*, Army Research Laboratory Technical Reports, 2002.

[8] Strehlow, W.H., Cook, E.L., *Compilation of Energy Band Gaps in Elemental and Binary Compound Semiconductors and Insulators*, J. Phys. Chem. Ref. Data, vol. 2, no. 1, pp. 163–200, 1973.

[9] Nakata, K., Fujishima, A., *TiO_2 photocatalysis: Design and applications*, J. Photochem. Photobiol. C Photochem. Rev., vol. 13, pp. 169–189, 2012.

[10] Mo S., Ching, W.Y., *Electronic and optical properties of three phases of titanium dioxide: Rutile, anatase, and brookite,* Phys. Rev. B, vol. 51, no. 19, pp. 23–32, 1995.

[11] Paola, A.D., Bellardita, M., Palmisano, L., *Brookite, the Least Known TiO_2 Photocatalyst,* Catalysts, vol. 3, no. 1, pp. 36–73, 2013.

[12] Ma, B., Goh, G.K.L., Ma, J., *Crystallinity and photocatalytic activity of liquid phase deposited TiO_2 films,* J. Electroceramics, vol. 16, no. 4, pp. 441–445, 2006.

[13] Banerjee, S., Gopal, J., Muraleedharan, P., Tyagi, A.K., Ra,j B., *Physics and chemistry of photocatalytic titanium dioxide: Visualization of bactericidal activity using atomic force microscopy,* Curr. Sci., vol. 90, no. 10, 2006.

[14] Reddy, K. M., Manorama, S.V., Reddy, *A.R., Bandgap studies on anatase titanium dioxide nanoparticles,* Mater. Chem. Phys., vol. 78, pp. 239–245, 2002.

[15] Sakai, N., Ebina, Y., Takada, K., Sasak,i T., *Electronic band structure of titania semiconductor nanosheets revealed by electrochemical and photoelectrochemical studies,* J. Am. Chem. Soc., vol. 126, no. 18, pp. 5851–8, 2004.

[16] Hashimoto K., Irie, H., Fujishima, A., *TiO_2 Photocatalysis: A Historical Overview and Future Prospects,* Jpn. J. Appl. Phys., vol. 44, no. 12, pp. 8269–8285, 2005.

[17] Ohtani, B., *Preparing Articles on Photocatalysis—Beyond the Illusions, Misconceptions, and Speculation,* Chem. Lett., vol. 37, no. 3, pp. 216–229, 2008.

[18] Grela, M.A., Coronel, M.E.J., Colussi A.J., *Quantitative Spin-Trapping Studies of Weakly Illuminated Titanium Dioxide Sols. Implications for the Mechanism of Photocatalysis,* vol. 3654, no. 95, pp. 16940–16946, 1996.

[19] Dogu, D., *The Photocatalytic Activity of Praseodymium Doped Titanium Dioxide*, PhD.Thesis, Middle East Technical University, 2012.

[20] He, C., Tian, B., Zhang, J., *Thermally stable* SiO_2*-doped mesoporous anatase* TiO_2 *with large surface area and excellent photocatalytic activity*, J. Colloid Interface Sci., vol. 344, no. 2, pp. 382–9, 2010.

[21] Zhang, Z., Wang, C., Zakaria, R., Ying, J.Y., *Role of Particle Size in Nanocrystalline* TiO_2 *-Based Photocatalysts*, Journal of Physical Chemistry B., pp. 10871–10878, 1998.

[22] Yasong, Z., Guowei, J., *Study on Properties of Composite Oxides* TiO_2/SiO_2, Chinese J. Chem. Eng., vol. 10, no. 3, pp. 349–353, 2002.

[23] Nguyen, T.V., Lee, H.C., Khan, M. Alam, Yang, O. B., *Electrodeposition of* TiO_2/SiO_2 *nanocomposite for dye-sensitized solar cell,* Sol. Energy, vol. 81, no. 4, pp. 529–534, 2007.

[24] Leary, R., Westwood, A., *Carbonaceous nanomaterials for the enhancement of* TiO_2 *photocatalysis,* Carbon N. Y., vol. 49, no. 3, pp. 741–772, Mar. 2011.

[25] Woan, K., Pyrgiotakis, G. and Sigmund, W., *Photocatalytic Carbon-Nanotube-*TiO_2 *Composites,* Adv. Mater., vol. 21, no. 21, pp. 2233–2239, 2009.

[26] Sonawane, R.S., Dongare, M. K., *Sol–gel synthesis of Au/*TiO_2 *thin films for photocatalytic degradation of phenol in sunlight,* J. Mol. Catal. A Chem., vol. 243, no. 1, pp. 68–76, 2006.

[27] Wu, M., Lin, G., Chen, D., Wang, G., He D., Feng, S., Xu, R., *Sol-Hydrothermal Synthesis and Hydrothermally Structural Evolution of Nanocrystal Titanium Dioxide*, no. 21, pp. 1974–1980, 2002.

[28] Young, S.K., *Overview of Sol-Gel Science and Technology,* in Army Research Laboratory-Technical Reports, 2002.

[29] Brinker, C.J., Scherer, G.W., *Sol-gel Science: The Physics and Chemistry of Sol-gel Processing,* Academic Press, San Diego, 908, 1990.

[30] Hanaor, D.a.H., Sorrell, C.C., *Review of the anatase to rutile phase transformation*, J. Mater. Sci., vol. 46, no. 4, pp. 855–874, 2010.

[31] Wang, G.J., Chou, S.W., *Electrophoretic deposition of uniformly distributed* TiO_2 *nanoparticles using an anodic aluminum oxide template for efficient photolysis,* Nanotechnology, vol. 21, 2010.

[32] Ovenstone, J., Yanagizawa, K., *Effect of hydrothermal treatment of amorphous titania on the phase change from anatase to rutile during calcination,* Chemistry Materials, vol 11, no.11, pp. 2770-2774, 1999.

[33] Yanagizawa, K., Yamamoto, Y., Feng, Q., Yamasaki, N., *Formation mechanism of fine anatase crystals from amorphous titania under hydrothermal conditions,* Journal of Materials Research, vol. 13, no. 04, pp. 825-829, 1998.

[34] Eder, D., Windle, A.H., *Morphology Control of CNT-*TiO_2 *hybrid materials and rutile nanotubes*, Journal of Materials Chemistry, 2008, 18, 2036-2043

[35] Yürüm, A., *The Synthesis of Titanium Dioxide Photocatalysts by Sol-Gel Method: The Effect of Hydrothermal Treatment Conditions and Use of Carbon Nanotube Template,* PhD.Thesis, Middle East Technical University, 2009.

[36] Zhao, B., Zhang, L., Wang, X., Yang, J., *Surface functionalization of vertically-aligned carbon nanotube forests by radio-frequency Ar/*O_2*plasma,* Carbon, vol. 50, pp 2710–2716, 2012.

[37] Biesinger, M.C., Leo W.M.L., Gerson, A.R., Smart, R.St.C., *Resolving surface chemical states in XPS analysis of first row transition metals, oxides and hydroxides: Sc, Ti, V, Cu and Zn*, Applied Surface Science, vol. 257, pp. 887–889, 2010.

[38] H. Liu, H. T. Ma, X. Z. Li, W. Z. Li, M. Wu, and X. H. Bao, *The enhancement of* TiO_2 *photocatalytic activity by hydrogen thermal treatment*, Chemosphere, vol. 50, no. 1, pp. 39–46, 2003.

[39] Sirisuk, A., Klansorn, E., Praserthdam, P., *Effects of reaction medium and crystallite size on* Ti^{3+} *surface defects in titanium dioxide nanoparticles prepared by solvothermal method*, Catalysis Communications, vol. 9, no. 9, pp. 1810– 1814, 2008.

[40] Chen X.Q., Liu, H.B., Gu, G. B., *Preparation of nanometer crystalline* TiO_2 *with high photo-catalytic activity by pyrolysis of titanyl organic compounds and photocatalytic mechanism*, Materials Chemistry and Physics, vol. 91, no. 2-3, pp. 317–324, 2005.

[41] Krzanowski, J.E., Leuchtner, R.E., *Chemical, Mechanical, and Tribological Properties of Pulsed-Laser-Deposited Titanium Carbide and Vanadium Carbide*, Jornal of. American Ceramic Society, vol. 80, no. 5, pp. 1277-1280, 1997.

[42] Jaeger, D., Patscheider, J., *A complete and self-consistent evaluation of XPS spectra of TiN,* Journal of Electron Spectroscopy and Related Phenomena, vol. 185, no. 11, pp 523-534, 2012.

[43] Wang, L., Sun Y.P., Xu, B.S., *Surface chemical structure of titania-silica nanocomposite powder*, Chinese Science Bulletin, vol. 53, no. 19, pp 2964-2972, 2008.

[44] Haque. M.M., Bahnemann, D., Muneer, M., *Photocatalytic Degradation of Organic Pollutants: Mechanisms and Kinetics,* Organic Pollutants Ten Years After the Stockholm Convention-Environmental and Analytical Update, Intech, Chapter 12, 2012.

APPENDIX A

PROPERTIES OF CARBON NANOTUBES

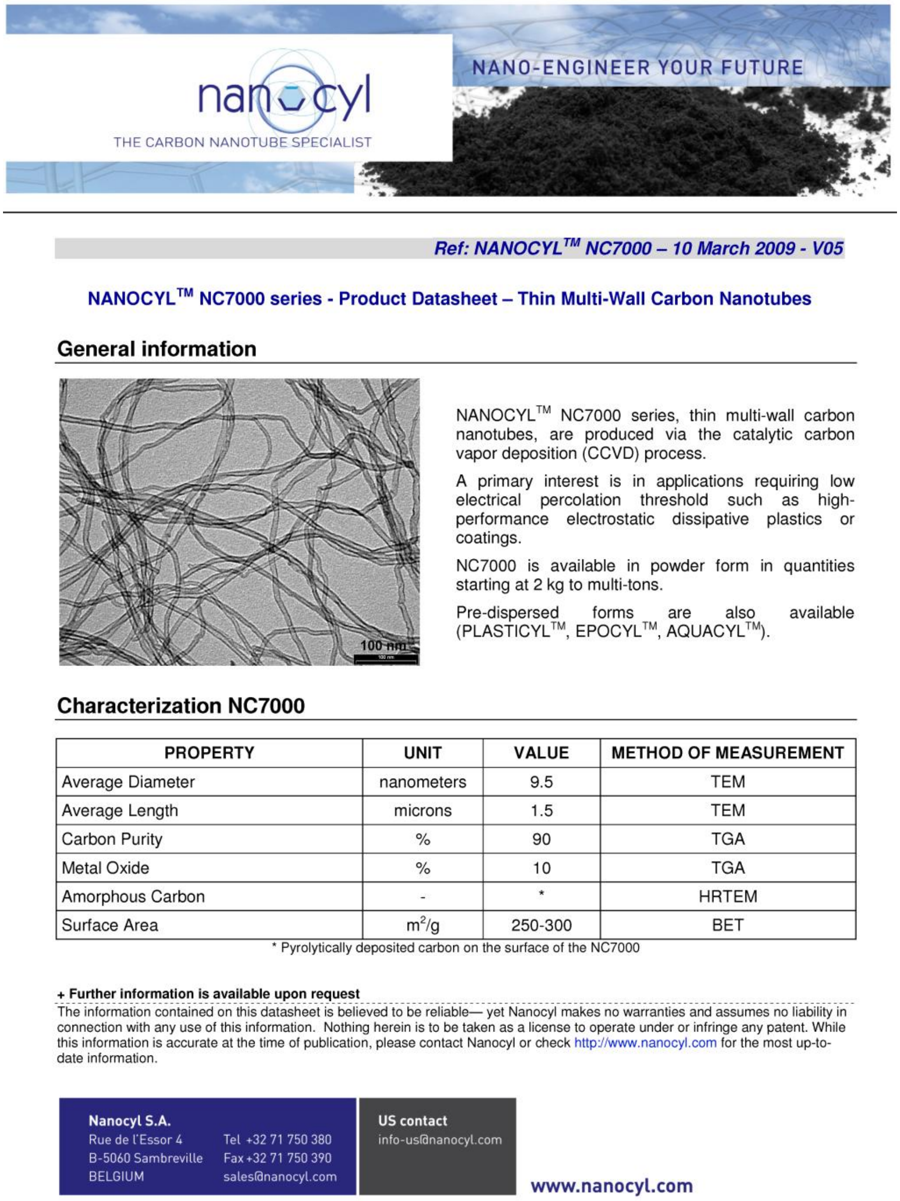

nanocyl
THE CARBON NANOTUBE SPECIALIST

NANO-ENGINEER YOUR FUTURE

Ref: NANOCYL™ NC7000 – 10 March 2009 - V05

NANOCYL™ NC7000 series - Product Datasheet – Thin Multi-Wall Carbon Nanotubes

General information

100 nm

NANOCYL™ NC7000 series, thin multi-wall carbon nanotubes, are produced via the catalytic carbon vapor deposition (CCVD) process.

A primary interest is in applications requiring low electrical percolation threshold such as high-performance electrostatic dissipative plastics or coatings.

NC7000 is available in powder form in quantities starting at 2 kg to multi-tons.

Pre-dispersed forms are also available (PLASTICYL™, EPOCYL™, AQUACYL™).

Characterization NC7000

PROPERTY	UNIT	VALUE	METHOD OF MEASUREMENT
Average Diameter	nanometers	9.5	TEM
Average Length	microns	1.5	TEM
Carbon Purity	%	90	TGA
Metal Oxide	%	10	TGA
Amorphous Carbon	-	*	HRTEM
Surface Area	m^2/g	250-300	BET

* Pyrolytically deposited carbon on the surface of the NC7000

+ Further information is available upon request

The information contained on this datasheet is believed to be reliable— yet Nanocyl makes no warranties and assumes no liability in connection with any use of this information. Nothing herein is to be taken as a license to operate under or infringe any patent. While this information is accurate at the time of publication, please contact Nanocyl or check http://www.nanocyl.com for the most up-to-date information.

Nanocyl S.A.
Rue de l'Essor 4
B-5060 Sambreville
BELGIUM

Tel +32 71 750 380
Fax +32 71 750 390
sales@nanocyl.com

US contact
info-us@nanocyl.com

www.nanocyl.com

APPENDIX B

X-RAY PHOTOELECTRON SPECTROSCOPY

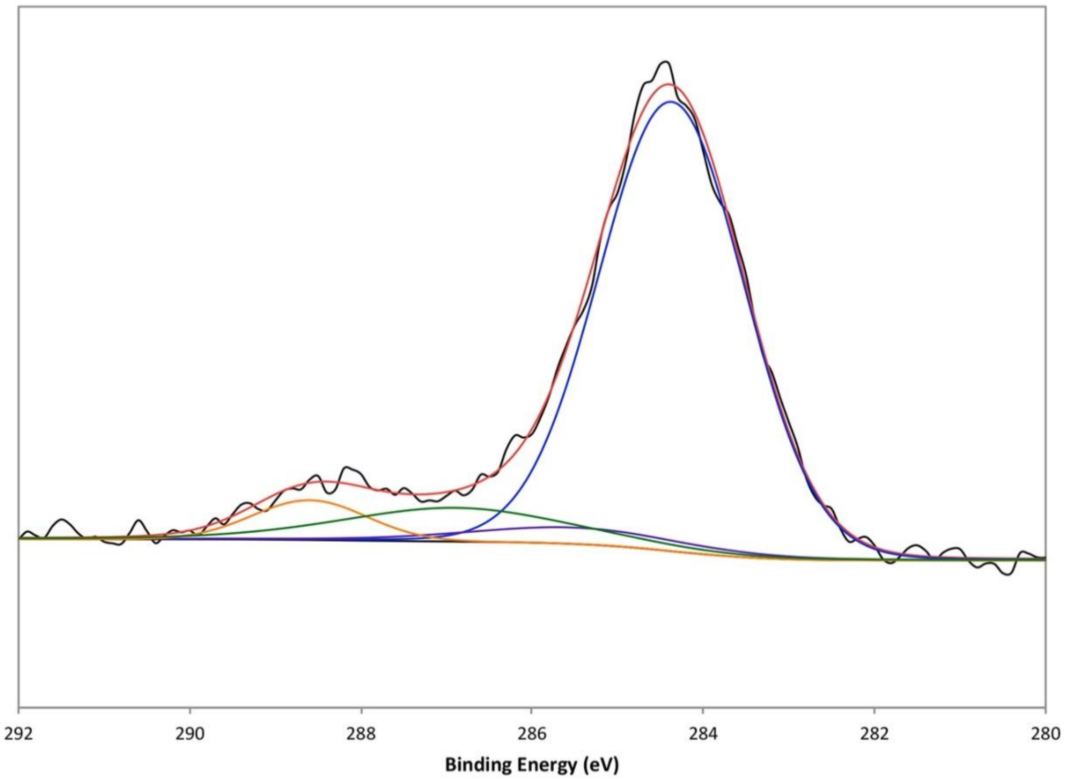

Figure B.1 C 1s XPS spectrum of C-A400

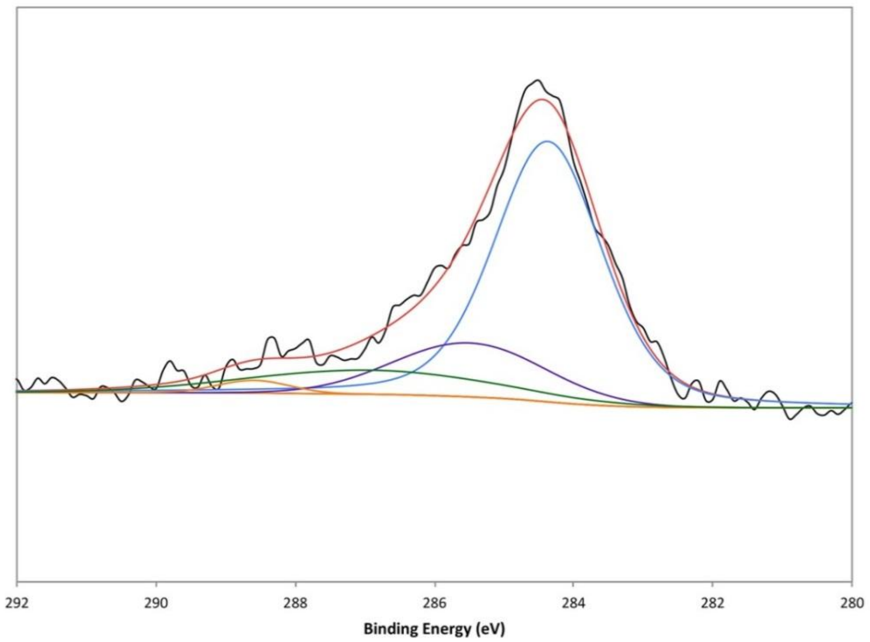

Figure B.2 C 1s XPS spectrum of C-A500

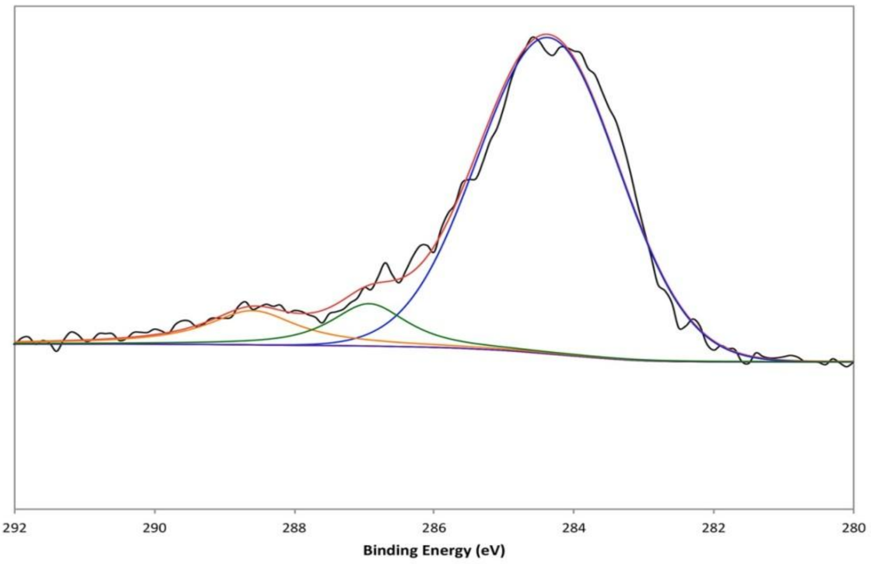

Figure B.3 C 1s XPS spectrum of C-N400

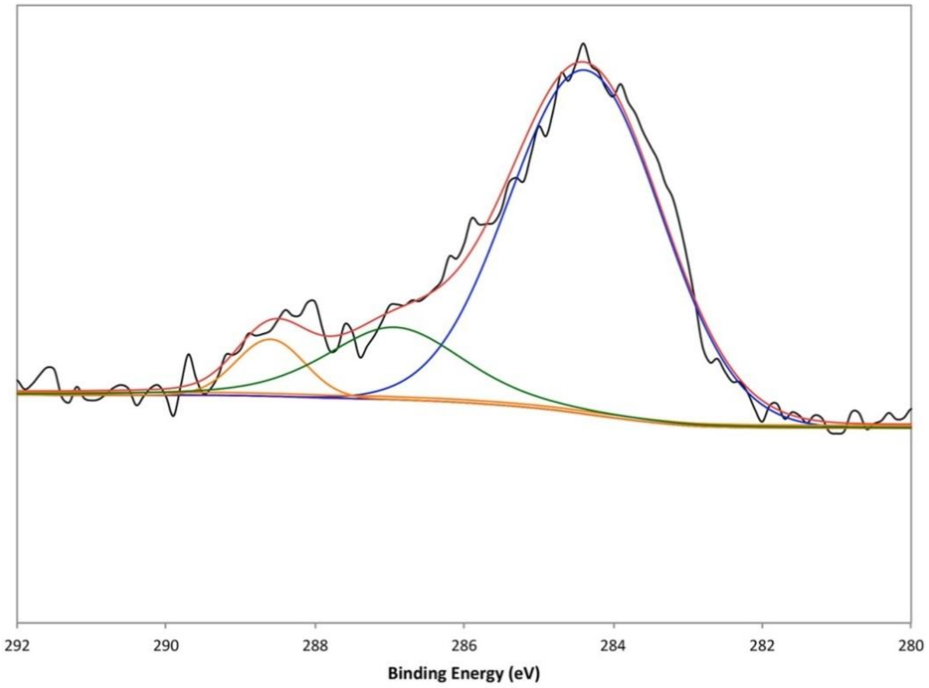

Figure B.4 C 1s XPS spectrum of C-N500

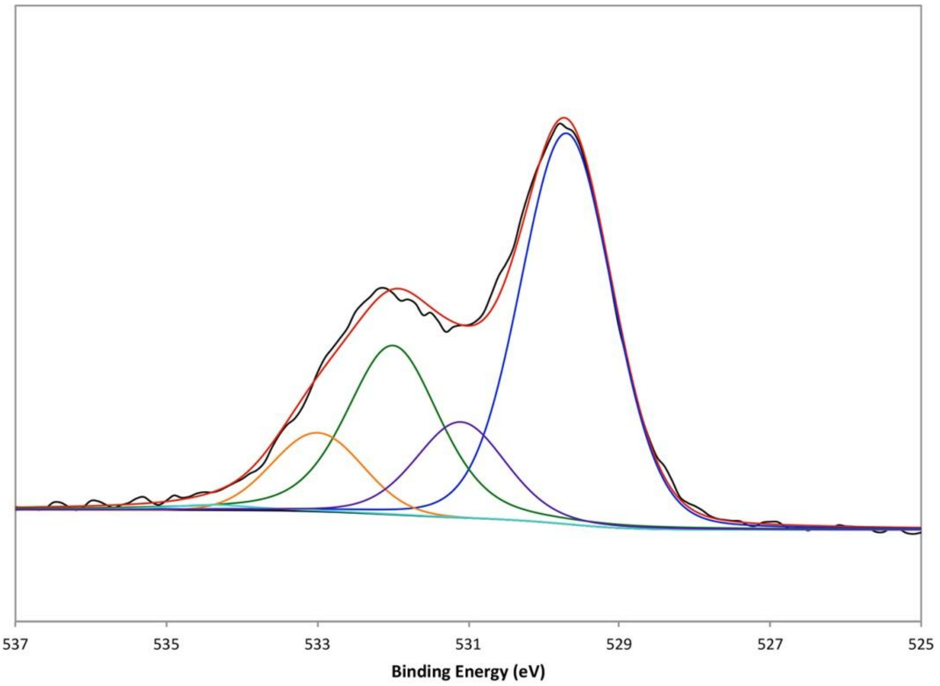

Figure B.5 O 1s XPS spectrum of C-A400

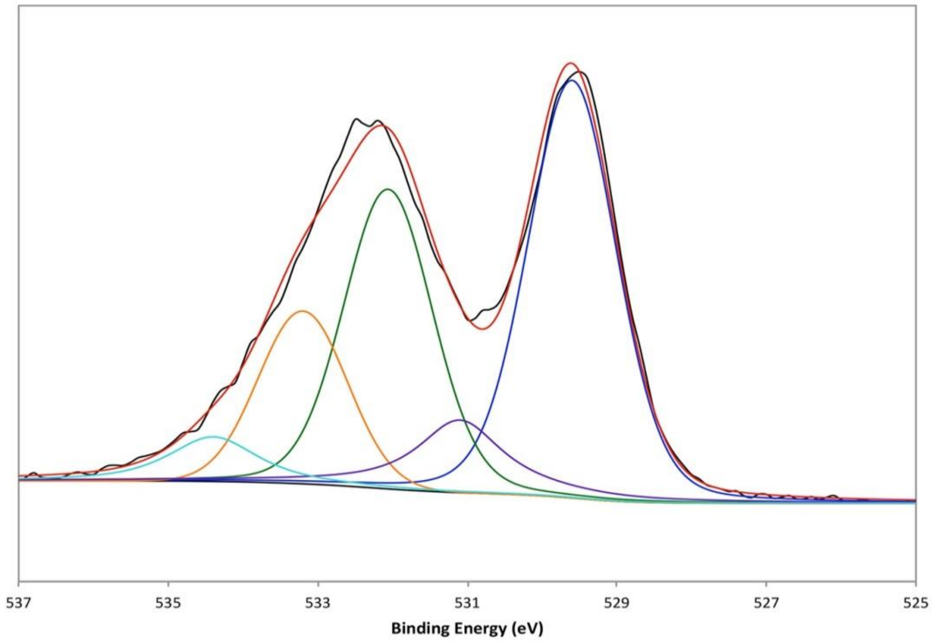

Figure B.6 O 1s XPS spectrum of C-A500

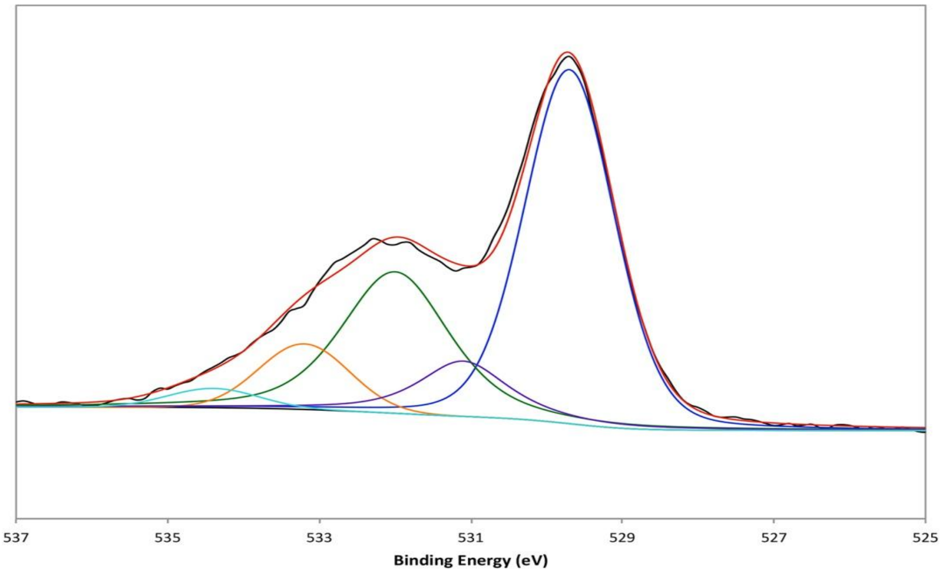

Figure B.7 O 1s XPS spectrum of C-N400

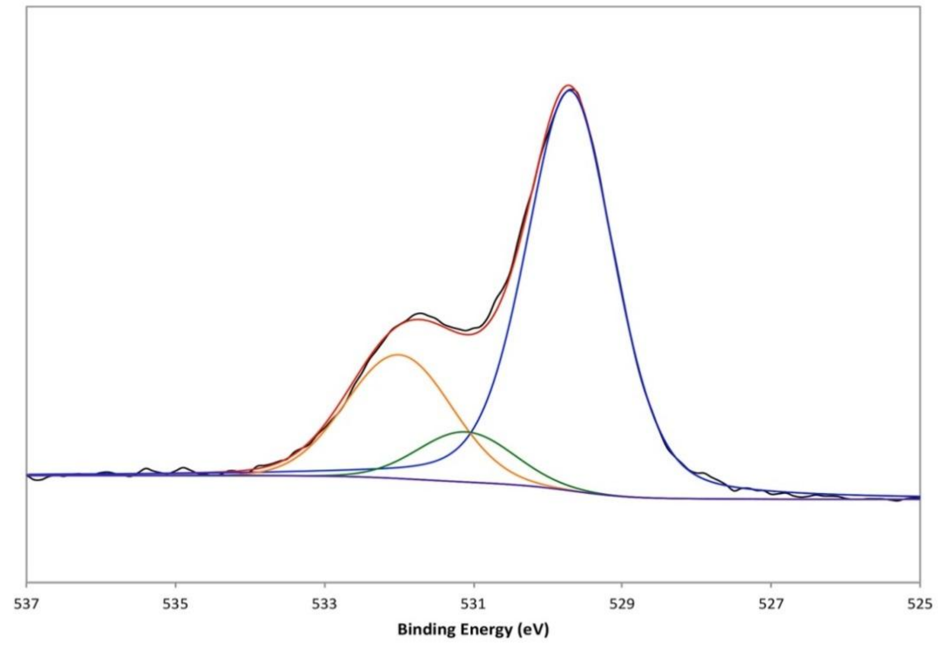

Figure B.8 O 1s XPS spectrum of C-N500

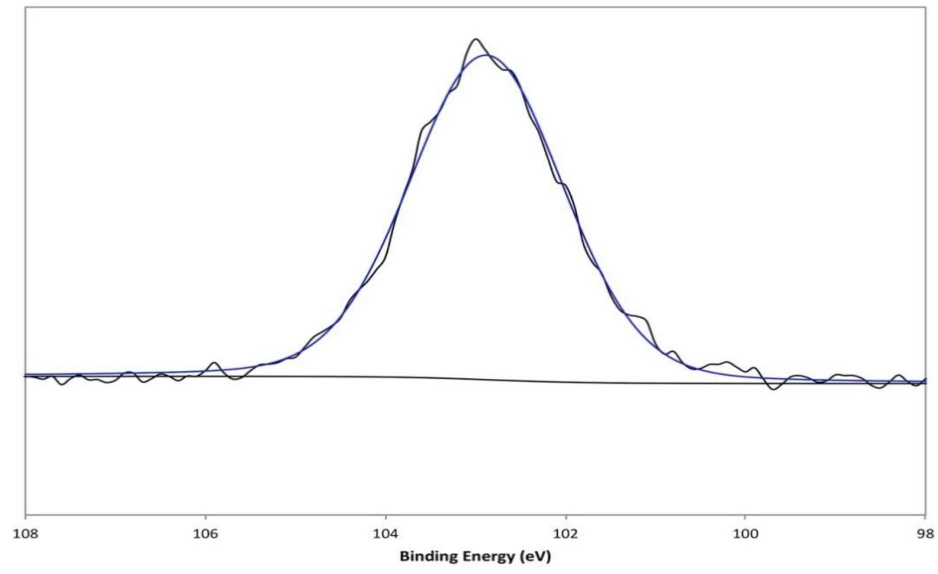

Figure B.9 Si 2p XPS spectrum of C-A400

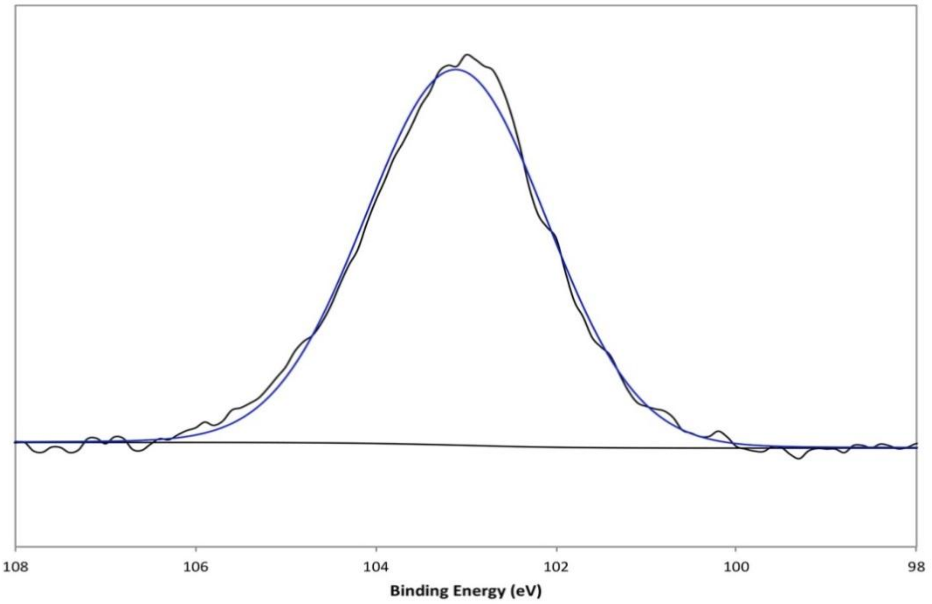

Figure B.10 Si 2p XPS spectrum of C-A500

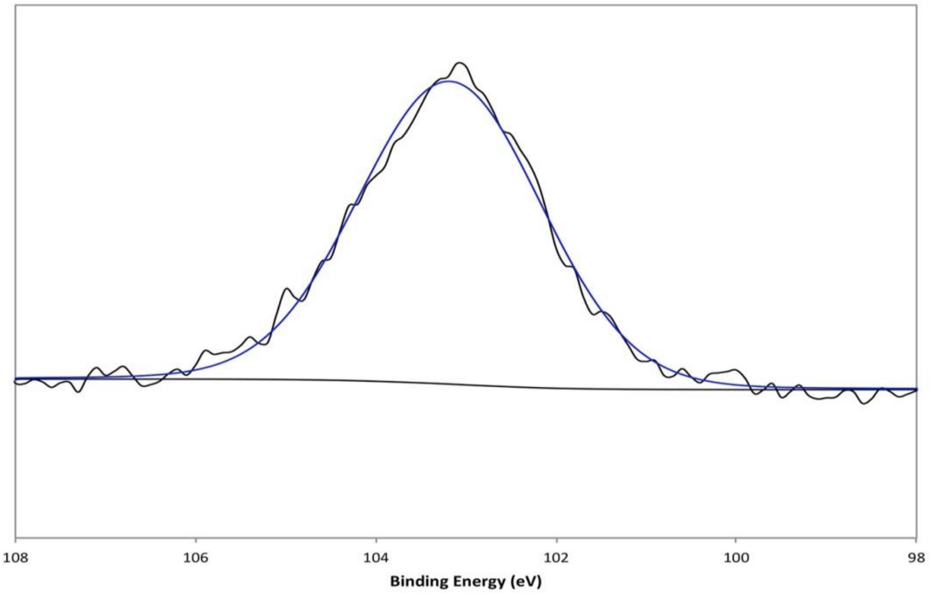

Figure B.11 Si 2p XPS spectrum of C-N400

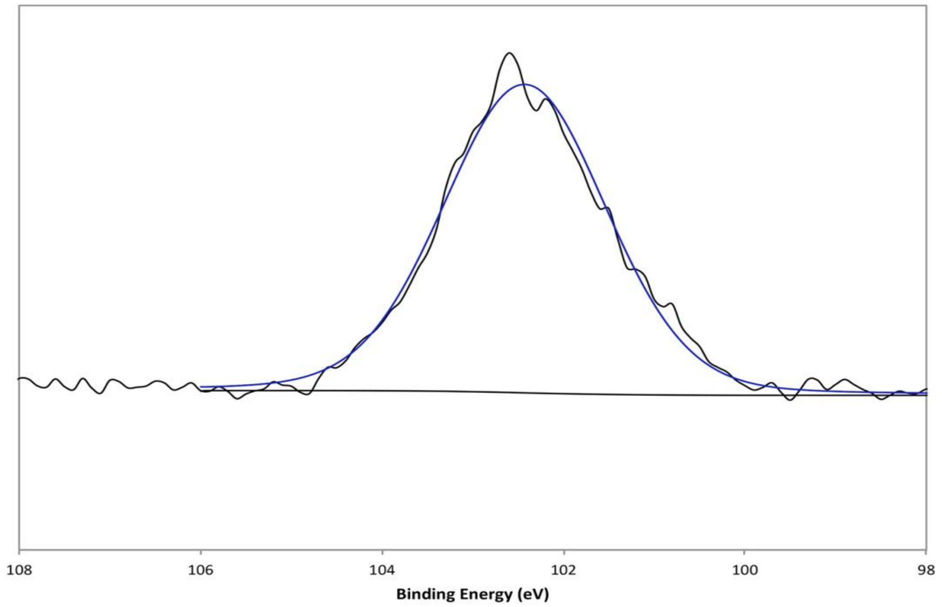

Figure B.12 Si 2p XPS spectrum of C-N500

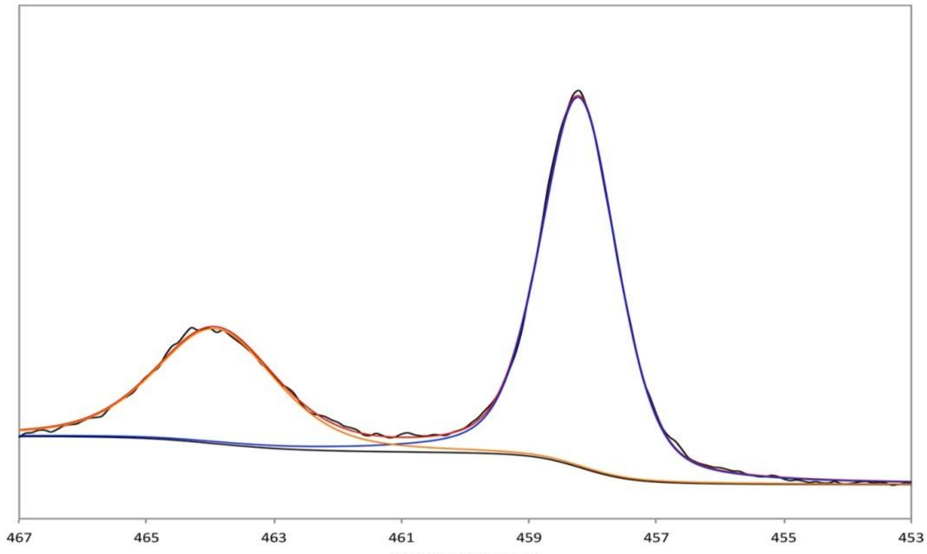

Figure B.13 Ti 2p XPS spectrum of C-A400

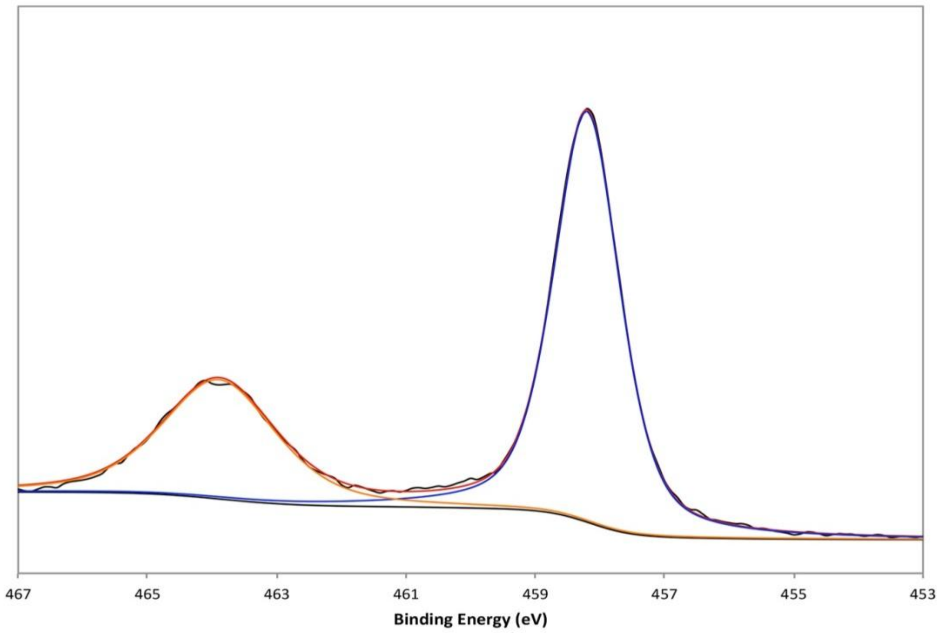

Figure B.14 Ti 2p XPS spectrum of C-A500

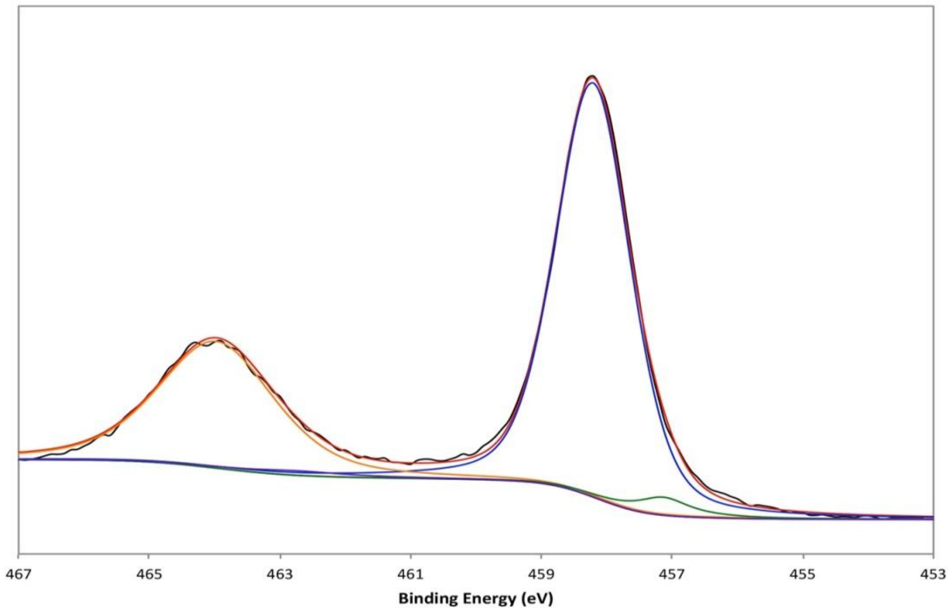

Figure B.15 Ti 2p XPS spectrum of C-N400

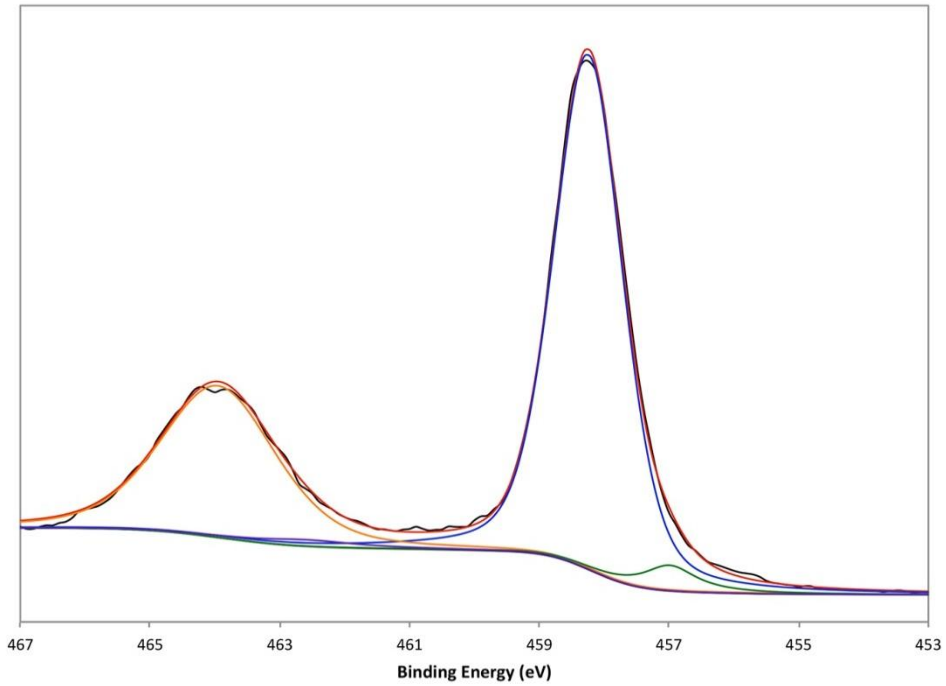

Figure B.16 Ti 2p XPS spectrum of C-N500

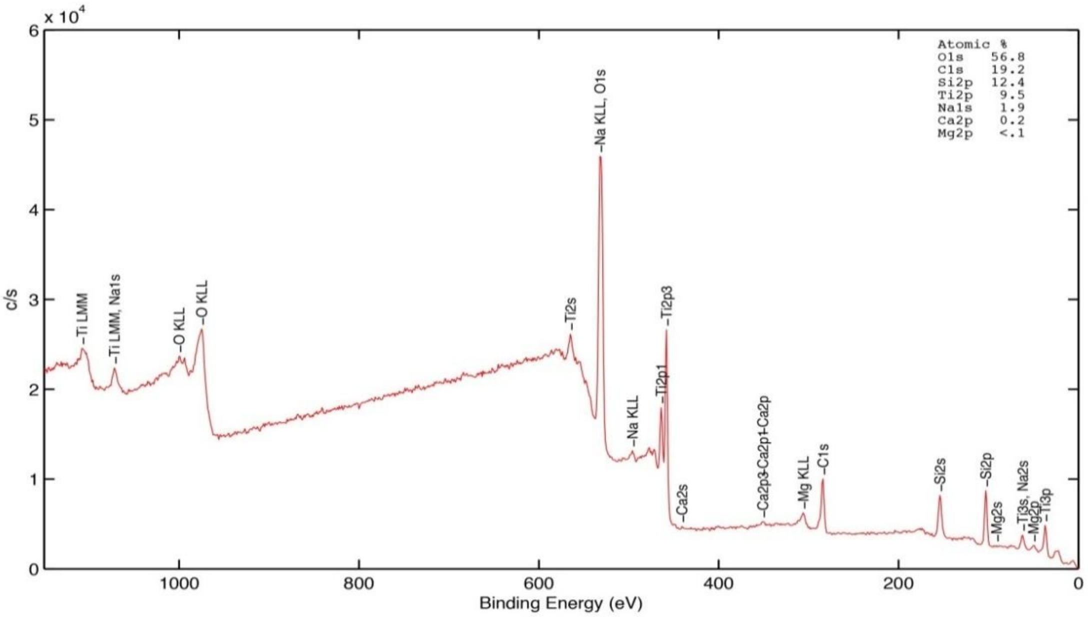

Figure B.17 Survey XPS scan of C-A300

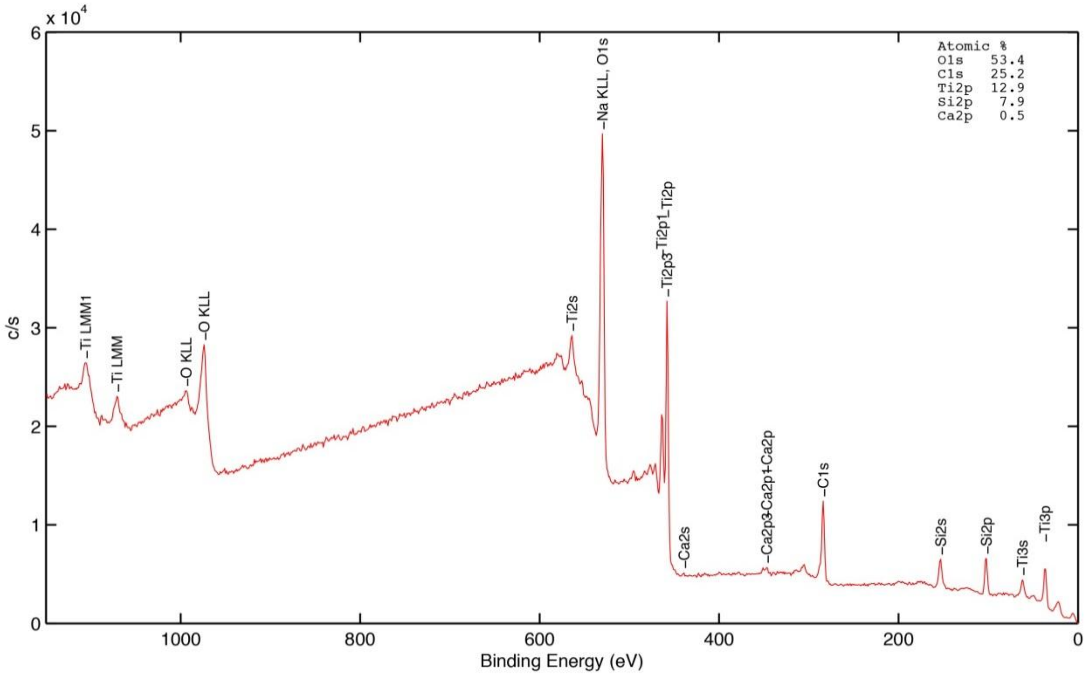

Figure B.18 Survey XPS scan of C-A400

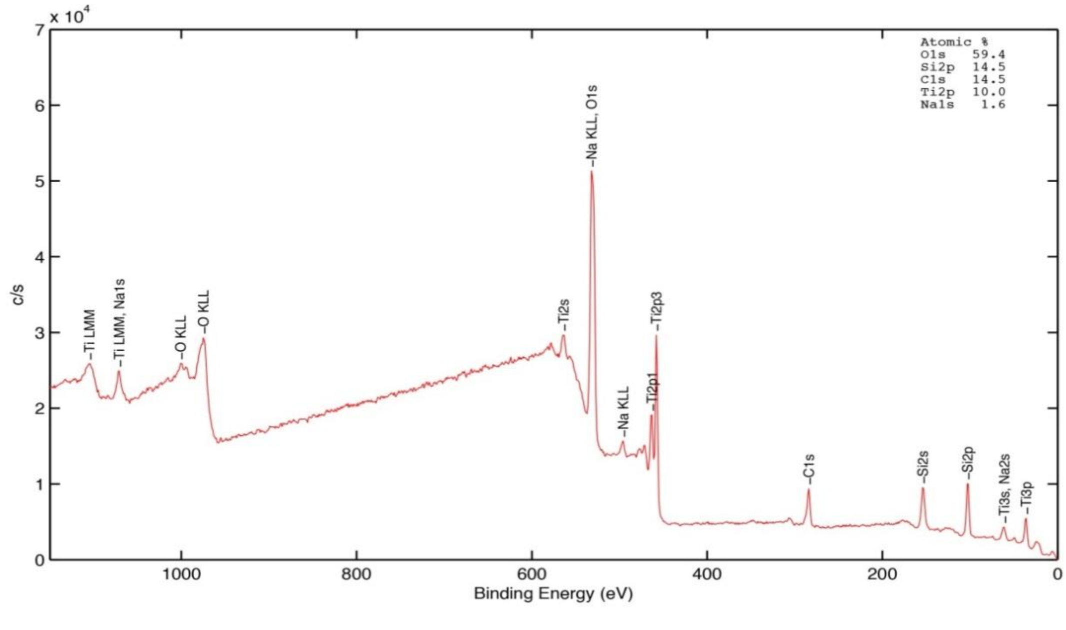

Figure B.19 Survey XPS scan of C-A500

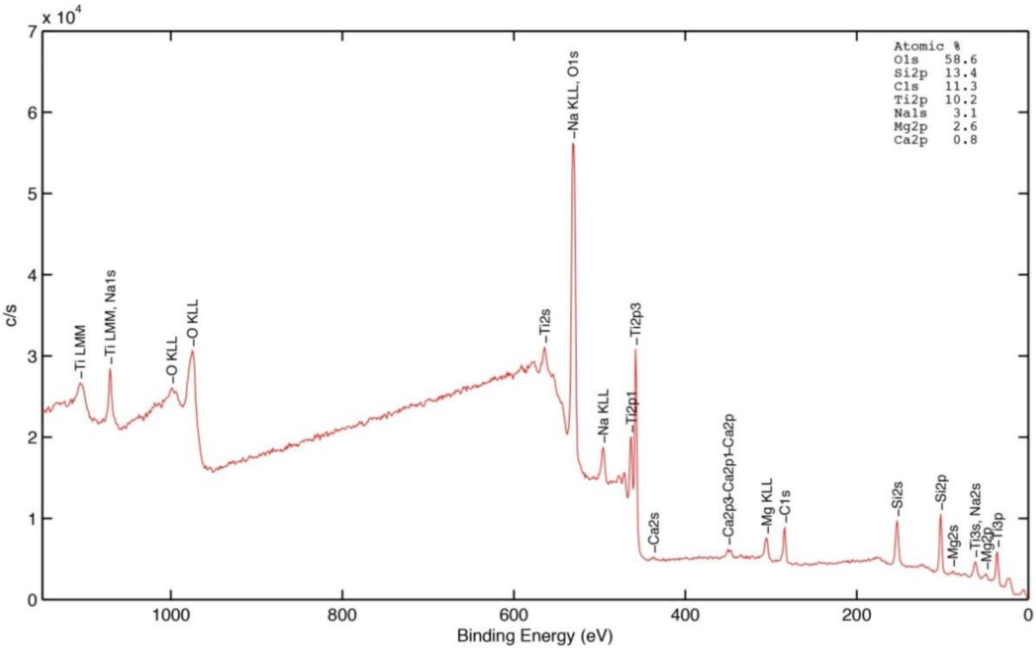

Figure B.20 Survey XPS scan of C-A600

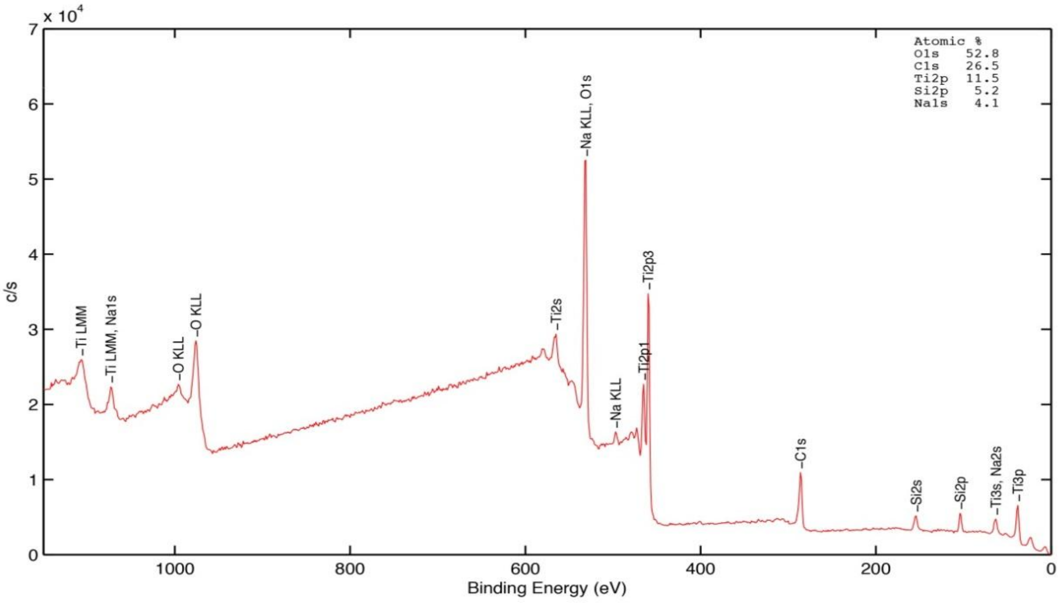

Figure B.21 Survey XPS scan of C-N300

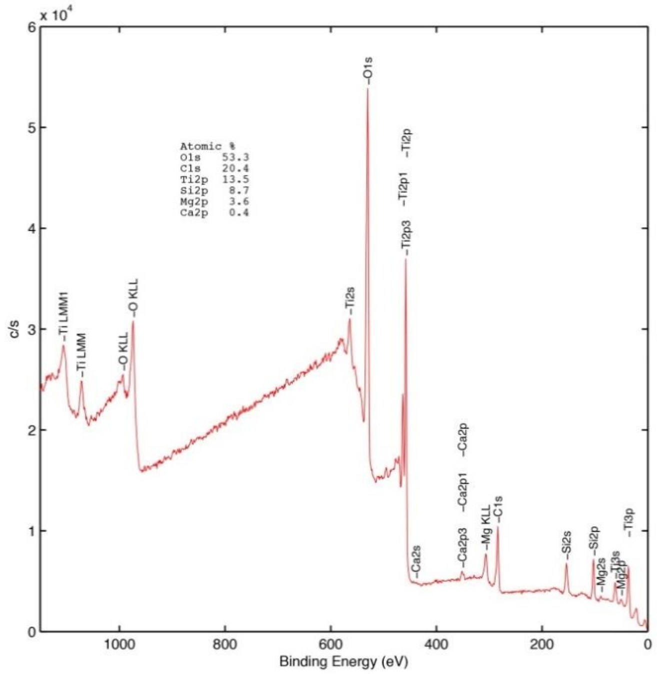

Figure B.22 Survey XPS scan of C-N400

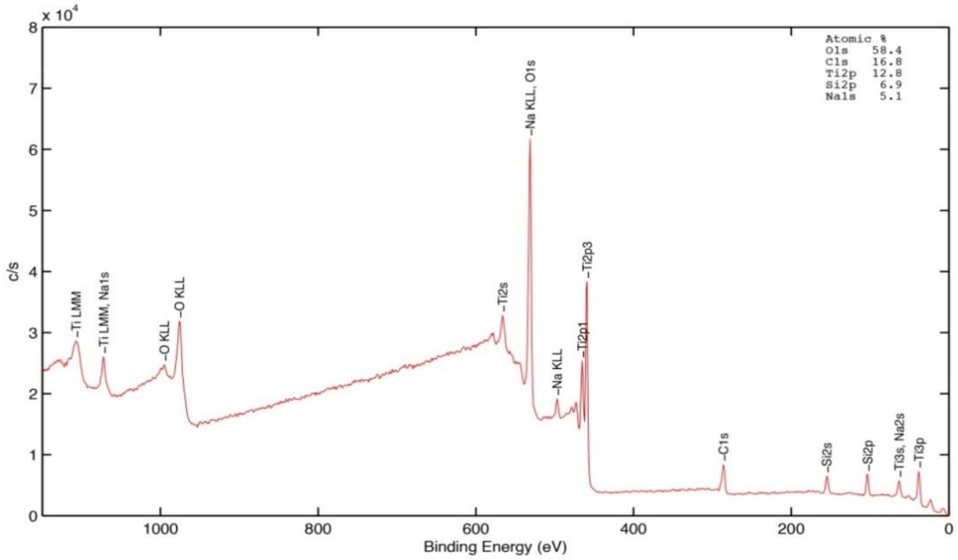

Figure B.23 Survey XPS scan of C-N500

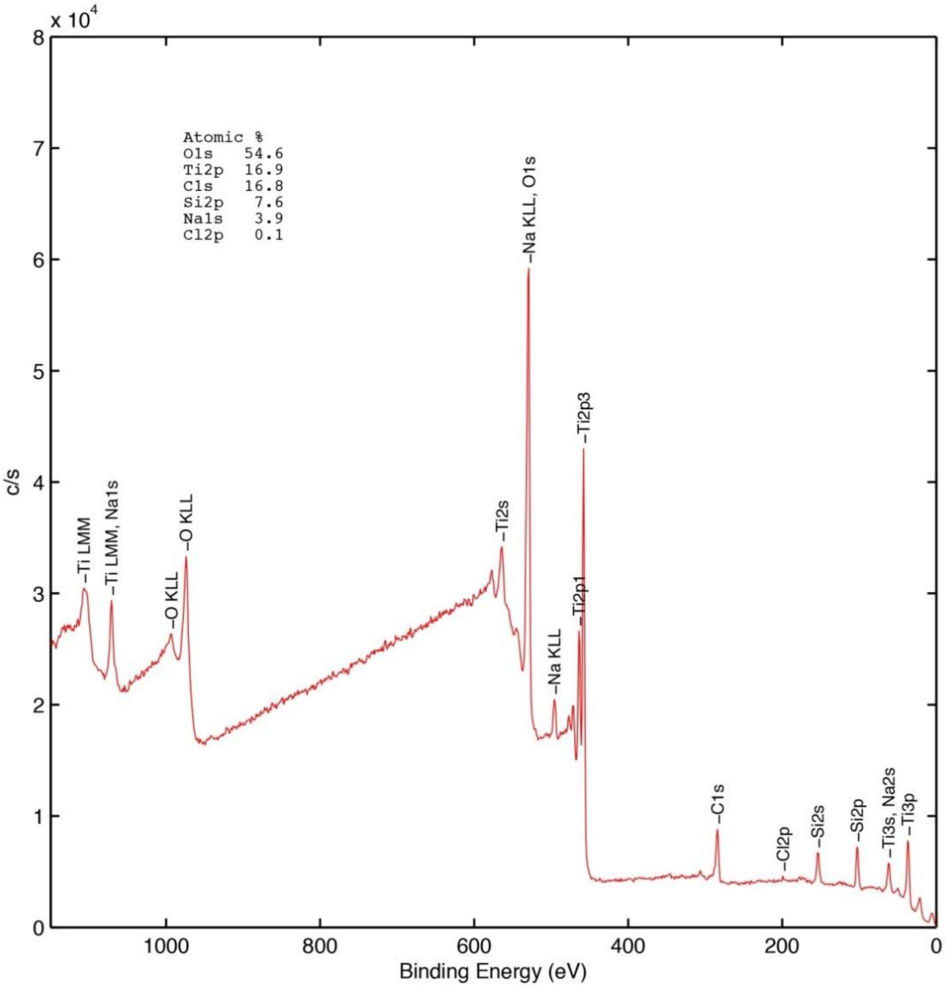

Figure B.24 Survey XPS scan of C-N600

APPENDIX C

BAND GAP CALCULATION

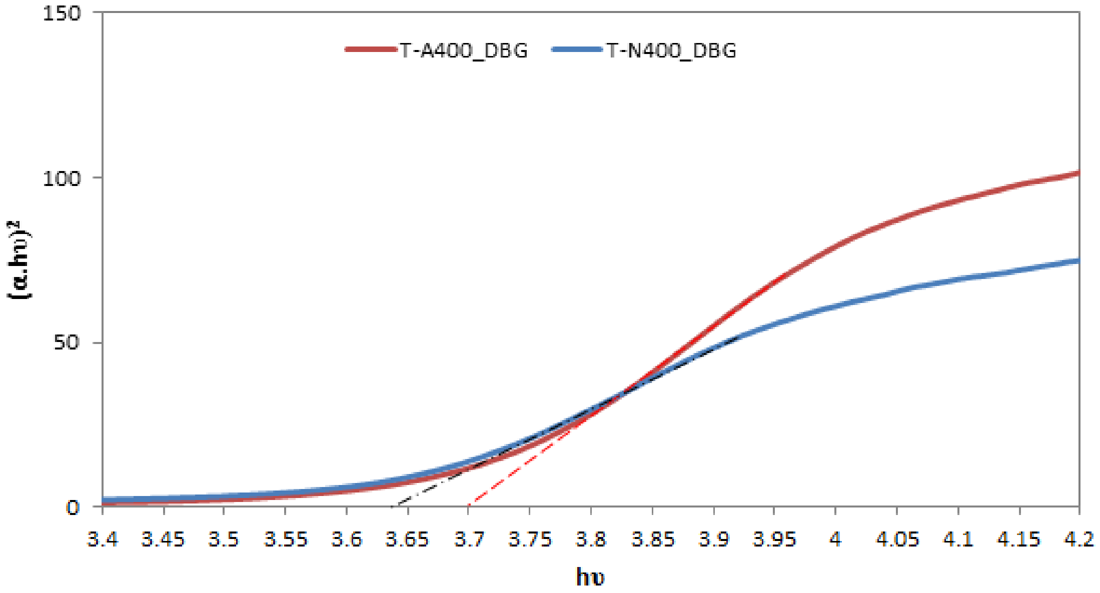

Figure C.1 Direct band gap determination of T-400 sample

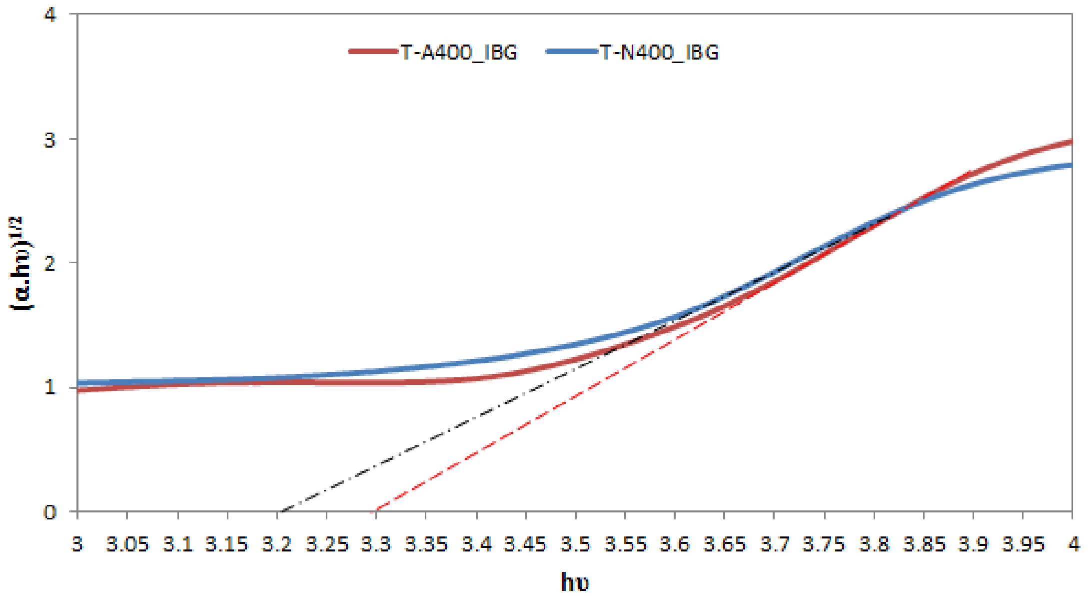

Figure C.2 Indirect band gap determination of T-400 sample

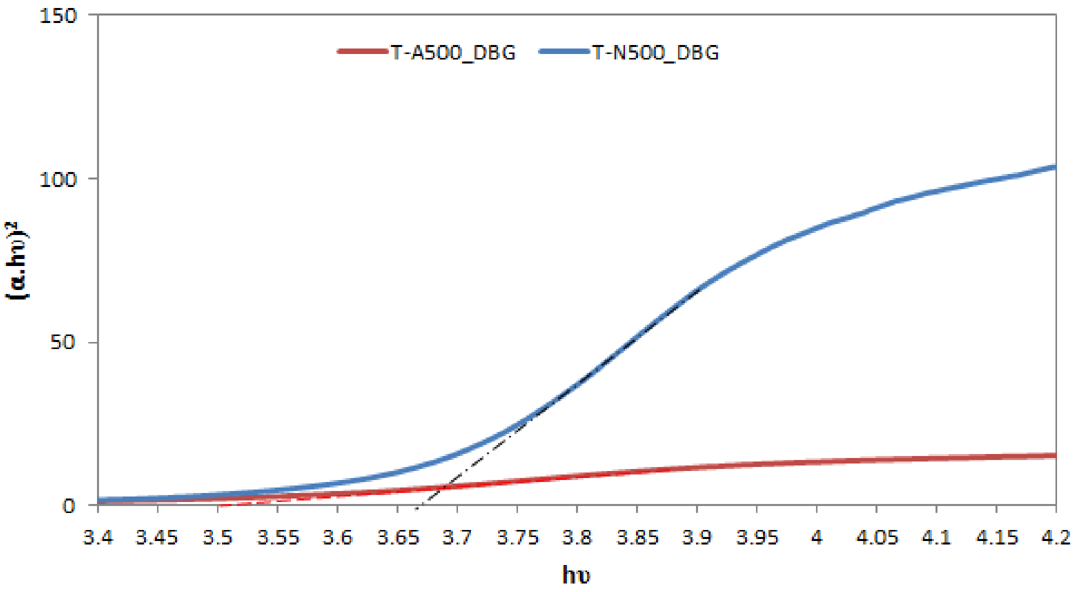

Figure C.3 Direct band gap determination of T-500 sample

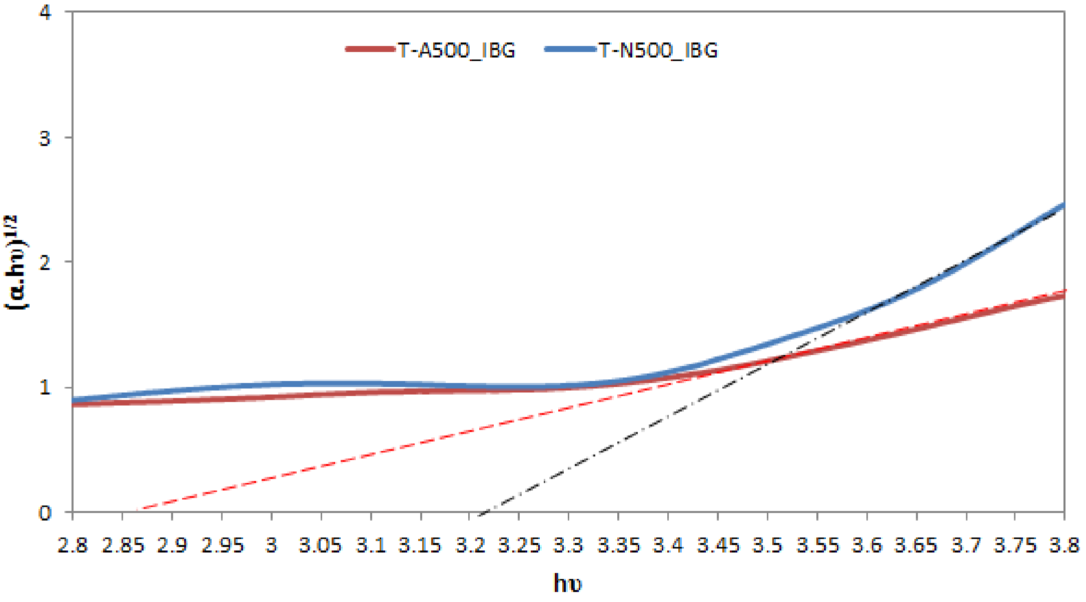

Figure C.4 Indirect band gap determination of T-500 sample

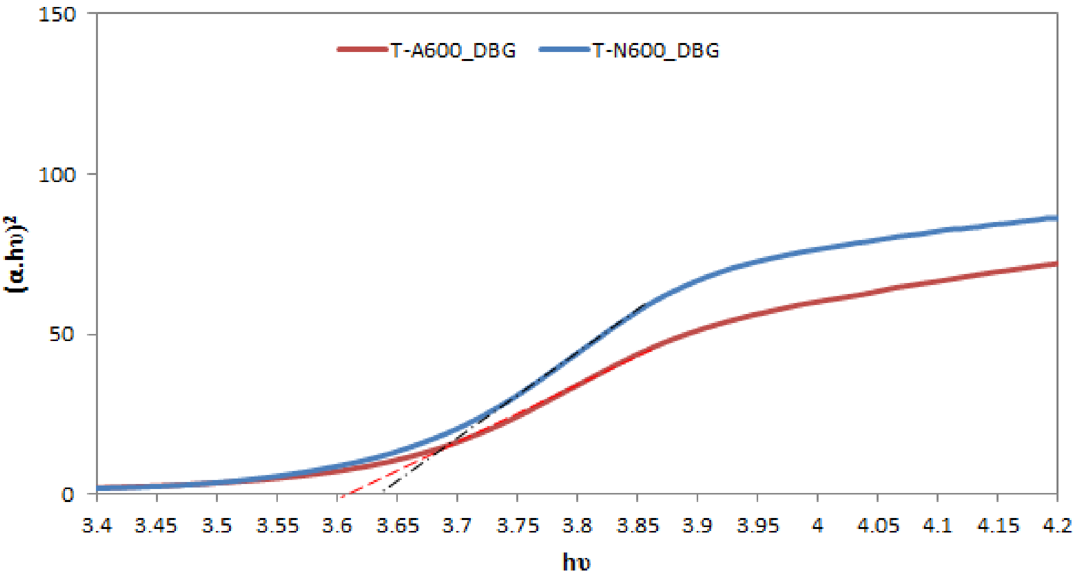

Figure C.5 Direct band gap determination of T-600 sample

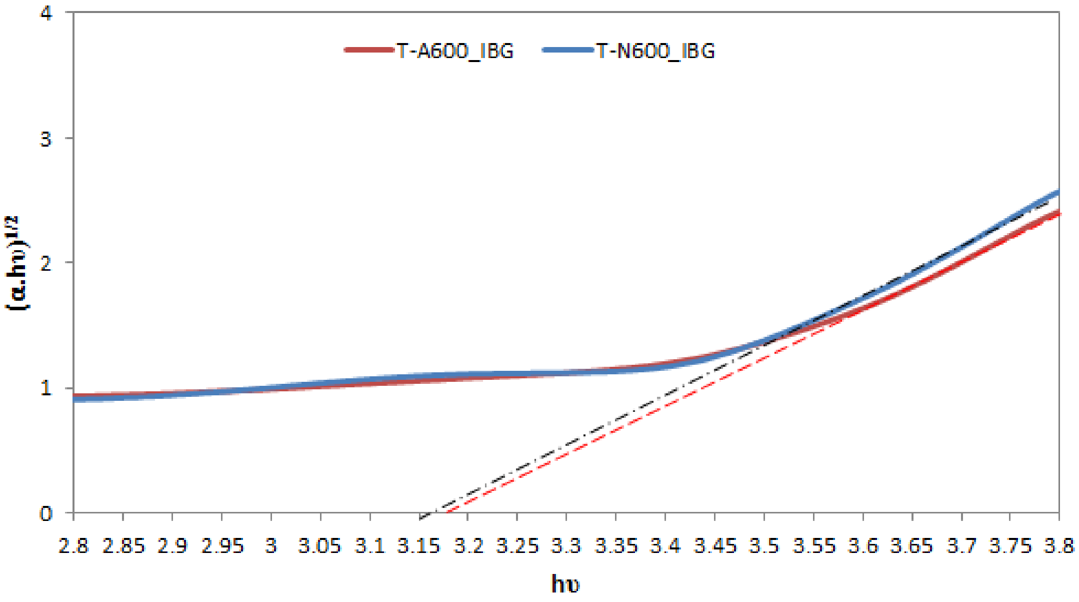

Figure C.6 Indirect band gap determination of T-600 sample

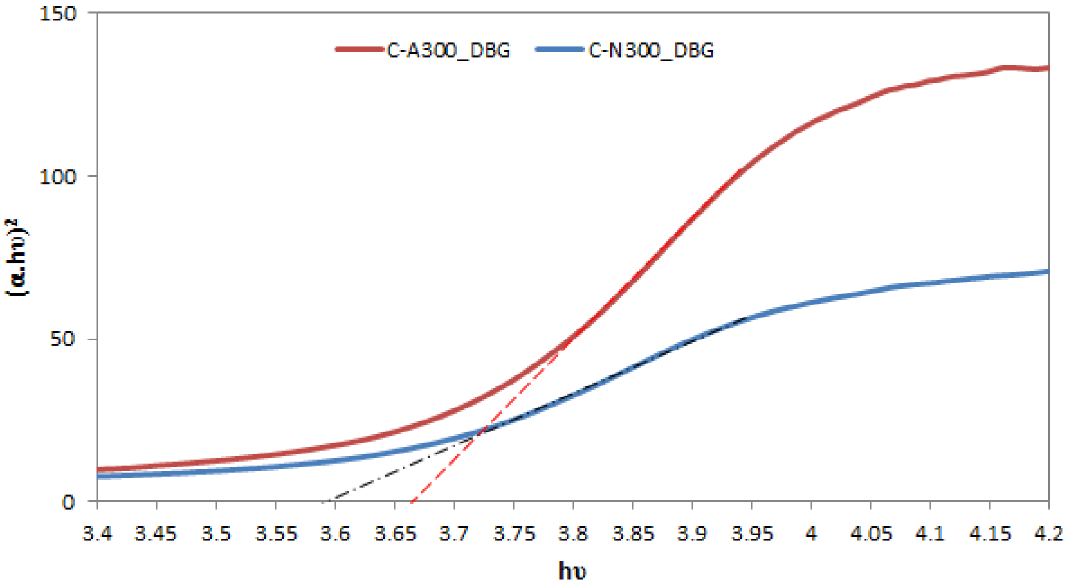

Figure C.7 Direct band gap determination of T-300 sample

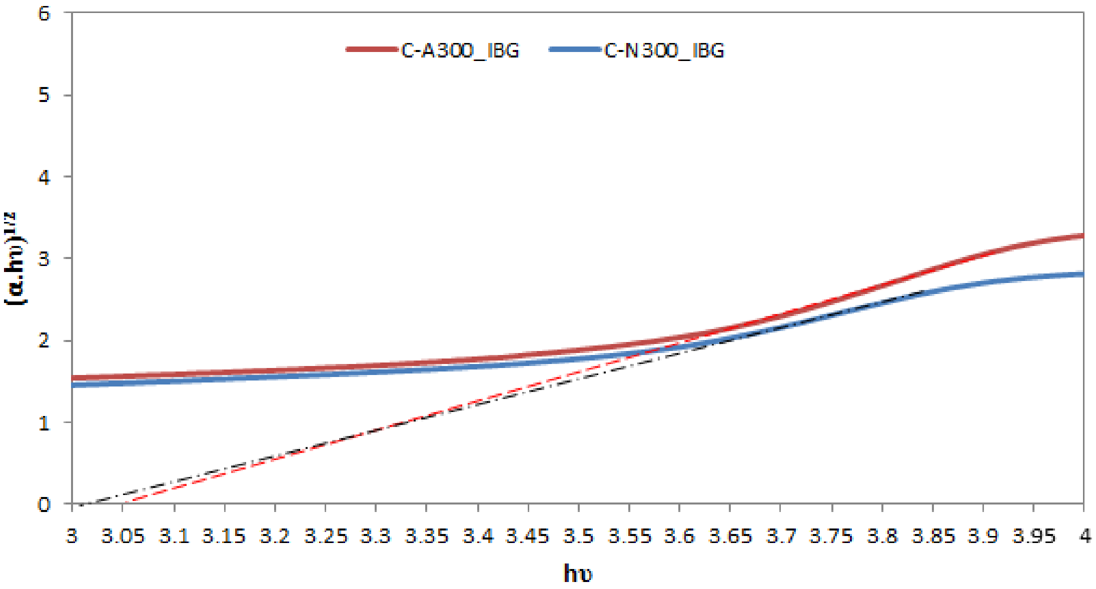

Figure C.8 Indirect band gap determination of C-300 sample

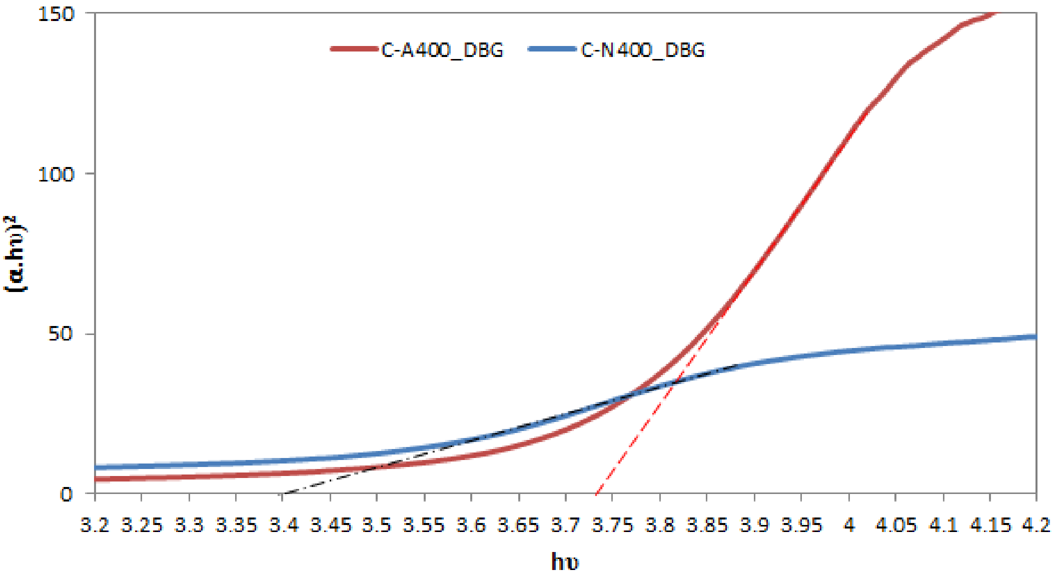

Figure C.9 Direct band gap determination of C-400 sample

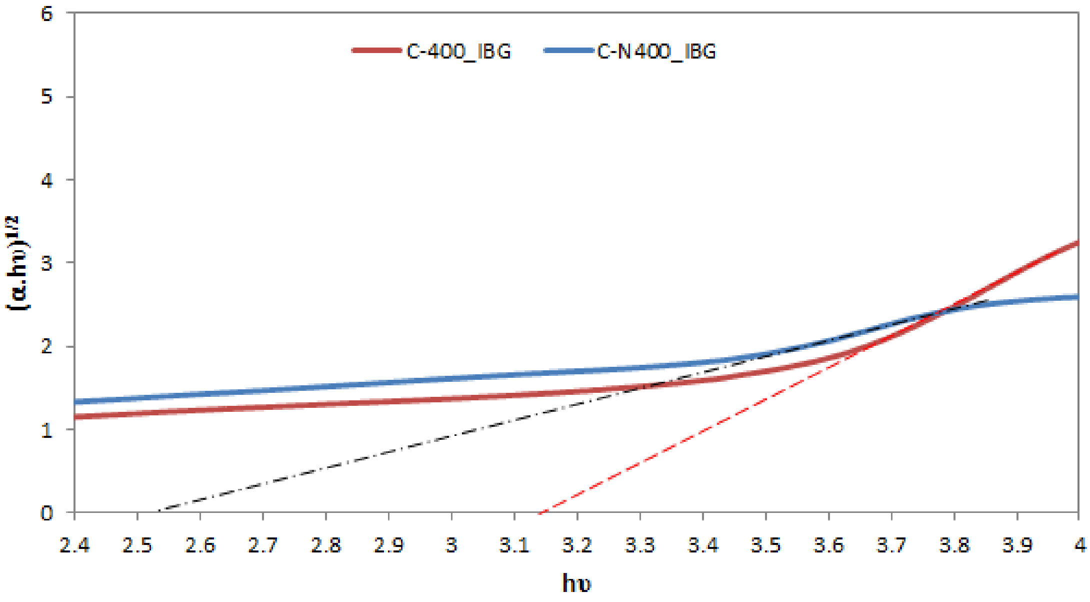

Figure C.10 Indirect band gap determination of C-400 sample

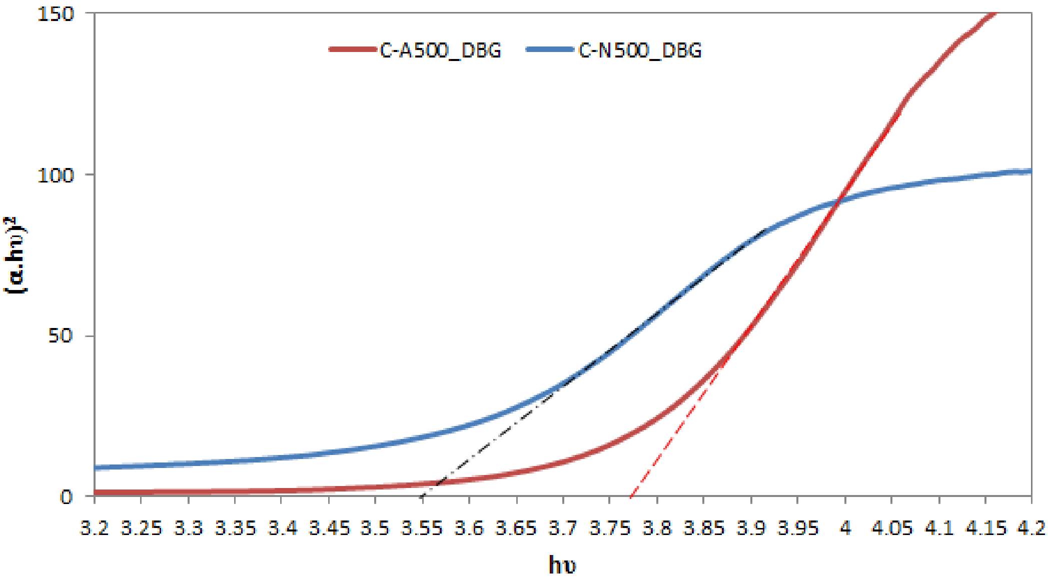

Figure C.11 Direct band gap determination of C-500 sample

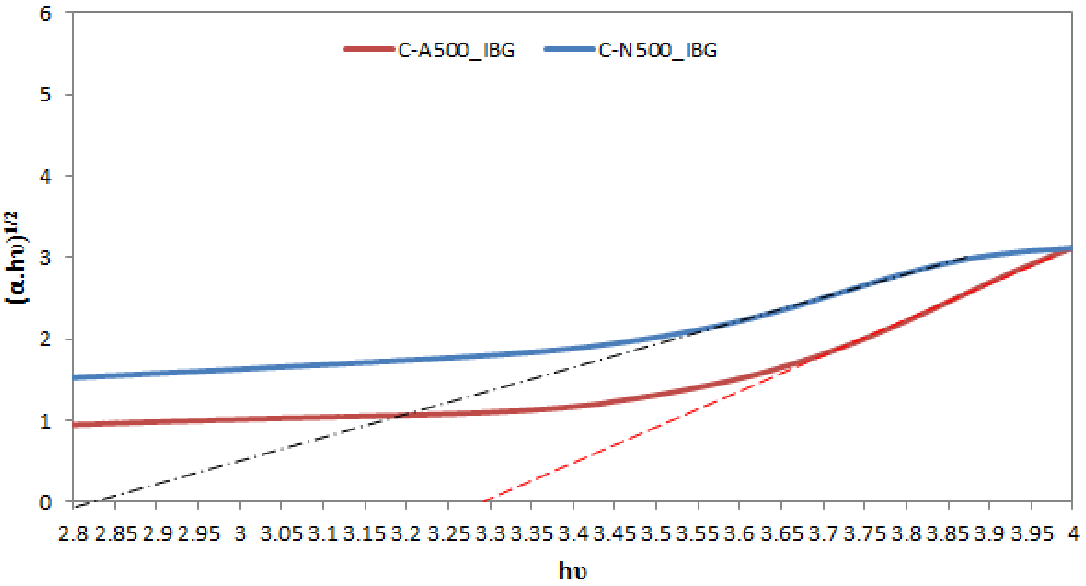

Figure C.12 Indirect band gap determination of C-500 sample

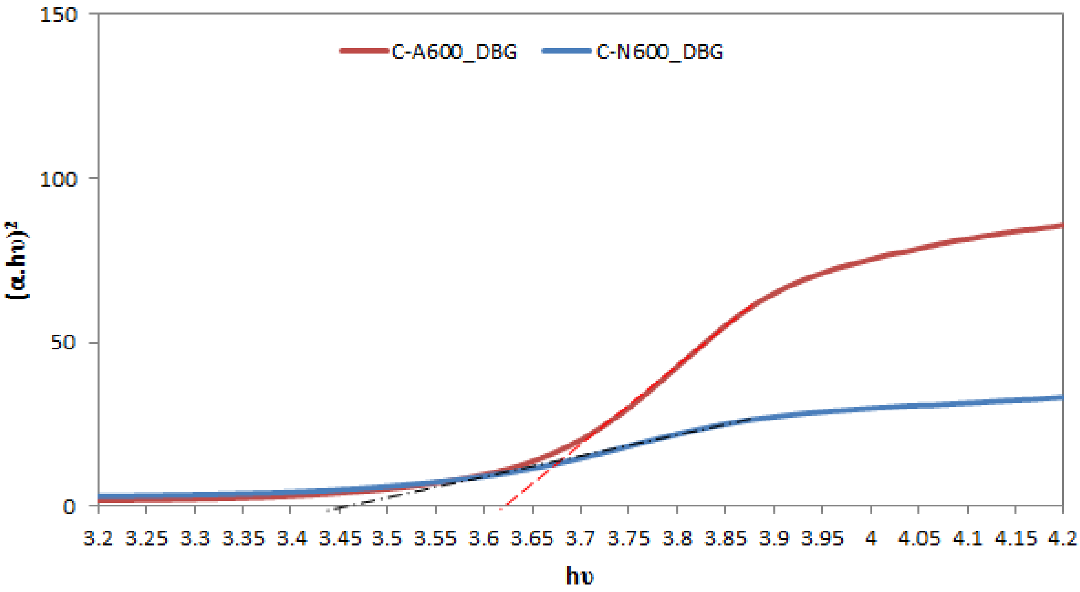

Figure C.13 Direct band gap determination of C-600 sample

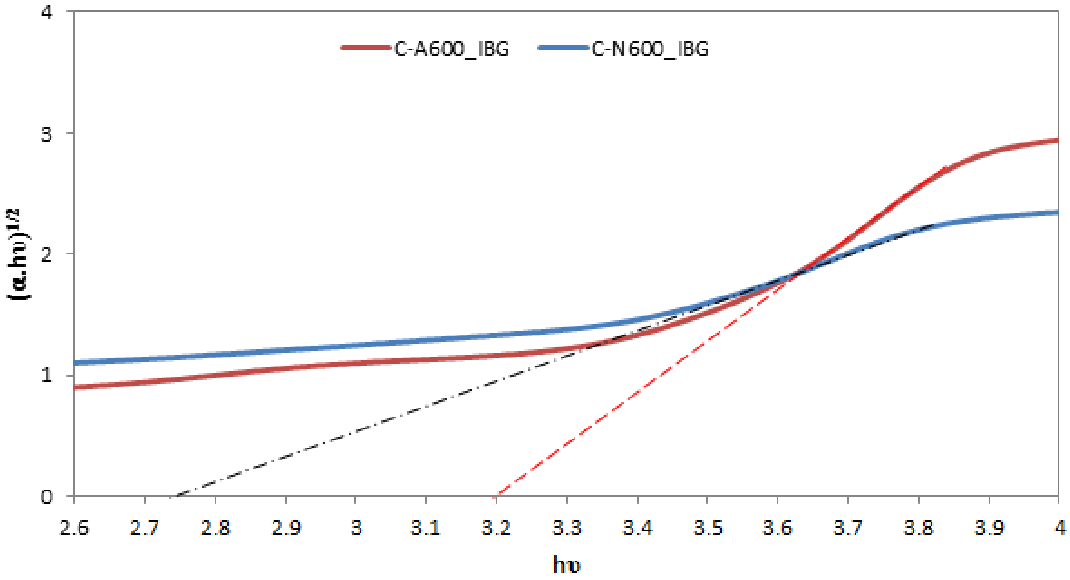

Figure C.14 Indirect band gap determination of C-600 sample

APPENDIX D

PHOTOCATALYTIC ACTIVITY TEST

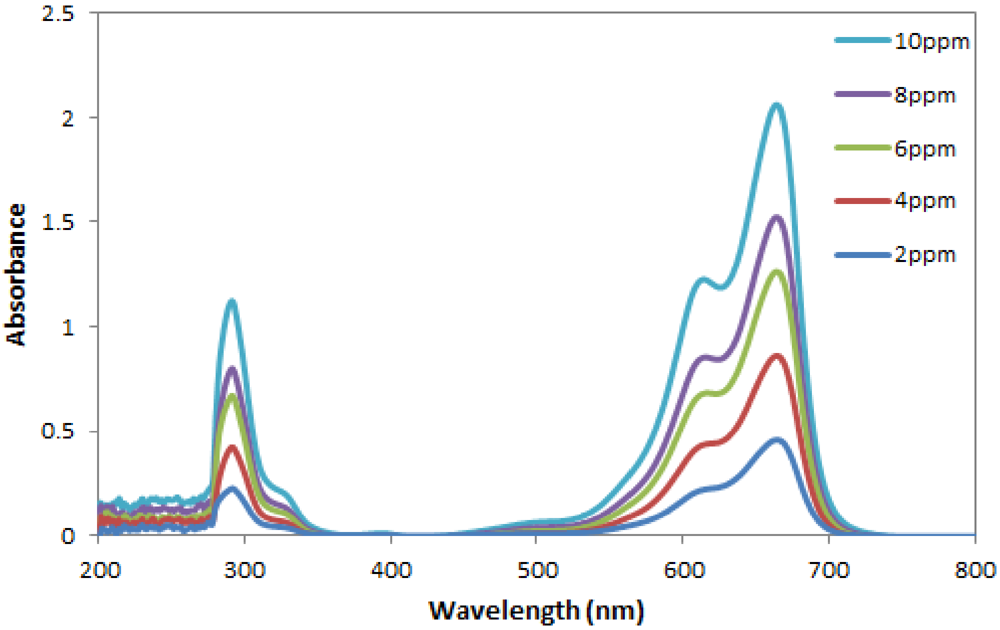

Figure D.1 UV-Vis Spectra of methylene blue solution at different concentrations

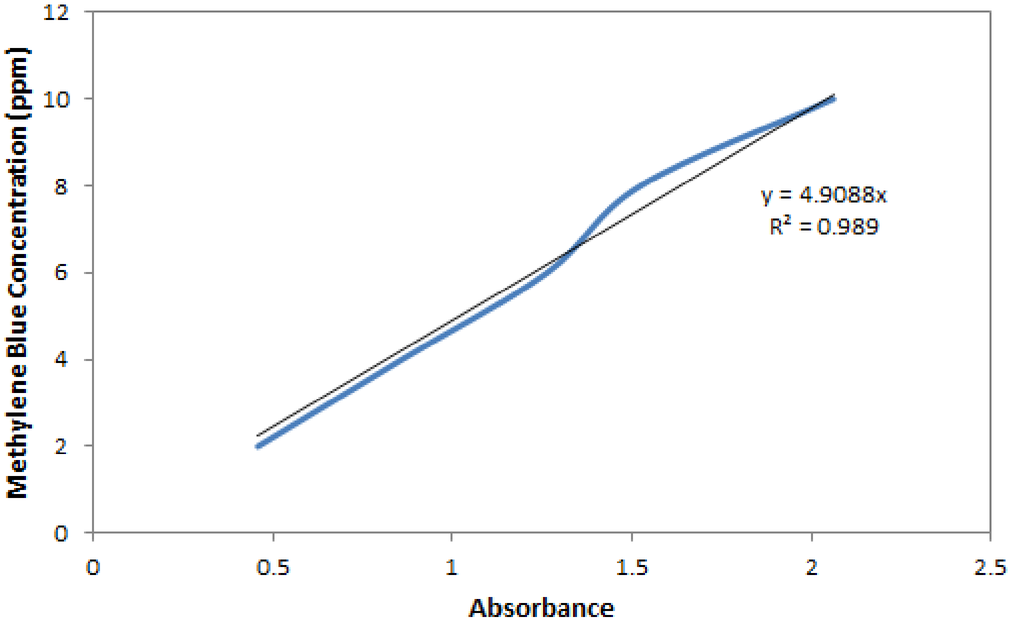

Figure D.2 Calibration line for the methylene blue degradation

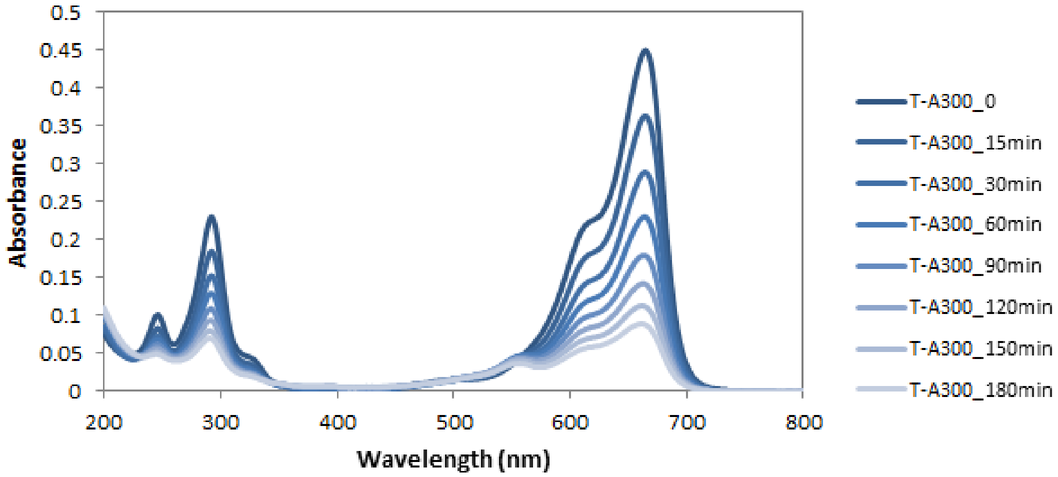

Figure D.3 Photocatalytic degradation of methylene blue solution by T-A300 under UV-C irradiation

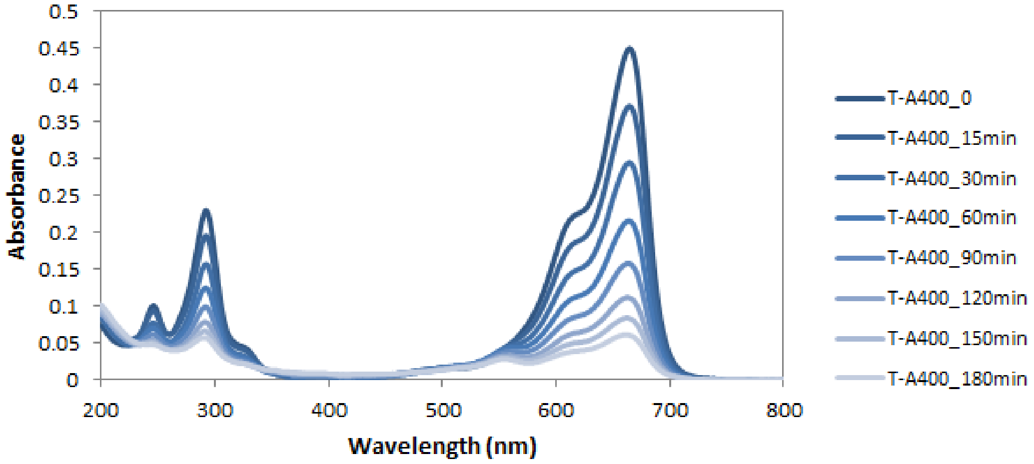

Figure D.4 Photocatalytic degradation of methylene blue solution by T-A400 under UV-C irradiation

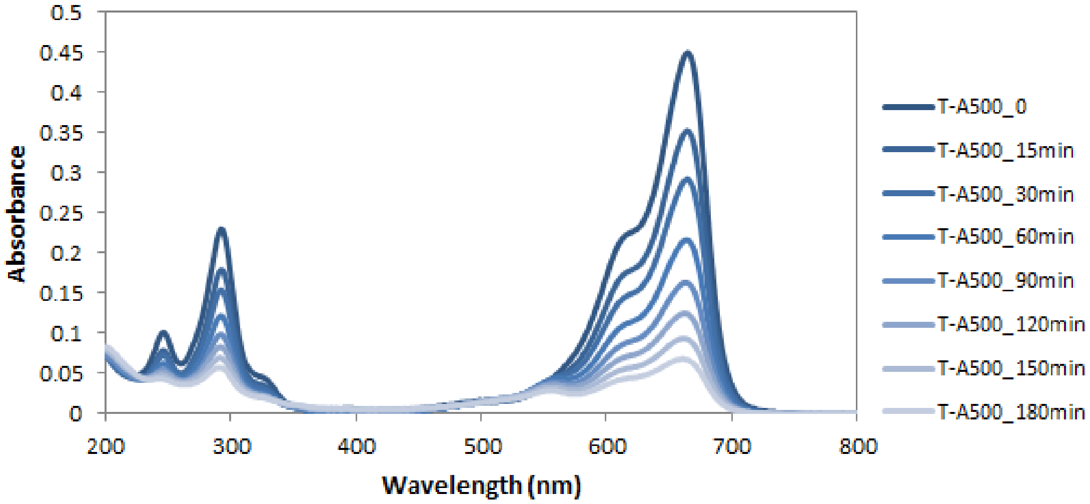

Figure D.5 Photocatalytic degradation of methylene blue solution by T-A500 under UV-C irradiation

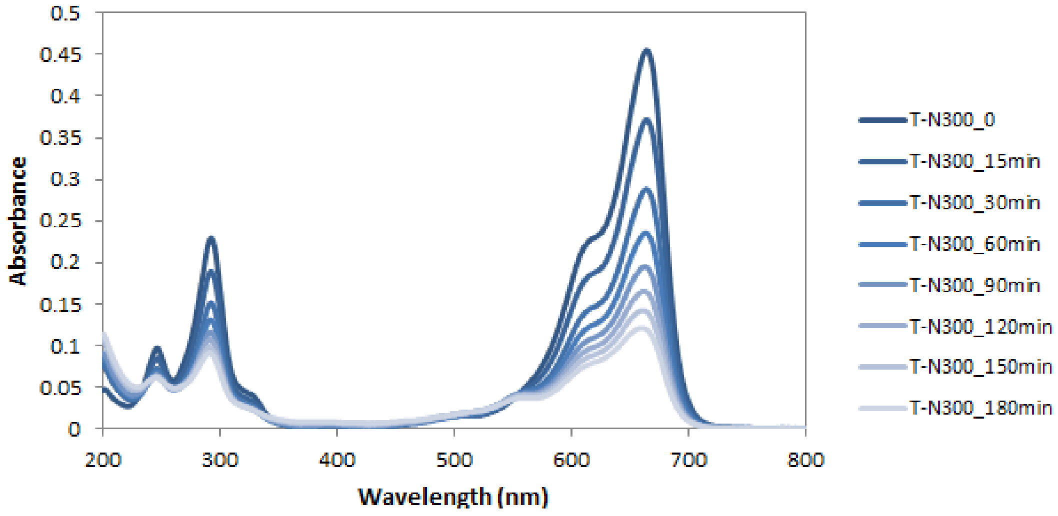

Figure D.6 Photocatalytic degradation of methylene blue solution by T-N300 under UV-C irradiation

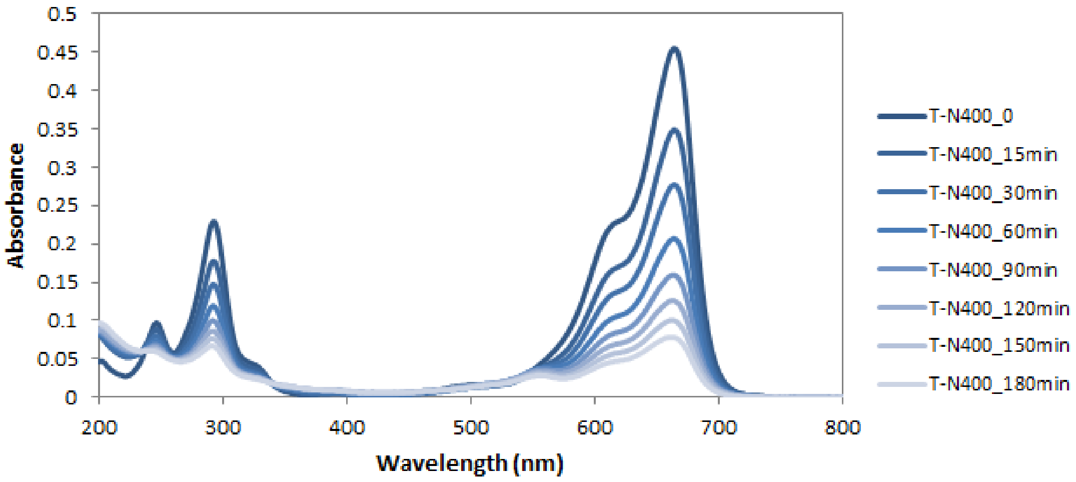

Figure D.7 Photocatalytic degradation of methylene blue solution by T-N400 under UV-C irradiation

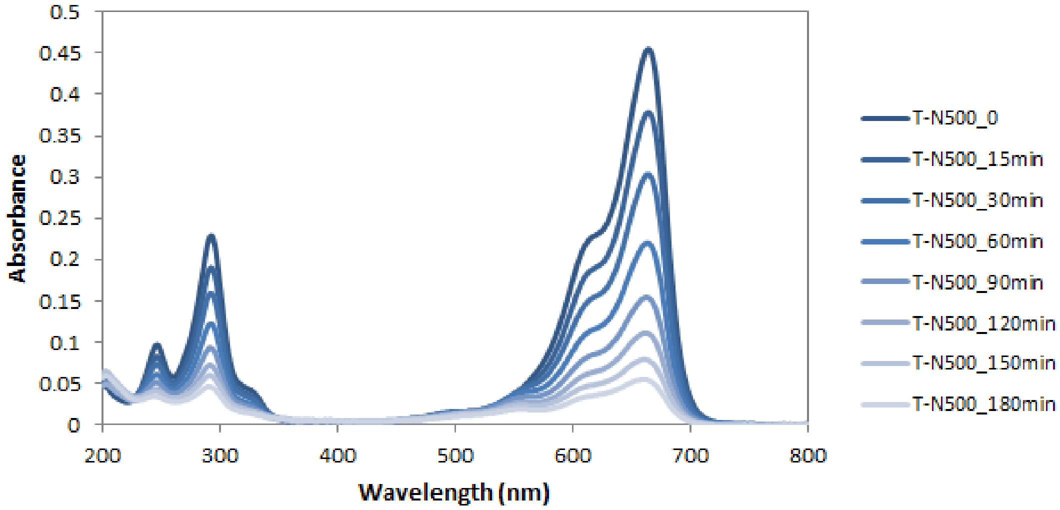

Figure D.8 Photocatalytic degradation of methylene blue solution by T-N500 under UV-C irradiation

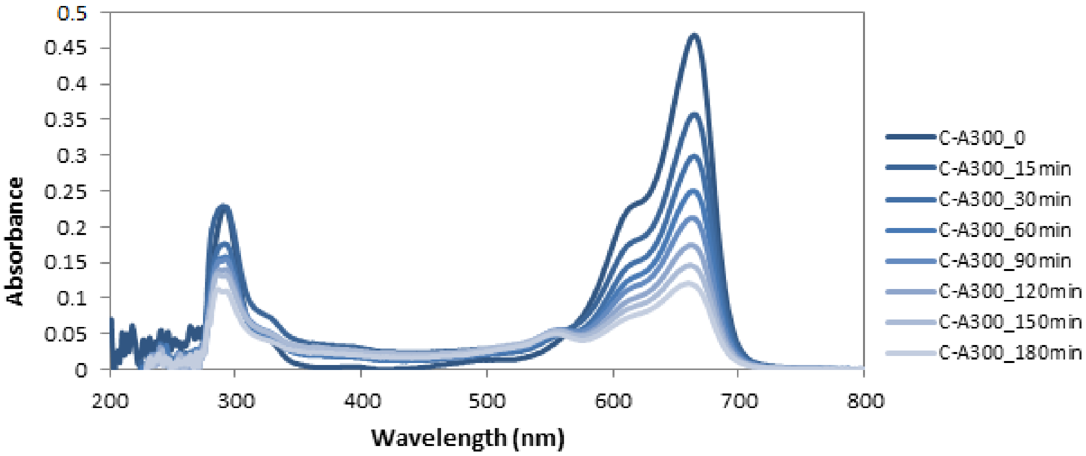

Figure D.9 Photocatalytic degradation of methylene blue solution by C-A300 under UV-C irradiation

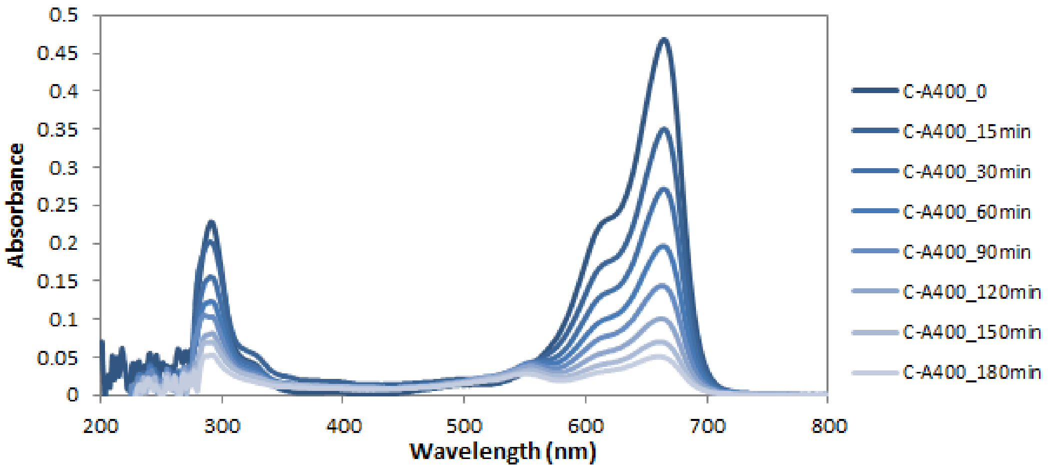

Figure D.10 Photocatalytic degradation of methylene blue solution by C-A400 under UV-C irradiation

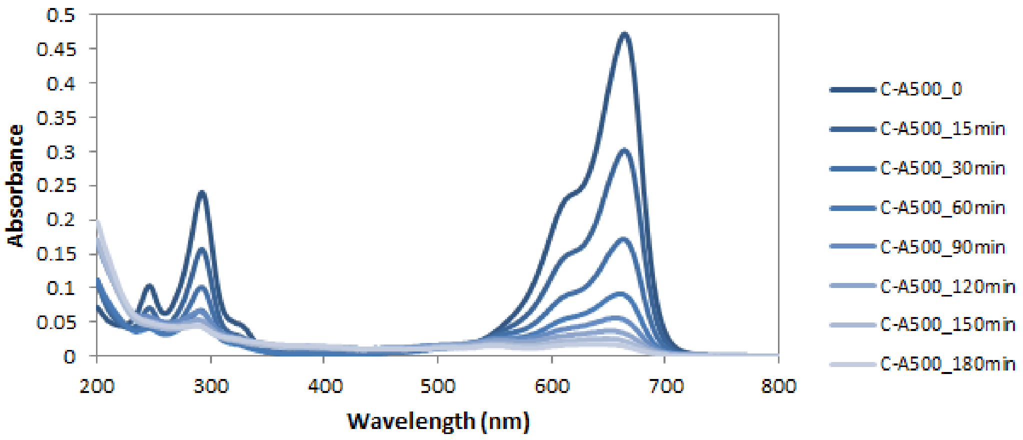

Figure D.11 Photocatalytic degradation of methylene blue solution by C-A500 under UV-C irradiation

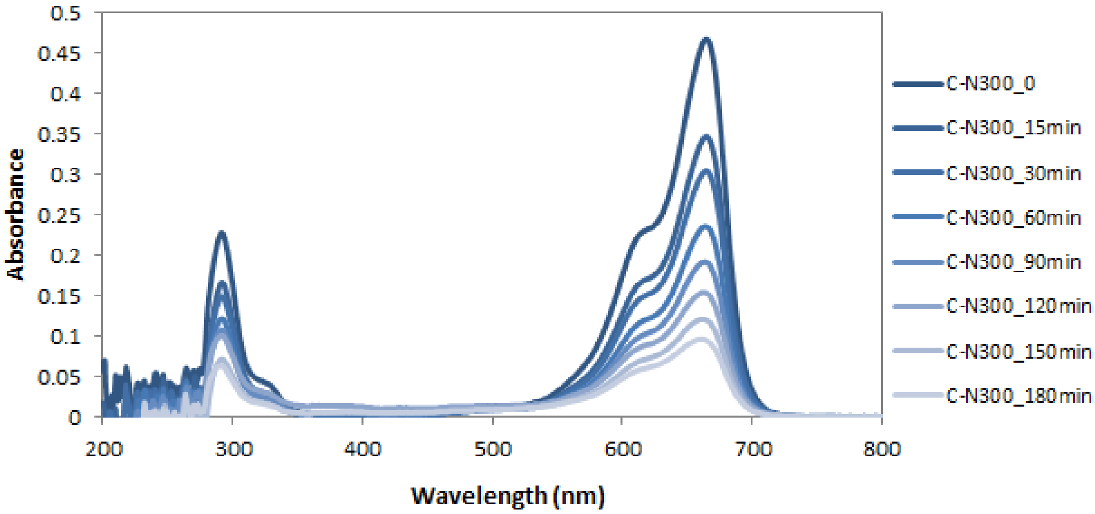

Figure D.12 Photocatalytic degradation of methylene blue solution by C-N300 under UV-C irradiation

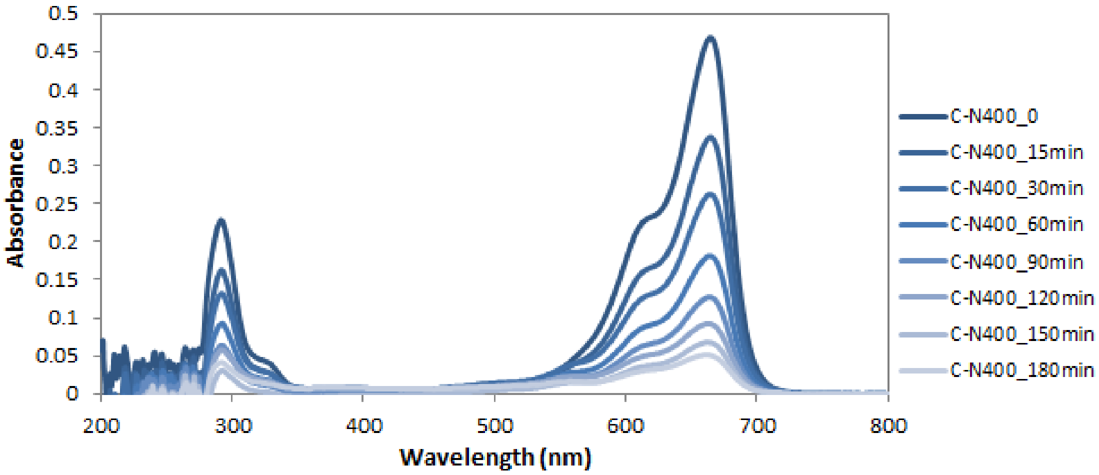

Figure D.13 Photocatalytic degradation of methylene blue solution by C-N400 under UV-C irradiation

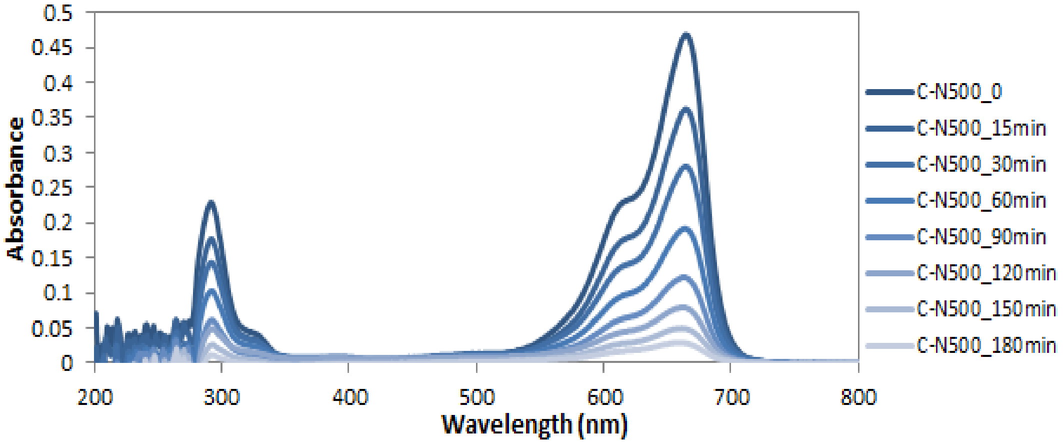

Figure D.14 Photocatalytic degradation of methylene blue solution by C-N500 under UV-C irradiation

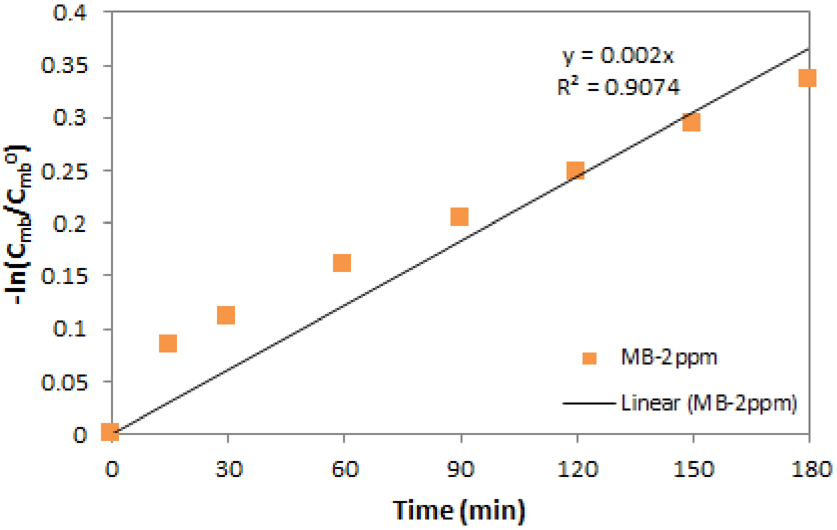

Figure D.15 Rate constant determination for self-degradation reaction of methylene blue

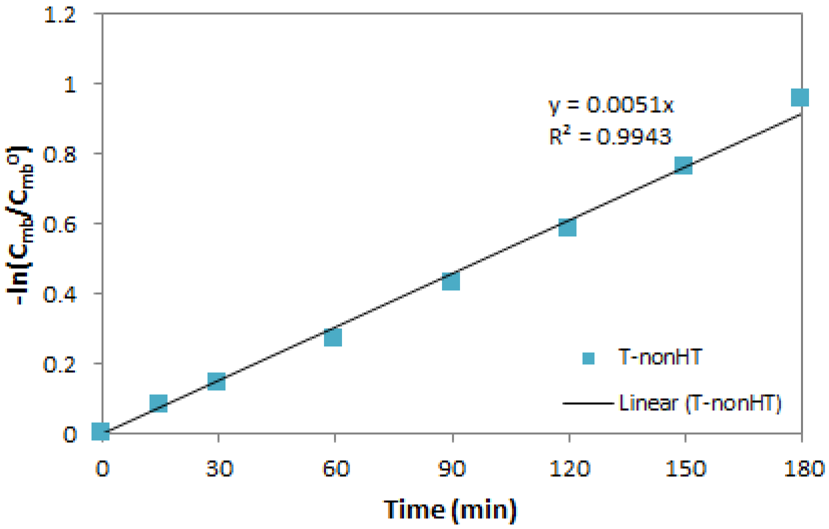

Figure D.16 Rate constant determination for photocatalytic degradation by T-nonHT

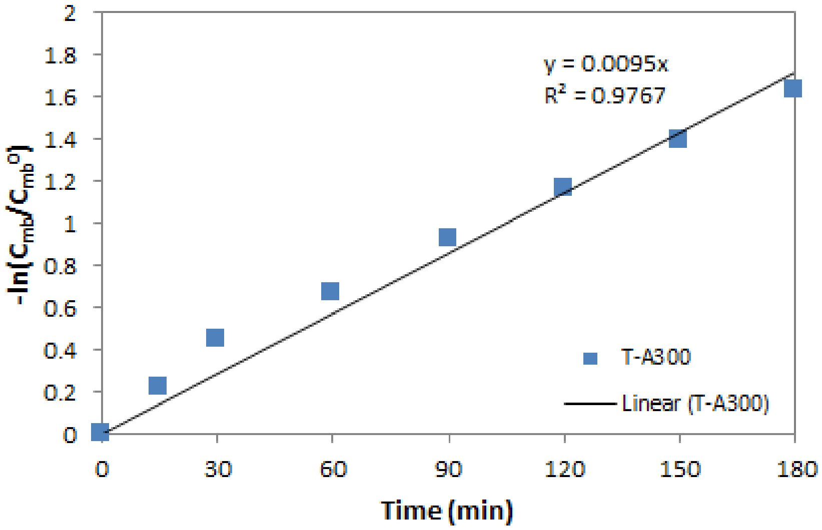

Figure D.17 Rate constant determination for photocatalytic degradation by T-A300

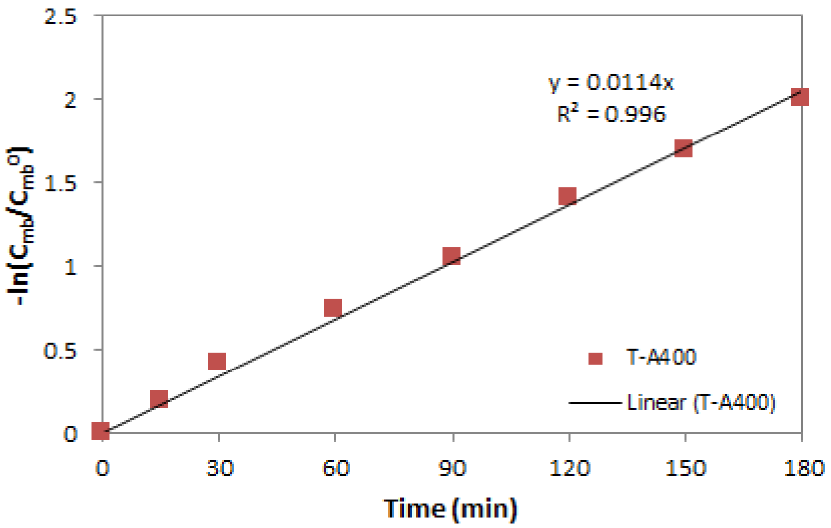

Figure D.18 Rate constant determination for photocatalytic degradation by T-A400

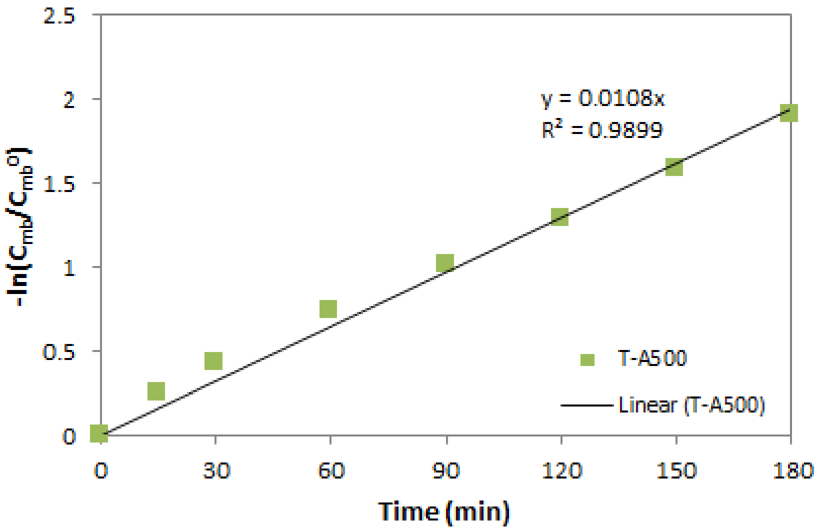

Figure D.19 Rate constant determination for photocatalytic degradation by T-A500

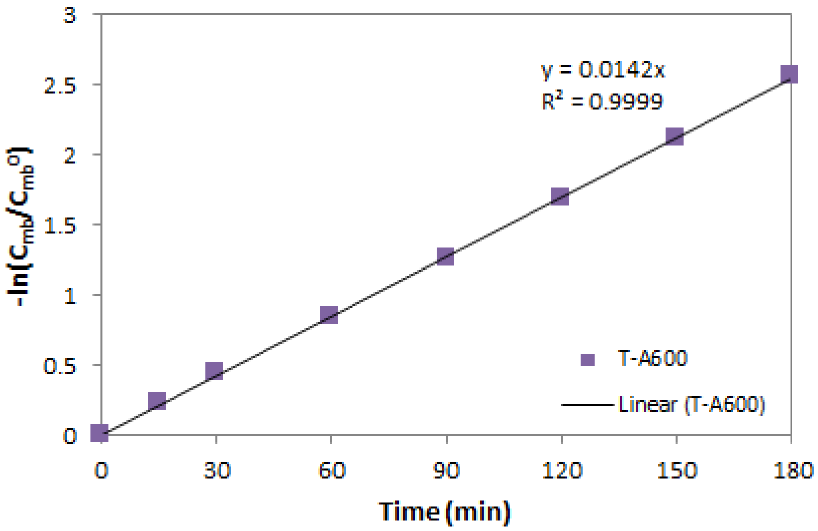

Figure D.20 Rate constant determination for photocatalytic degradation by T-A600

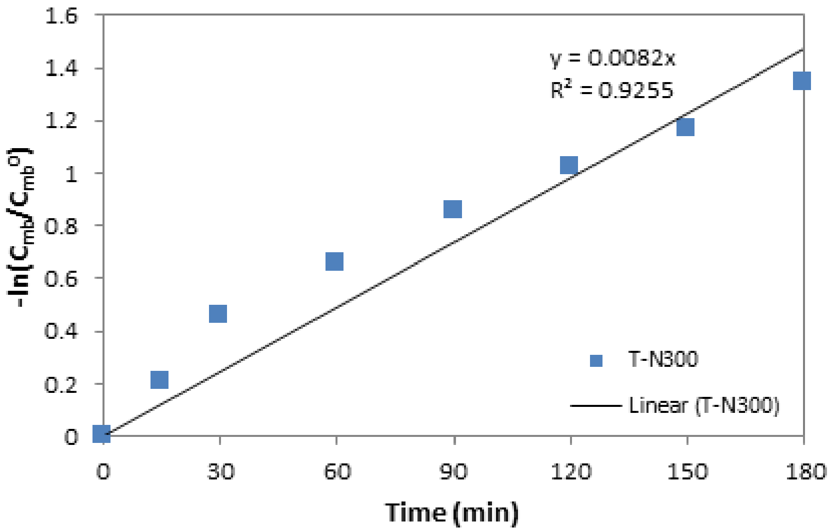

Figure D.21 Rate constant determination for photocatalytic degradation by T-N300

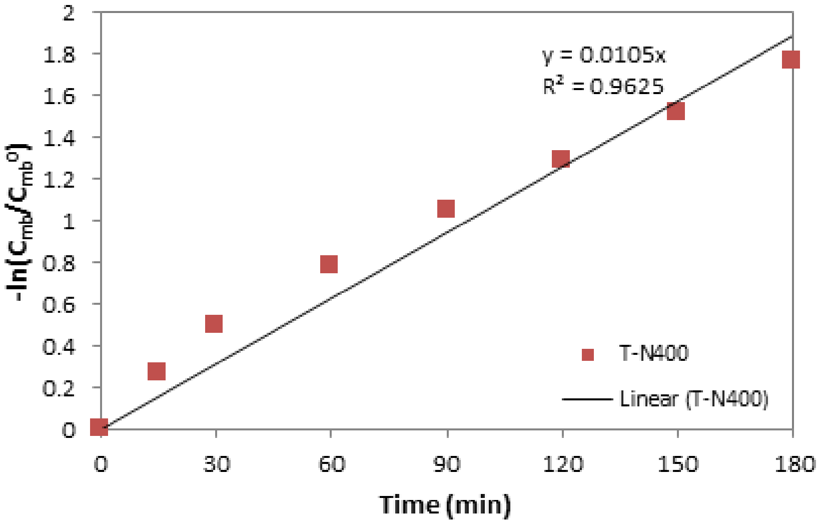

Figure D.22 Rate constant determination for photocatalytic degradation by T-N400

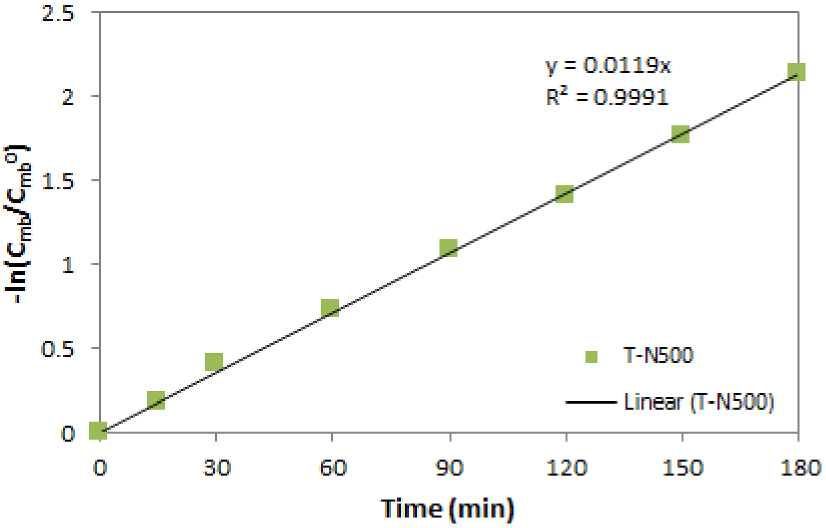

Figure D.23 Rate constant determination for photocatalytic degradation by T-A500

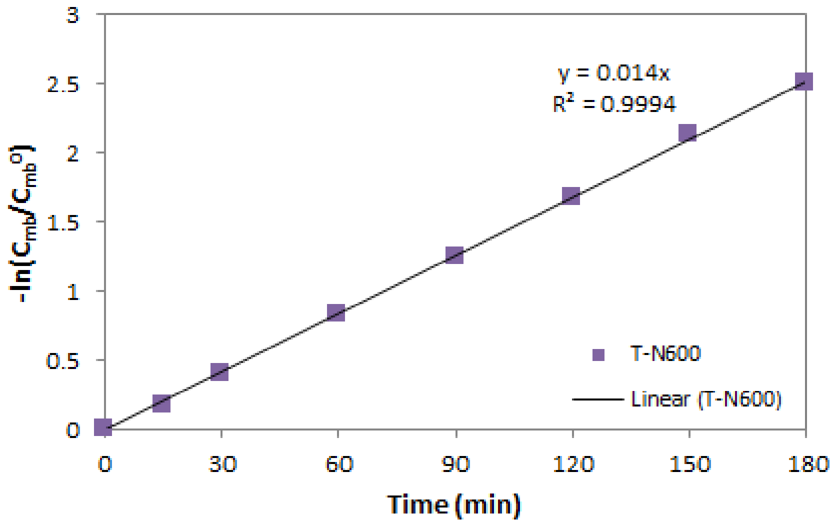

Figure D.24 Rate constant determination for photocatalytic degradation by T-A600

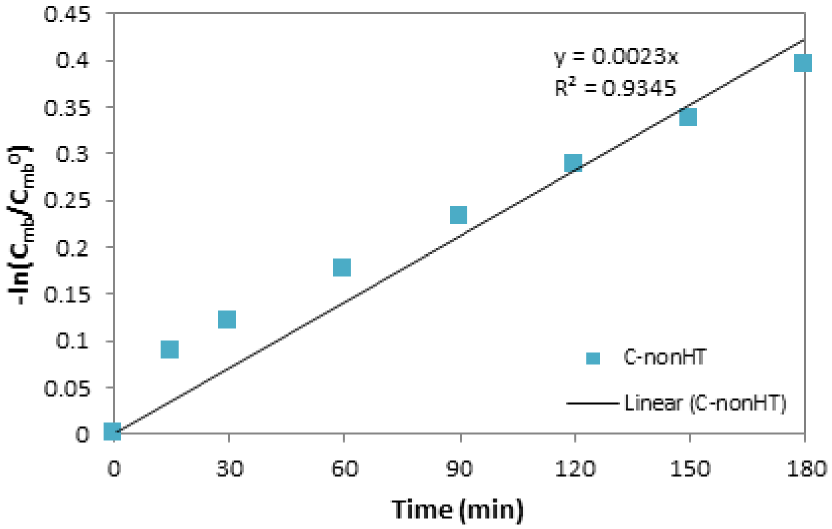

Figure D.25 Rate constant determination for photocatalytic degradation by C-nonHT

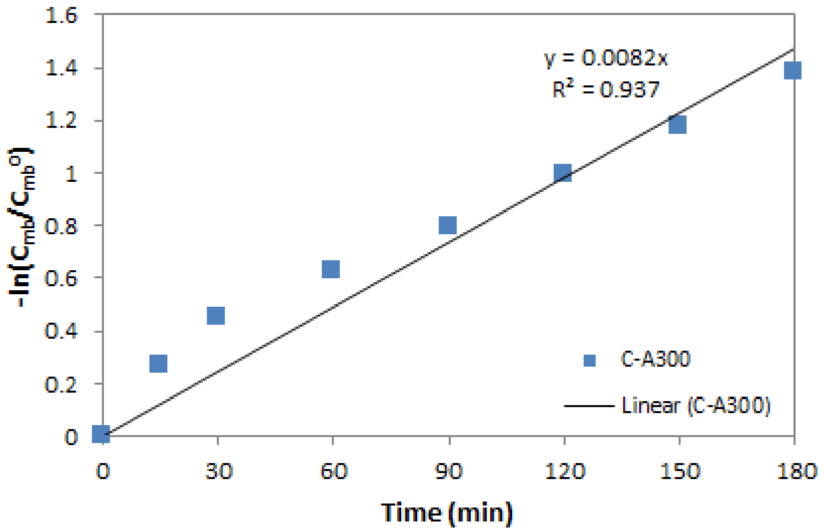

Figure D.268 Rate constant determination for photocatalytic degradation by C-A300

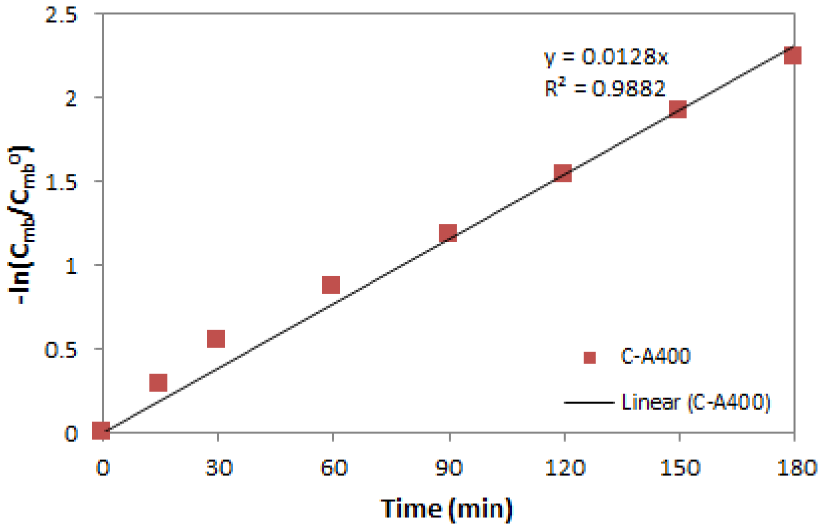

Figure D.27 Rate constant determination for photocatalytic degradation by C-A400

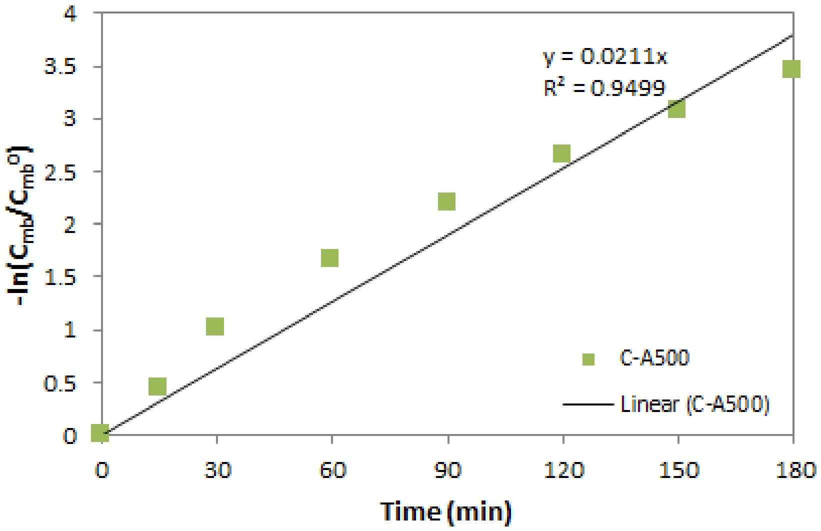

Figure D.28 Rate constant determination for photocatalytic degradation by C-A500

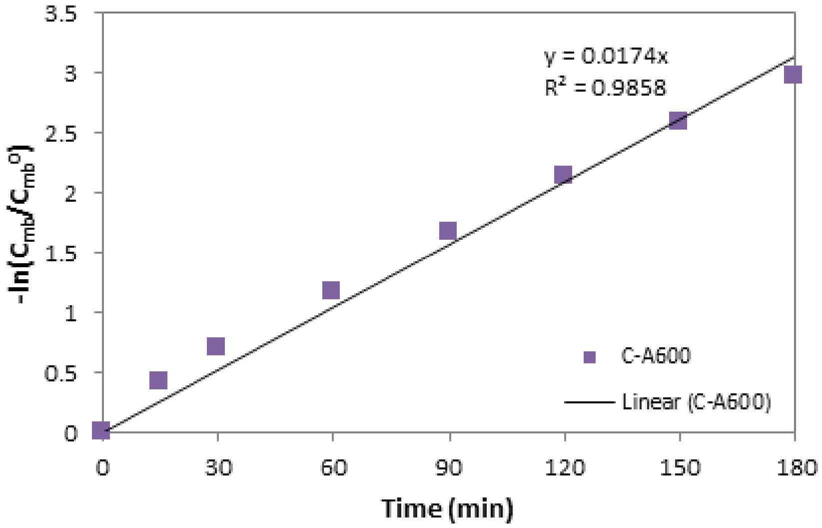

Figure D.29 Rate constant determination for photocatalytic degradation by C-A600

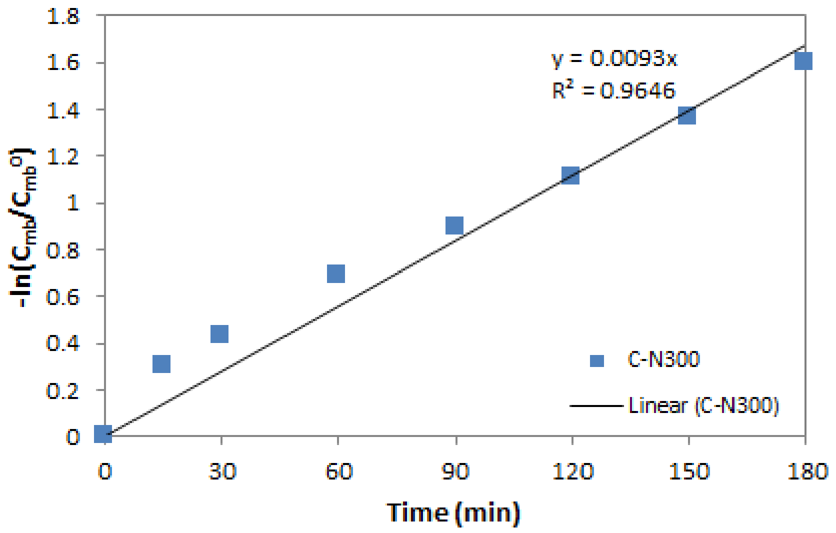

Figure D.30 Rate constant determination for photocatalytic degradation by C-N300

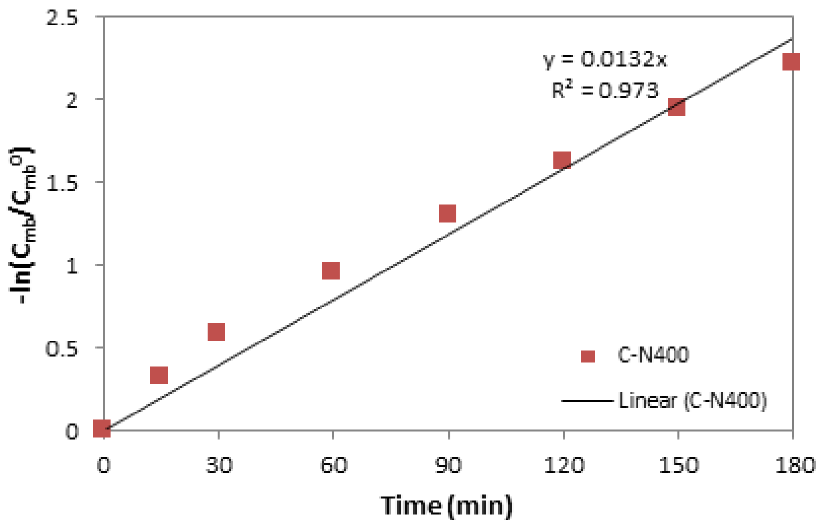

Figure D.31 Rate constant determination for photocatalytic degradation by C-N400

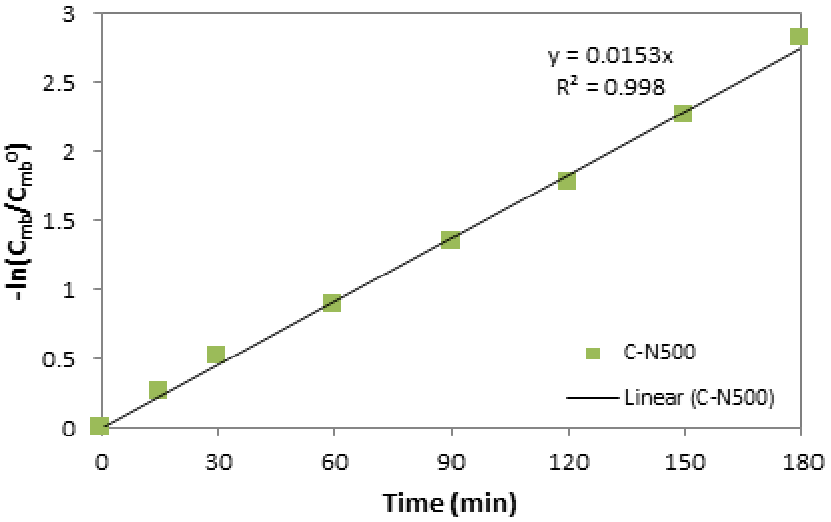

Figure D.32 Rate constant determination for photocatalytic degradation by C-N500

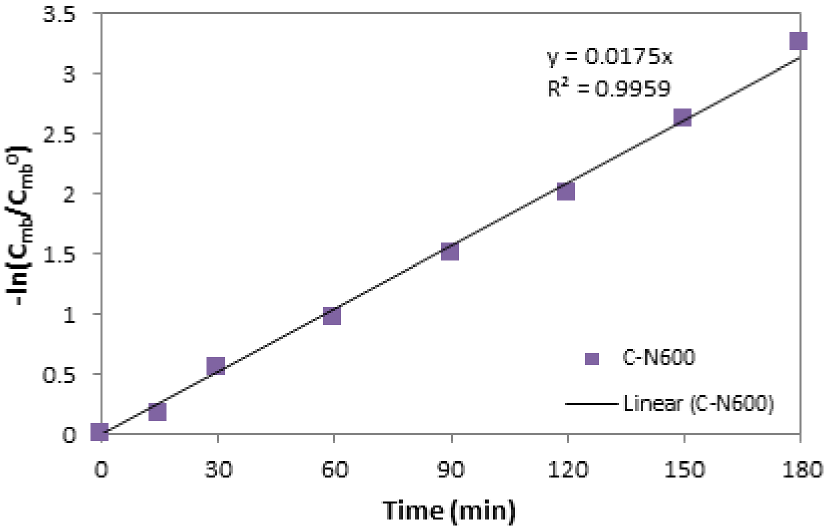

Figure D.33 Rate constant determination for photocatalytic degradation by C-N600